72-29,894

KIRK, Jr., Harold Glen, 1941-
IDENTIFICATION OF RELATIVISTIC PARTICLES EMITTED FROM 16.2 GeV/c PION NUCLEON COLLISIONS IN EMULSION.

The University of Oklahoma, Ph.D., 1972
Physics, nuclear

THE UNIVERSITY OF OKLAHOMA

GRADUATE COLLEGE

IDENTIFICATION OF RELATIVISTIC PARTICLES EMITTED FROM 16.2 GeV/c PION NUCLEON COLLISIONS IN EMULSION

A DISSERTATION

SUBMITTED TO THE GRADUATE FACULTY

in partial fulfillment of the requirements for the

degree of

DOCTOR OF PHILOSOPHY

BY

HAROLD G. KIRK, Jr.

Norman, Oklahoma

1972

IDENTIFICATION OF RELATIVISTIC PARTICLES EMITTED FROM

16.2 GeV/c PION-NUCLEON COLLISIONS IN EMULSION

APPROVED BY:

DISSERTATION COMMITTEE

ACKNOWLEDGMENT

Sincere appreciation is extended to Dr. J. R. Burwell for his initial suggestion which led to this work, for his guidance throughout the experiment and for his invaluable criticisms during the preparation of the manuscript for this dissertation.

The author gives special thanks to Dr. R. G. Fowler and Dr. H. J. Fischbeck for their kind cooperation in allowing him the use of their multichannel analyzers for this work.

My gratitude also goes to Miss Stephanie Michels for her valuable assistance during the data procurement phase of the work, especially for her diligent work during my absence.

Finally, to Mrs. Mary Lou Stokes, I give my sincere thanks for a job well done in the preparation of the manuscript for this work.

TABLE OF CONTENTS

TABLE OF CONTENTS (Cont'd.)

LIST OF TABLES

LIST OF ILLUSTRATIONS

LIST OF ILLUSTRATIONS (Cont'd.)

ABSTRACT

Grain density measurements have been made on the tracks of relativistic particles emitted from 16.2 GeV/c Π^--nucleon collisions in Ilford K-5 emulsion. The grain densities have been determined directly from the gap length distributions as well as from track lacunarity and the more traditional blob density. These results, when combined with multiple Coulomb scattering data previously obtained, allow for the identification of fast non-stopping particles.

The restricted rate of energy loss by ionization in Ilford K-5 emulsion for fast singly charged particles is found to be well described by the Sternheimer equation with the energy cutoff T_{max} = 100 KeV.

Because of experimental constraints imposed, the track selection was mostly confined to the fast forward particle tracks leaving the collision sites. Most of these particles are found to be pions, with kaons and electrons also present. The quantity of kaons observed appears to be substantially higher than expected.

CHAPTER I

INTRODUCTION

Preliminary Remarks

In studying the strong interaction by means of high energy collisions, the ultimate task of the experimenter is to locate all of the particles emitted from the collision sites and to measure all the kinematical variables associated with each particle. This is a formidable task and no single technique has been developed which can do this comprehensively. One major obstacle to this ideal experiment involves the difficulties incurred in detecting neutral particles. For charged particles, detection is easier, but measuring the complete set of kinematical variables still proves to be an elusive goal which is achieved only in certain types of strong interaction events.

Excluding the geometry of the strong interaction event, the kinematical variables consist of three quantities: energy, momentum, and velocity. If the particle's mass (identity) is known, only one of these three variables is needed to completely specify the kinematical properties of the particle; otherwise, in the absence of information concerning the particle's mass, two of these quantities are needed. By geometrical properties of the interaction we speak of the directions in which the particles are emitted from the interaction site. Experiments using track forming devices such as bubble chambers or nuclear emulsions have been extremely successful in determining the geometry of the interaction but have had only limited success in determining the kinematical properties completely.

The basic techniques available in nuclear emulsion research for measuring these kinematic variables are multiple Coulomb scattering, which allows measurements of $P\beta$ (P is the particle momentum while β is the velocity of a particle in units of c); range measurements, from which a particle's energy can be determined; and ionization measurements, which yield information concerning the particle's velocity. If one wishes to study relativistic particles which do not stop in the emulsion, then the range-energy technique is no longer available and one is confined to multiple Coulomb scattering and ionization measurements in order to extract the complete kinematical information available for each particle. It is the purpose of this work to explore and define the techniques whereby these two methods of measurements can be consolidated and the kinematical variables of a particle completely described.

The Emulsion

The Ilford K-5 emulsion used in this experiment consists of silver bromide crystals embedded in a matrix of gelatin and water. The composition of Ilford K-5 emulsion [1] is given in Table 1 by per cent weights and per cent atoms.

The silver bromide crystals are responsible for rendering the paths of the charged particles visible. A crystal can be rendered developable by an ionizing charged particle which passes through the crystal and transfers a small portion of the particle's energy to it. During the development process, silver atoms are released from those crystals which have been rendered developable and these atoms then

Table 1

COMPOSITION OF ILFORD K-5 EMULSION

Element	Per Cent Weight	Per Cent Atoms
Ag	47.5±.7	12.8
Br	34.9±.5	12.7
I	.3±.0	.01
C	7.2±.2	17.5
H	1.4±.03	40.7
O	6.5±.01	12.0
N	1.9±.05	4.0
S	.2±.0	.2

coalesce into grains of silver. The undeveloped silver bromide crystals are removed from the emulsion, leaving behind the silver grains which have developed along the path of the ionizing particle. The gelatin and water base transmit light easily, but the silver grains are opaque and hence the path of the ionizing particle becomes clearly visible with the aid of a microscope.

The linear density of the silver grains is the track parameter directly related to the ionization energy loss rate of a charged particle passing through the emulsion. Unfortunately, the grain density is normally not directly observable due to the fact that each of the blobs which are strewn along the particle path can actually contain more than one silver grain; consequently, the track parameter most commonly measured for lightly ionizing particles is the blob density rather than the grain density.

The emulsion stack used in this investigation was exposed to a beam of 16.2 GeV/c negative pions at the CERN synchrotron in Geneva, Switzerland and is designated the Berkeley Я Stack. The University of Oklahoma high energy laboratory has fifty-six pellicles from this stack, which is one-third of the original exposed stack.

The gelatin in the emulsion readily absorbs and releases water causing the emulsion to be very sensitive to the water content of the atmosphere about it. For this reason, the entire stack is kept at constant temperature and humidity to prevent expansion and contraction of the emulsion.

Previous Experiments

The identification of relativistic particles in nuclear emulsions has been previously attempted [2 - 5] with limited success. The results are marginal because in most cases the errors reported are too large to permit a clear identification of individual fast particles; thus, the particle identification may be valid on a statistical basis but not necessarily for each individual particle. Under these circumstances it is difficult to determine whether or not the experimental data verifies the theoretical relationships governing the ionization energy loss rate.

Another feature common to these experiments is that all of them use the blob density as the measured track parameter. The blob density is either used directly in the data analysis [3 - 5], or attempts are made to convert blob density into grain density [2], for subsequent analysis. In this experiment, a different approach is taken in that an attempt is made to take advantage of the exponential nature of the gap length (the distance between adjacent resolvable blobs) distribution, thus allowing a direct measurement of the grain density. In addition, the blob density and a third track parameter, the lacunarity (the total gap length per unit track length), is measured for each track. By using these three parameters, we can extract more information from the track structure than we could obtain from any one parameter alone; information which should improve the accuracy of the measurements of the grain density.

Event Selection

All events used in this investigation were located by scanning along the beam tracks. The scanners were especially trained for locating electromagnetic events, which are very difficult to find due to the fact that the beam particle does not perceptively change directions and the produced particles consist of not more than two lightly ionizing particles. We are, therefore, confident that the resulting sample of events is unbiased with regard to the locating of white ($N_H \leq 1$, where N_H is the number of heavy tracks leaving the event) or dark ($N_H > 1$) stars.

It is generally assumed that a dark star is caused by the interaction of a beam pion with a nucleus in the emulsion resulting in many heavy fragments being ejected from the site of the interaction. White stars, on the other hand, are considered to be possible pion-nucleon collisions with the nucleon being either completely free, as in the case of a hydrogen proton, or bound to a nucleus as is surely the case for all neutrons and many protons. This does not preclude the beam pion from interacting with an individual nucleon in a nucleus. Since the average binding energy of a nucleon is on the order of 8 MeV and the beam pions have momenta of 16.2 GeV/c, these nucleons can effectively be considered free.

A study of pion-nucleon interactions utilizing these white star events has been done in this laboratory [6]. This investigation included the further examination of all recorded white star events in order to eliminate events which are most likely not pion-nucleon interactions. All the shower particles of the remaining five hundred events had their space angles (the angle between the shower particle track and the beam direction) measured. In addition, all light tracks which travelled two thousand microns or more before leaving the emulsion pellicle were measured for $P\beta$ by the multiple Coulomb scattering method.

In this work we will take these $P\beta$ measurements; and, by utilizing the information available in the grain densities of the lightly ionizing tracks, attempts will be made to learn the identities of the fast particles producing those tracks.

CHAPTER II

GRAIN DENSITY THEORY

Introductory Remarks

The production of a grain along the path of an ionizing particle is a random process analogous to radioactive decay or collision probabilities. As one follows the path of the particle there is a certain probability per unit path length that a crystal of silver bromide will be rendered developable. We shall assume that this probability is directly proportional to the energy loss rate of the particle which penetrates the silver bromide crystal. This is often written as

$$g = -Q \frac{1}{\rho} \left(\frac{dE}{dx}\right) \tag{2-1}$$

where Q is the constant of proportionality and $-\frac{1}{\rho}(dE/dx)$ is the energy loss rate in a medium with density ρ. The constant of proportionality may depend on such factors as degree of development of the plate, the time interval between exposure and development, the temperature at exposure and development, type of emulsion, etc. There is ample evidence that the degree of development varies with the location in a pellicle; in particular, close attention will be placed on the variation of grain density as a function of depth. Such a variation has been noticed by many observers.

In this experiment, the constant of proportionality will be removed by comparing the grain density measurements of the shower tracks to the grain density possessed by the 16.2 GeV/c negative pion beam particles. If the grain density of a beam particle is g_o, then the quantity

$$g^* = g/g_o = (dE/dx)/(dE/dx)_o \qquad (2\text{-}2)$$

may be defined.

We shall analyze in a following section the relationship between the quantity g* and the Pβ that a particle possesses, but first the calculation of the energy loss rate will be discussed.

The Energy Loss Rate

The theoretical value of the energy loss rate, - dE/dx, is given by the Bethe-Bloch Formula [7,8]

$$-\frac{1}{\rho}\left(\frac{dE}{dx}\right) = \frac{2\pi n z^2 e^4}{mc^2\beta^2\rho}\left[\ell n\,\frac{2mc^2\beta^2 w_{max}}{I^2(1-\beta^2)} - 2\beta^2-\delta-U\right] . \qquad (2\text{-}3)$$

In this equation

n = number of electrons per cm^3 in the stopping substance

mc^2 = rest energy of the electron (.511 MeV)

z = the charge of the particle (in this work all shower particles are assumed to have $z = 1$)

β = the velocity of the particle in units of c

I = mean excitation potential of the atoms in the stopping substance

w_{max} = maximum energy transfer possible from the incident particle to an electron

ρ = mass density of the stopping material.

The quantity w_{max} has been shown by Bhabha [9] to be

$$w_{max} = \frac{E-\mu^2 c^4}{\mu c^2[\frac{\mu}{2m} + \frac{m}{2\mu} + \frac{E}{\mu c^2}]} \tag{2-4}$$

where μ and E refer to the mass and total energy of the incident particle. Notice that this is the only place in the Bethe-Bloch equation in which the mass of the incident particle appears.

δ is a correction term needed for highly relativistic particles. It is the density effect correction which is due to the polarization of the medium at relativistic velocities. It must be taken into consideration for this experiment.

U is a correction term needed for extremely slow particles and is due to the non-participation of the inner-most electron shells (K,L, etc.) of the atoms. It need not be considered here.

In our application to grain density measurements we are interested in a more restricted energy loss, that occurring directly along the path of the particle. Clearly, for electrons carrying away large amounts of energy (the so called delta rays or knock on electrons), the loss of energy will not affect the production of grains along the particle path. Therefore, we must apply an energy cut off, T_{max}, below the kinematical limit w_{max}. The value of T_{max} has given experimental physicists difficulty for many years. Early calculations used values of T_{max} in the range of 2 to 5 KeV [10]. This is the energy an electron needs to leave the site of a silver bromide crystal. Later experiments, however, yielded higher values on the order of 30 KeV [11] to 100 KeV [12]. The determination of this quantity shall be of concern when the analysis of the data is considered.

The equation for the restricted energy loss is found by considering separately two types of collisions, close and distant [13]. The close collisions are the collisions in which the electrons are ejected with high velocities, i.e. the delta rays. The close collisions do not contribute to the restricted energy loss. The energy loss rate due to these collisions is given [13] by

$$-\frac{1}{\rho}(dE/dx)_{close} = \frac{2\pi ne^4z^2}{mc^2\beta^2\rho}\left[\ell n\,\frac{W_{max}}{T_{max}} - \beta^2\right] . \qquad (2\text{-}5)$$

The energy loss rate due to distant collisions is given [14] by

$$-\frac{1}{\rho}(dE/dx)_{distant} = \frac{2\pi ne^4z^2}{mc^2\beta^2\rho}\left[\ell n\,\frac{2mc^2\beta^2T_{max}}{I(1-\beta^2)} - \beta^2 - \delta - U\right] . \qquad (2\text{-}6)$$

We shall refer to Eq. (2-6) as the restricted energy loss rate. Clearly, from Eqs. (2-3), (2-5) and (2-6)

$$-\frac{1}{\rho}(dE/dx)_{total} = -\left[\frac{1}{\rho}(dE/dx)_{close} + \frac{1}{\rho}(dE/dx)_{distant}\right] .$$

The Sternheimer Equation

Equation (2-6) has been considered by Sternheimer [15] and the correction term δ evaluated. This equation, in Sternheimer's notation, is

$$-\frac{1}{\rho}(dE/dx) = \frac{A}{\beta^2}\left[B + 0.69 + 2\,\ell n\,\beta\gamma + \ell n\,T_{max} - \beta^2 - \delta\right] \qquad (2\text{-}7)$$

where β and γ have their usual meanings,

$$A = \frac{2\pi ne^4}{mc^2\rho} , \qquad (2\text{-}8)$$

and

$$B = \ln \frac{mc^2 \text{ (meV)}}{I^2} . \tag{2-9}$$

The correction term δ is evaluated as follows: consider the parameter $X = \log_{10} (\beta\gamma)$, then

$$\delta = 0 \qquad \text{for} \qquad X \leq X_o , \tag{2-10}$$

$$\delta = 2 \ln \beta\gamma + C + a(X_1 - X)^m \tag{2-11}$$

$$\text{for} \qquad X_o < X < X_1 ,$$

and

$$\delta = 2 \ln \beta\gamma + C \qquad \text{for} \qquad X \geq X_1 \tag{2-12}$$

where

$$C = -2 \ln(\frac{I}{h\nu_\rho}) - 1 . \tag{2-13}$$

$\nu_\rho = (ne/\pi m)^{\frac{1}{2}}$ is the plasma frequency of the electrons. The parameters a and m in Eq. (2-11) are chosen so that $\delta = 0$ at $X = X_o$, thus giving the condition

$$\delta = 2 \ln \beta\gamma + C + a(X_1 - X_o)^m = 0 .$$

The values of these constants (except of course for T_{max}) have been tabulated by Sternheimer [16] for various stopping materials. The results for two important materials are given in Table 2.

Table 2

VALUES OF THE STERNHEIMER EQUATION PARAMETERS FOR TWO IMPORTANT MATERIALS

Material	I(eV)	A	B	- C	a	m	X_1	X_o
AgBr	573.8	0.0671	14.25	5.95	0.0235	4.03	4	0.30
Emulsion	372.6	0.0698	15.12	5.55	0.0220	4.01	4	0.23

Let us consider the general nature of the Sternheimer equation. Notice that if we assume a constant value of z, the restricted energy loss rate has only one variable, β. For low values of β the energy loss rate is inversely proportional to the square of the particle velocity. As $\beta \to 1$, however, we find that the dominant term becomes $\ln \beta^2/1-\beta^2$ which increases with β. This rise in the energy loss rate after a minimum value is referred to as the relativistic rise. Although it is apparent from the Bethe-Bloch formula (Eq. 2-3), the effect was not verified experimentally until 1950 [17]. We thus have a minimum grain density for singly charged particles which occurs in the vicinity of $\beta \simeq .97$ ($\gamma \simeq 4$). The relativistic rise would continue indefinitely if it were not for the density effect. The first term in Eq. (2-11) cancels the term in the Bethe-Bloch equation responsible for the relativistic rise. The density effect begins in the region of $X = X_0$ ($\beta \simeq .89$ or $\gamma = 2.2$) and assumes the form of Eq. (2-12) at $X = X_1$ ($\gamma \simeq 10{,}000$). This is illustrated in Fig. 1. Note that the parameter I in the Bethe-Bloch equation is cancelled by the C parameter in Sternheimer's density effect correction, δ. This means that only the parameter T_{max} is available to adjust the amount of the relativistic rise. The combination T_{max}/I^2 does, however, influence the low velocity side of the curve and hence the location of the minimum can be affected by the choice of I.

g^* Vs $P\beta$ Curves

In our calculations we are interested in the ratio of the restricted energy loss rate for particles of various velocities compared to the restricted energy loss rate for 16.2 GeV/c pions. The velocity of the beam pions is (we set c = 1)

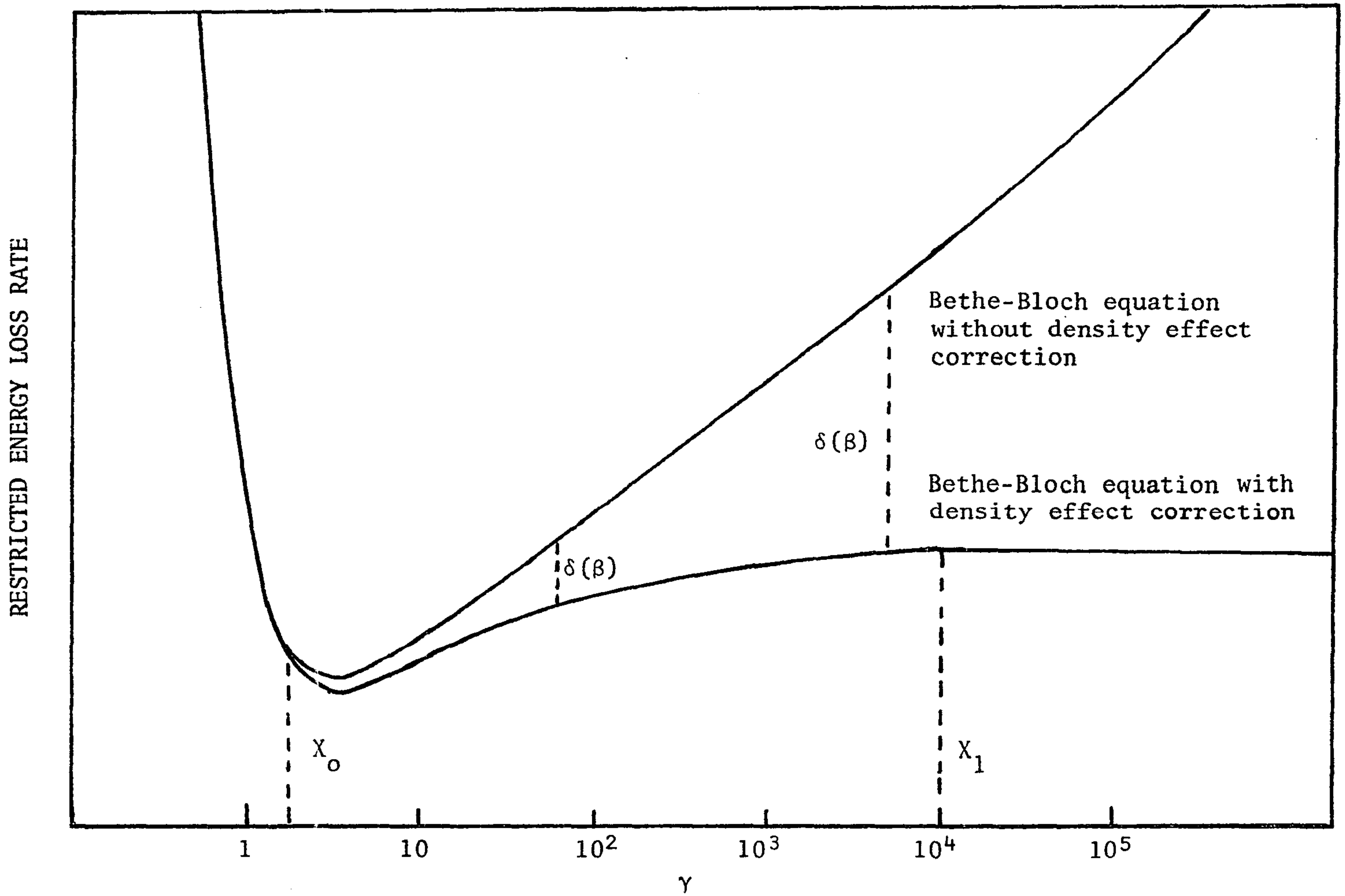

Figure 1. A schematic diagram of the restricted energy loss rate with and without the density effect correction.

$$\beta = \frac{P}{E} = \frac{P}{\sqrt{P^2+M^2}} \quad . \tag{2-14}$$

Using P = 16.2±.64 GeV/c and M = .1396 GeV we get β = .9999629±.0000029 which gives γ = 116±5.

Because we will eventually be interested in comparing the grain density results with the values of Pβ already determined from multiple Coulomb scattering measurements, it is convenient to select a velocity variable related to Pβ. Thus

$$\beta^2 = \frac{P\beta}{E}$$

or

$$\beta^2\gamma = P\beta/M \ . \tag{2-15}$$

Hence, Pβ/M is a function of β, as is g*, and the two can be correlated.

We utilize Eq. (2-7) to calculate the values of g*; the parameters used in this equation are selected from Table 2. It is important to select those applying to AgBr, because we are interested in the restricted energy loss rate in the silver bromide crystals and not that in the emulsion matrix. If we were performing calculations on the energy-range relationship, we would be interested in the total energy loss for the entire emulsion and would therefore use the parameters in Table 2 applicable to the entire emulsion.

In Fig. 2, g* is plotted vs Pβ/M for 3 values of T_{max}: 2, 5 and 100 KeV. The essential feature noted is that variations in T_{max} change the value of the minimum g*. The location of the minimum does move somewhat along the Pβ/M axis as a result of T_{max}/I^2 varying, but this is not nearly as pronounced as the change in the minimum ionization of

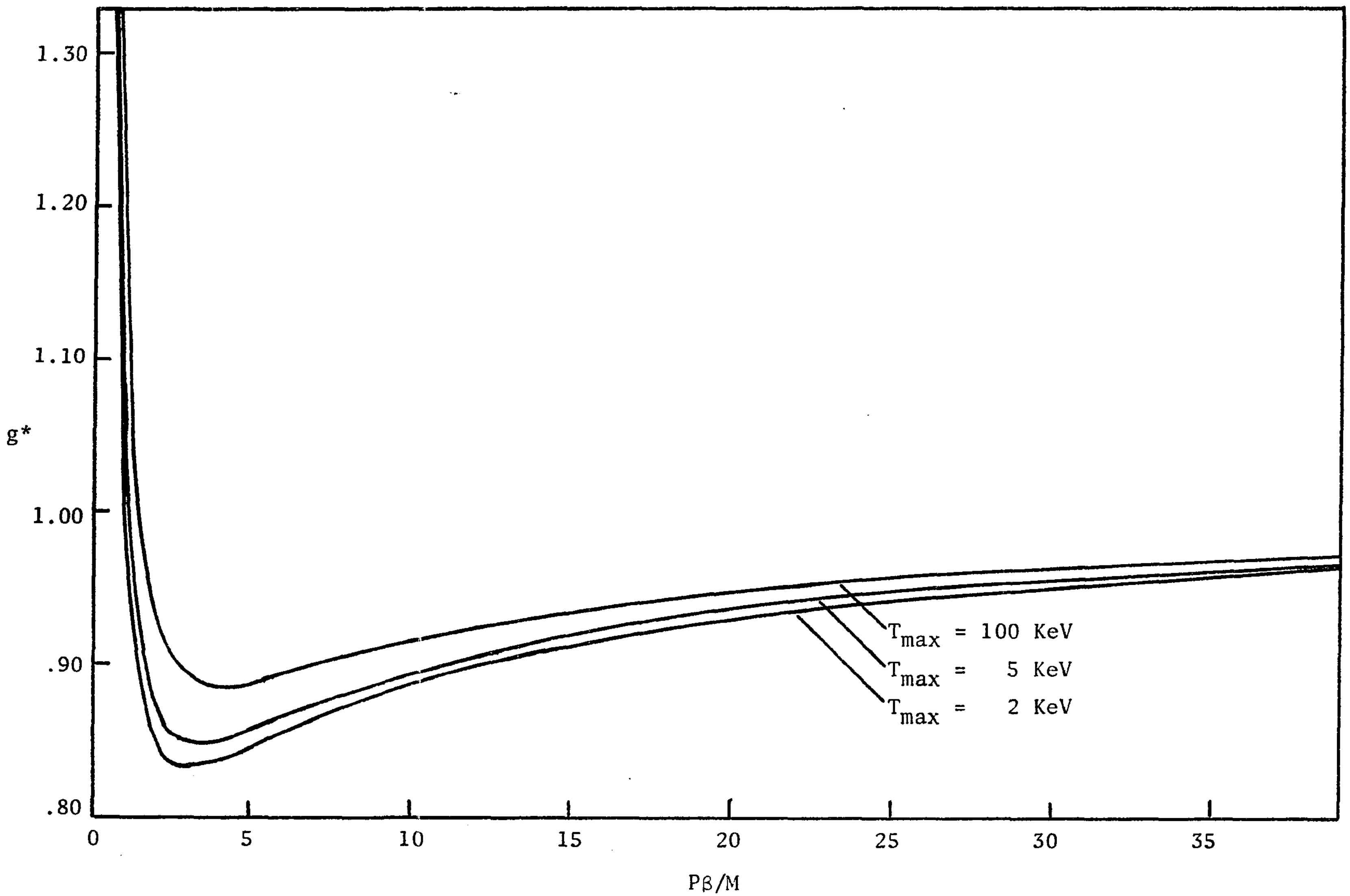

Figure 2. g* vs Pβ/M for three values of T_{max}.

a particle relative to the beam pion. We note rises from g_{min} to g_o on the order of 17%, 15% and 12% for T_{max} = 2 KeV, 5 KeV and 100 KeV respectively. The beam grain density g_o is not the same as the grain density in the plateau region of the g* vs Pβ/M curve. The plateau occurs at the extreme relativistic region of the curve (γ>10,000) where the density effect completely cancels the relativistic rise. One should add approximately 2% to the above percentages in order to get an idea of the per cent rise to the plateau. The proper choice of the parameter T_{max} will be examined in the data analysis section.

The relationship between g* and Pβ/M provides us with the opportunity to obtain a set of g* vs Pβ curves - one for each mass M. Tables have been prepared based upon Eq. (2-7) and Eq. (2-15) giving the values of g* vs Pβ for five types of particles: pions, kaons, protons, sigmas and deuterons. These tables calculated for different values of T_{max} ranging from 1 KeV to 100 KeV, are given in Appendix A. The mass used for each particle is given in Table 3.

Table 3[18]

PARTICLE MASSES

Particle	Mass (GeV)
Π (pion)	.1396
K (kaon)	.4938
P (proton)	.9383
Σ (sigma)	1.1940
D (deuteron)	1.8755

Figure 3 shows a plot of g* vs Pβ for the five particles listed

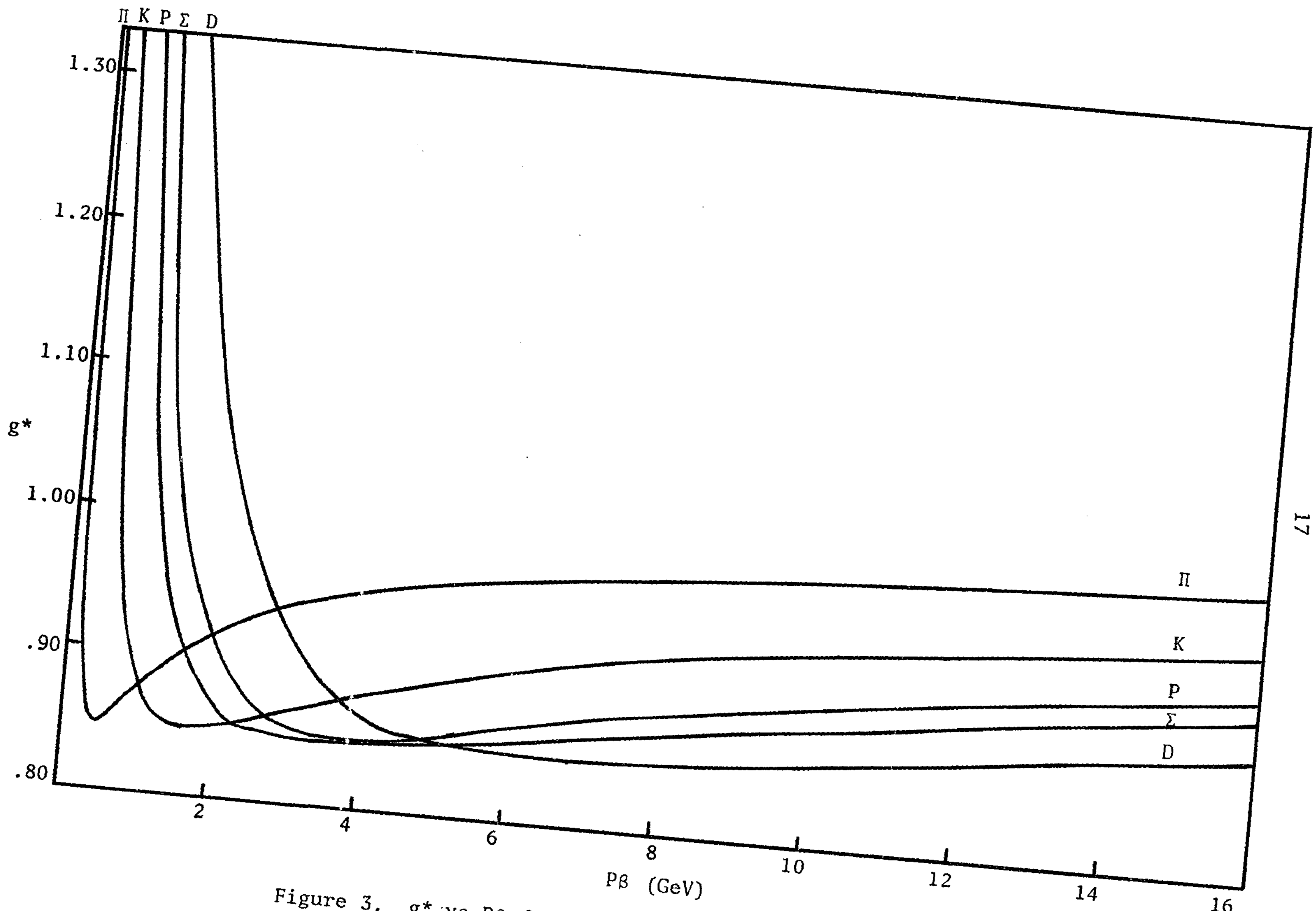

Figure 3. g* vs Pβ for five particles. T_{max} = 5 KeV is assumed.

in Table 3. For this plot T_{max} was chosen to be 5 KeV. The relationship between g* and $P\beta/M$ provides the opportunity to identify unknown shower particles by measuring g* and $P\beta$ for each particle and observing where the plot of these measured values falls on the graph. This identification method has been attempted previously [2] without a clear demonstration of success. The basic problems that arise when this method of identification is used are the errors involved in the measurements and the regions of ambiguity that occur as a result of the many points where the curves overlap. For example, it is considered most unlikely that protons and sigmas can be separated from one another. To do so at energies below 2 GeV would require $P\beta$ measurements with errors consistently less than 10%. Such accuracy has not been obtained for this experiment where the accepted $P\beta$ values have errors on the order of 20%. Separation of protons and sigmas at higher energies would require measurements of grain density with errors consistently less than .75%. These errors are not achieved in this experiment. These difficulties involved in particle identification are further compounded by an uncertainty in the precise amount of the relativistic rise, i.e. an uncertainty in the correct value of T_{max}.

Track Parameters

A track in a nuclear emulsion consists of a series of blobs interrupted by gaps. These blobs may consist of one developed grain of silver or may consist of two or more grains which have coalesced into one unresolvable unit. From Fig. 4 let s be the distance between the centers of adjacent grains. We show seven grains in Fig. 4, but only six resolvable blobs.

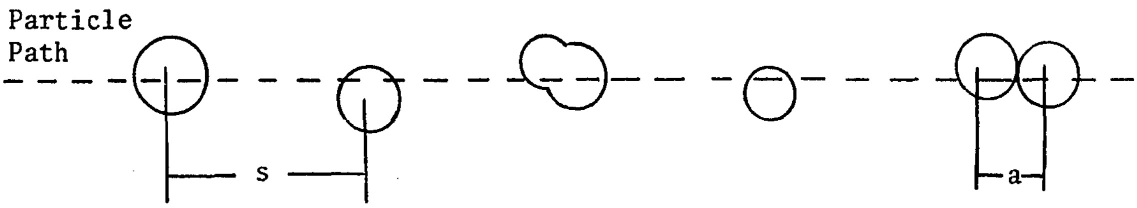

Figure 4. Typical track configuration.

We will refer to the grain density as g and the blob density as B.

Let "a" be the minimum distance between centers by which two adjacent grains must be separated in order for them to be resolved. The gap length ℓ between two adjacent grains then is given by $\ell = s - a$. We define the quantity $\alpha \equiv \langle a \rangle$ which shall be referred to as the resolution. In this single quantity we can account for the size of the grains, the optical resolution of the microscope, and the observational and measuring characteristics of the scanner.

Let us return to the proposition that the formation of grains along an ionizing track is an event determined by the laws of probability. To simplify the discussion, a simple model will be used in which grains are rendered developable at intermittent points along the particle path and that around each point a grain of diameter α is developed (See Fig. 5).

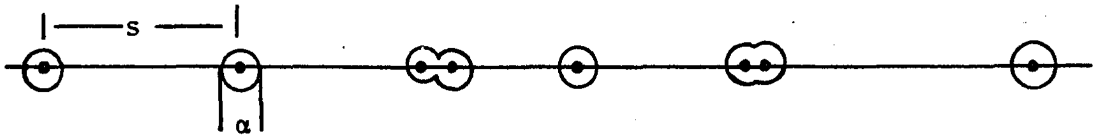

Figure 5. Idealized track structure.

If the probability per unit path length of rendering grains developable is a constant, λ, then

$$\frac{dP}{ds} = \lambda. \tag{2-16}$$

We get

$$dP = -\frac{dN}{N} = \lambda ds \quad ,$$

which gives

$$N(s) = N_o\, e^{-\lambda s}$$

where $\lambda = 1/\bar{s}$ and thus

$$N(s) = N_o\, e^{-s/\bar{s}} \quad . \tag{2-17}$$

Physically, over a total distance D, N_o such points have been deposited along the particle path with distances s between points. N(s) is the total number of gaps of length s or greater. The fact that the gap lengths are indeed distributed exponentially was first observed by O'Ceallaigh [19].

Let us divide Eq. (2-17) by the total distance D. The quantity $H(s) = N(s)/D$ is the gap length density distribution and N_o/D is the definition for the grain density g. Further, $\bar{s} = D/N_o = 1/g$; hence Eq. (2-17) becomes

$$H(s) = ge^{-gs} \quad . \tag{2-18}$$

We now consider the growth of the grains about the points, each to a diameter α. Actually, it is not necessary for the grain growth to be uniform, as the exponential nature of the gap length distribution can not be destroyed by any random distributions of grain diameters, but for purposes of illustration, the uniform diameter α

will suffice. Obviously all gap lengths smaller than α will disappear as the two adjacent grains grow into one unresolvable blob. The density of gaps remaining is given by

$$\mathcal{H}(\alpha) = g\ e^{-g\alpha}\ . \tag{2-19}$$

But the number of gaps remaining is equal to the number of blobs, hence $\mathcal{H}(\alpha)$ is equal to the blob density B giving

$$\boxed{B = ge^{-g\alpha}}\ . \tag{2-20}$$

This is an important equation relating the desired grain density with the more easily observable blob density. This equation provides the basis for most of the measurements of the grain density.

Let us now consider ℓ to be the distance from the end of one blob to the beginning of the following blob, i.e. the open distance between the opaque blobs. We will refer to this, in all that follows, as the gap length. This is equivalent to replacing the s in Eq. (2-18) with $\ell + \alpha$. Thus

$$\mathcal{H}(\ell+\alpha) = H(\ell) = g\ e^{-g(\ell+\alpha)} \tag{2-21}$$

$$H(\ell) = g\ e^{-g\alpha}e^{-g\ell}$$

$$\boxed{H(\ell) = B\ e^{-g\ell}}\ . \tag{2-22}$$

Note that H(0) = B as would be expected; that is, the blob density is equal to the total gap density. Equation (2-22) is significant because it provides the basis for obtaining the grain density g from the gap length distribution $H(\ell)$.

Yet another important track parameter is the lacunarity L of a track, defined as that fraction of the track which consists of gaps, that is

$$\text{Lacunarity} = \frac{\text{Total gap length measured}}{\text{Total length of track measured}} \quad .$$

From the gap length distribution, $H(\ell)$, one gets

$$L = - \int_0^\infty \ell \left(\frac{dH}{d\ell}\right) d\ell \quad ,$$

or

$$\boxed{L = e^{-g\alpha}} \quad . \qquad (2\text{-}23)$$

The use of this equation along with Eqs. (2-20) and (2-22) to permit the analysis of grain density measurements will be described in the next section.

The Measurement of Grain Density

Because the blob density is the track parameter most easily measured, Eq. (2-20) has been the starting point for most measurements of the grain density. All that is required for the measurement is for the observer to follow the track and count the unresolved blobs that lie along the path of the track. Unfortunately, the parameter α in this equation must be determined before this technique can be used. This parameter changes from observer to observer, and perhaps even for each observer as the experiment progresses and as the experimental procedures change. There are several methods for solving this problem. The first is to simply ignore it and assume that B is proportional to g. This is only approximately true for grain densities near minimum ionization. Secondly, α can be estimated. Given B, the solution to Eq. (2-20) for g is not very sensitive to the value of α, and g^* is even less sensitive, as long as the change in α is within reasonable limits, say 20%. Table 4 illustrates this point assuming values of B_0 (beam blob density) = .26/μ and a shower particle blob density B_1 = .24/μ.

Table 4

GRAIN DENSITIES FOR VARIOUS ALPHAS
WITH B_1 = .24/μ, B_0 = .26/μ and $b^* = B_1/B_0$ = .923

α(microns)	.40	.45	.50	.55	.60	.65	.70	.75	.80
g_0(per μ)	.292	.297	.302	.308	.314	.320	.327	.334	.342
g_1(per μ)	.267	.271	.275	.280	.285	.290	.295	.301	.308
$g^*=g_1/g_0$	.914	.912	.911	.909	.907	.905	.903	.900	.898

The most common method of using Eq. (2-20) is to measure the blob densities of tracks of known grain densities and thus determine α for each observer. The grain density of a track may be measured by performing two measurements of $H(\ell)$ defined by Eq. (2-22). If one knows $H(\ell_1)$ and $H(\ell_2)$, then g may be determined as follows,

$$\frac{1}{B} H(\ell_1) = e^{-g\ell_1}$$

$$\frac{1}{B} H(\ell_2) = e^{-g\ell_2}$$

$$\frac{H(\ell_1)}{H(\ell_2)} = e^{g(\ell_2-\ell_1)}$$

$$g = \frac{1}{\ell_2-\ell_1} \ln \frac{H(\ell_1)}{H(\ell_2)} \quad . \tag{2-24}$$

If we set $\ell_1 = 0$ then $H(\ell_1) = B$ and we have

$$g = \frac{1}{\ell_2} \ln \frac{B}{H(\ell_2)} \tag{2-25}$$

$H(\ell_2)$ is measured by using a micrometer scale and counting the number of gaps which are equal to or greater than ℓ_2. This is a tedious and time consuming measurement.

Once g is known for several tracks, measurements on these tracks by different observers may then be used to determine the values of α for these observers, who will then perform grain density measurements on tracks of unknown grain density by the blob counting method. This is the most common procedure now in use for measuring the grain densities of lightly ionizing tracks.

The method chosen for measuring grain densities in this experiment differs from the previously described procedure. We have chosen to measure g directly from the gap length distribution $H(\ell) = Be^{-g\ell}$. This is a generalization of the procedure culminating in Eq. (2-24). Instead of measuring $H(\ell)$ at two different points ℓ_1 and ℓ_2, we will measure the distribution at one hundred or more values of ℓ and then find the value of g from the distribution $H(\ell)$ which will best fit the data. The method of least squares will be the criterion for the best fit. This measurement would be impractical unless some way to automate the processing of data were found. Fortunately the multichannel analyzer, an instrument which is ideally suited for this type of measurement, is readily available. The application of the multichannel analyzer to the measurement of g will be discussed in the experimental procedure chapter.

Equation (2-23) provides yet another way to determine the grain density of a track. As in the case of determining g from the blob density, the value of the parameter α must first be found before the track lacunarity can be used to estimate the grain density.

Experimentally, the lacunarity proves to be very useful, because it tends to be an accurately measurable track parameter. This is easily seen by considering that the most difficult task in blob counting is deciding how to count what may or may not be two blobs in close proximity to each other; that is, in deciding whether or not two or more grains are resolvable. While these decisions have an important bearing on the measured value of the blob density, they do not adversely affect the measurement of the lacunarity, because the gap lengths in question are very small and do not contribute much to the final measured value of L. It is therefore not surprising to find the per cent standard deviation of B larger than that of the lacunarity L. Typical values determined from remeasuring tracks found standard deviations of B on the order of 0.9% while those of L on the order of 0.5%. Both B and L will prove useful, as they permit the determination of grain densities which are independent of the grain density determined from the gap length distribution.

The track on which the grain density is measured, in general, dips or rises in the emulsion. This angle, in unprocessed emulsion, is called the dip angle. Figure 6 shows a typical configuration.

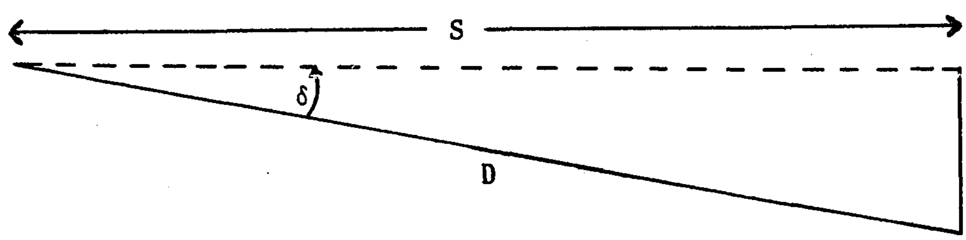

Figure 6. Schematic view of a dipping track.

The track being measured dips into the emulsion with a dip angle δ. The total track length measured is S. The result of the measurement yields a value g_m for the grain density. Then we have the total number of grains, $N = g_m S$. In reality these N grains are distributed along the path with distance D. Then the true grain density is $g = N/D$ which gives

$$g = g_m \; S/D \; ,$$

or

$$g = g_m \cos\delta \; . \tag{2-26}$$

Thus, to correct for the dipping of tracks we multiply the measured grain density by the cosine of the dip angle. This general result holds true regardless of the method used to measure the grain density.

CHAPTER III

EXPERIMENTAL PROCEDURE

The Basic Concept

Most multichannel analyzers on the market today are capable of two forms of analysis: pulse height analysis and multiscaling. For this experiment the multiscaling mode is used. Two different analyzers have been used: the Nuclear Data 2200 and the Nuclear Data 1100. The principle differences between the two are the size of the memory core and the pulse height analysis capabilities. For the purposes of this experiment the analyzers do not differ.

Multiscaling in a multichannel analyzer means that the analyzer behaves like a set of scalers which can be alternately switched on and off. The time in which each scaler is on is referred to as the dwell time. Actually, there is but one scaler with the information being stored in separate memory cores, each memory unit (scaler) being referred to as a channel. In this experiment almost exclusive use is made of 256 channels. Once the multiscaling action is initiated, it may be allowed to proceed through all 256 channels or it may be terminated at some intermediate channel.

The key factors necessary for obtaining the gap length distribution from the multichannel analyzer are:

(1) a constant speed motor system to drive the microscope stage,

(2) a remote means for initiating, terminating and reinitiating the multiscaling action,

(3) a constant impulse rate into the scaler.

Figure 7 illustrates the principles of this measurement. For illustration purposes we consider 15 channels. It is assumed that the microscope stage is being driven at a constant rate of 4 microns/sec.

	1	1	1	1	1	1	1	1	1						
CHANNEL	1	2	3	4	5	6	7	8	9	10	11	12	13	14	15

Figure 7a. Scaler contents after one gap length has been measured.

	20	16	12	9	6	4	3	3	2	1	1	1			
CHANNEL	1	2	3	4	5	6	7	8	9	10	11	12	13	14	15

Figure 7b. Scaler contents after twenty gap lengths have been measured.

The observer operates a tap key in which the multiscaling action is terminated by depressing the key and initiated by releasing the key. By observing the track as it passes the vertical crosshair of the microscope eyepiece, the measurement can be made. The tap key is in the depressed position when the cross-hair is over a blob and is in the released position when it is over a gap. Figure 7a is a schematic diagram of the measurement of a single gap length. Suppose the dwell time for each channel is .25 seconds and we have a pulser which delivers four pulses per second. We expect, therefore, one count in each channel as long as the multiscaling is allowed to continue. Because the speed of the microscope stage is 4 microns/sec we find that each channel represents a distance of 1 micron (speed × dwell time). We see that the first gap length measured is 9 microns. As a result of the characteristics of the multichannel analyzer in use for this experiment, this actually means that the gap length was at least 9 microns but not 10 microns, for the analyzer will record nothing in the tenth channel if the scaling is not allowed to proceed for the full amount of the dwell time. This is true regardless of the number of pulses delivered to the scaler during this time period. The measurement of this first gap was terminated by depressing the tap key. This caused the analyzer to stop multiscaling, to reset and be prepared to begin multiscaling from the first channel again. The measurement of the second gap length was begun by again releasing the tap key. The counts resulting from this measurement are added to those already recorded from the previous measurement so that the count in each channel displays an accumulation of measurements. Figure 7b shows the result of this procedure after the measurement of 20 gap lengths. It is seen that all twenty of these gaps are one micron or greater in length, that 16 gaps are two microns in length or greater, and that the longest gap length is 12 microns. This is, of course, the gap length distribution $H(\ell)$ (actually $N(\ell)$ since it is not yet a density) that is to be measured. In addition to the distribution $H(\ell)$, we also have information needed to obtain the blob density B and the lacunarity L. Let us assume that the total track length in this measurement was 100 microns. The total number of blobs (or gaps) is found in the first channel, thus giving a blob density for this measurement of $B = 20/100\mu = .20$ per μ. The value found in the first channel will actually have to be adjusted upward to account for the gaps which are shorter than one micron and hence not registered in the first scaler. This is less of a problem the shorter the dwell time becomes. In the actual runs, a dwell time of .04 seconds was used, corresponding to about .16 to .18 microns, depending on the speed of the microscope stage. Nevertheless, even when these smaller increments are used, the value of the first channel is adjusted upward slightly in order to obtain the measured blob density.

The lacunarity is found by simply adding the values found in all the channels, which is 78 in this case. Thus the total gap length was 78 microns. This total length should be adjusted to account for the loss of information in the incomplete channel of each measurement. We may assume that on the average each gap ends half way into the incomplete channel, thus in this example .5 microns is added to each gap. We then get a lacunarity of (78+10)/100 = .88 for this measurement [in general, L = (total count + $\frac{1}{2}$ blob count × channel distance increment)/total distance of measurement].

Microscope

The microscope used for all measurements in this experiment is a Leitz Ortholux binocular microscope mounted on a stage which was built at the University of Oklahoma Physics Department machine shop. The stage has 1 mm pitch screws which allow motion in two perpendicular directions both of which are perpendicular to the optical axis. The stage permits travel of 14 cm in the y direction and 18.5 cm in the x direction. The construction of the stage was such as to provide for the motion along the x direction to be as linear as possible. The emulsion plate holders, which are mounted in this stage, allow for 360°

rotation, permitting the alignment of all shower tracks along the x direction. This is the direction used for all grain density measurements. The distance along the x direction is measured by a precision micrometer dial (Ames gauge) which permits measurements to within one micron. The screw drive is also calibrated in microns, but is not as accurate as the Ames gauge. However, it is used in all measurements and the results obtained checked with the results on the Ames gauge allowing gross errors to be discovered. This procedure was found to be indispensable due to the occasional difficulty of reading the Ames gauge when the stage motion is registered in the reverse direction on the dial. This reverse reading occurs for all shower tracks while the beam tracks are registered in the forward direction.

The objective used is a Koristka 100X oil immersion lens with a numerical aperture of 1.25 and a 530 micron working distance. The eyepieces are Leitz periplan GF10X. These lenses, combined with the inherent body-tube magnification of 1.25X, give a total magnification of 1250X.

The fine focus of the microscope permits measurements along the optical axis (z axis) to within one micron. All depth measurements are made from the event or track to the top of the emulsion. This is done in one continuous motion so that any play in the fine focus mechanism will not spoil the measurement.

Motor and Stage Drive

An AC-DC motor is used in conjunction with a variable speed control to allow for a selection of the drive speed. The motor is a 1/15 horsepower Dayton model 4K868 gearmotor which has a gear ratio of 1787/1.

The drive speed is further reduced by a 15/1 gear. As a result, the speed of the drive shaft of the microscope stage is on the order of one-quarter r.p.m. One complete revolution of the stage drive results in advancing the stage 1000 microns; hence, speeds in the range of 4 μ/sec are attained. By utilizing the maximum range on the variable speed control, the drive speed may be increased to 15 μ/sec or decreased to zero. The normal speeds used in the grain density measurements range from 4.0 μ/sec to 4.5 μ/sec.

The variable speed control has another function more important than that of speed selection. Its main purpose is to regulate the motor so that regardless of the speed selected (up to the maximum allowable by the motor) that speed will remain constant. The device does this by varing the power supplied to the motor as the resistant torque fluctuates. If the stage should have a position which offers more resistance than usual to the advancement of the stage, the speed control will sense the increasing torque being applied to the electric motor and deliver more power, thus preventing the motor drive from slowing down.

A further improvement in the system is achieved by placing a lead fly wheel directly between the microscope and the motor-gear assembly. The purpose of the addition is twofold: to further smooth the speed drive and to dampen disturbing motor vibrations which would otherwise make the measurements impossible - on both accounts the device has proven successful. The lead fly wheel is 2.5 cm thick, has a diameter of 23 cm and weighs 25 lbs.

A timer is attached to the system in order that the time in which the motor is operating can be measured. The timer is a Canberra

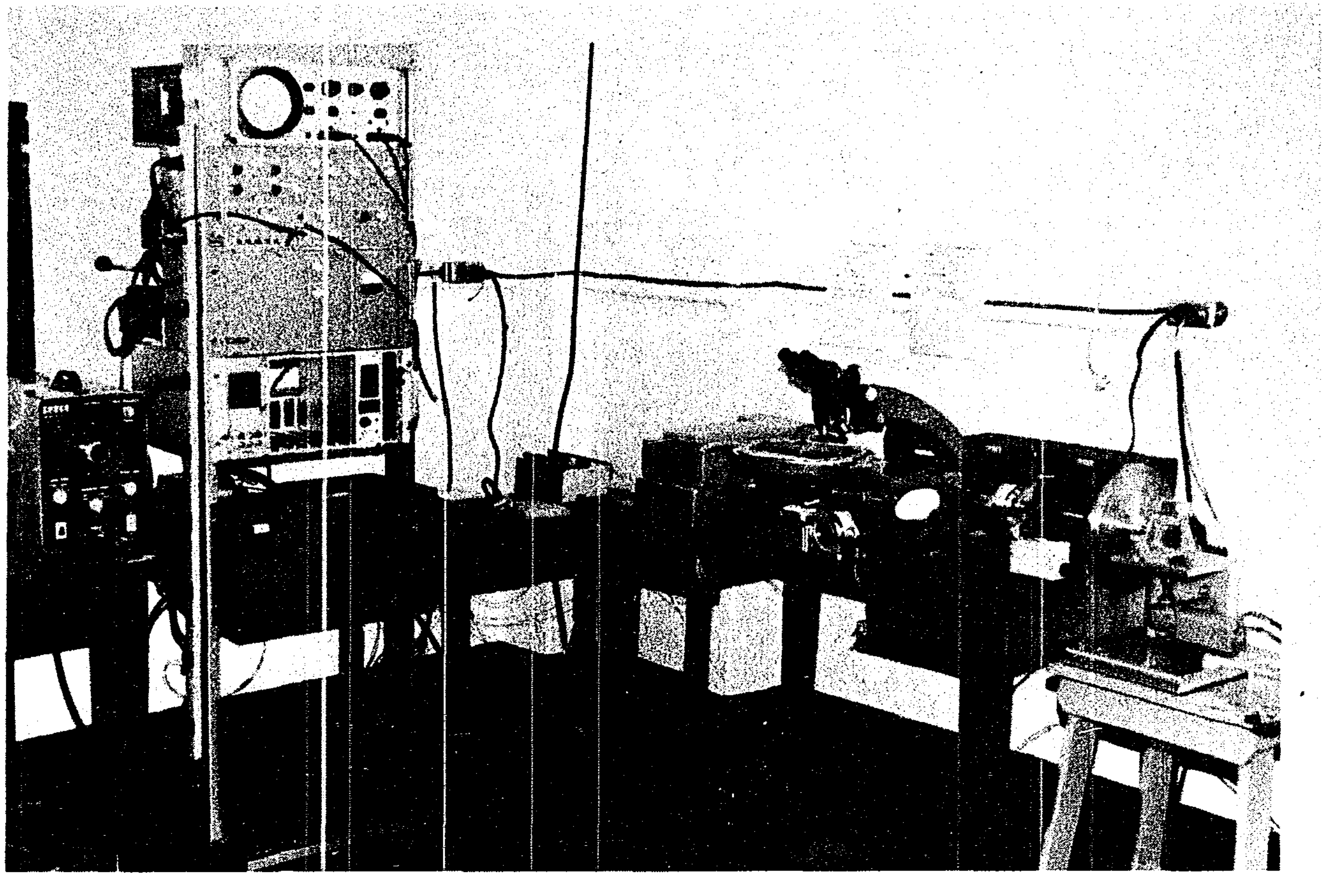

Figure 8. Overall view of the apparatus used in this experiment. On the right is the microscope coupled to the motor drive assembly. The rack on the left contains, from top to bottom, an oscilloscope for immediate viewing of the results, the Nuclear Data 2200 multichannel analyzer, the Canberra scaler/timer model 890, and the high speed parallel printer. The audio oscillator is on the extreme left.

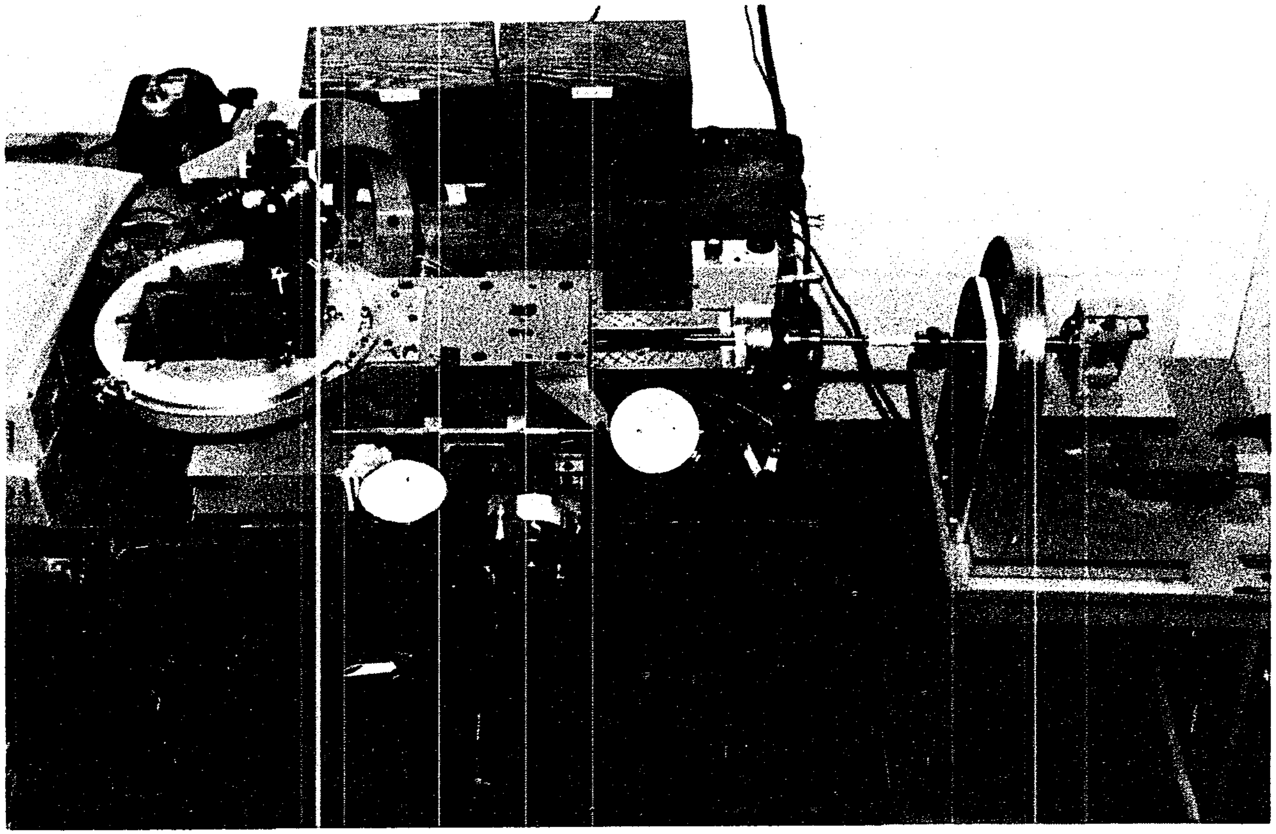

Figure 9 . Detailed view of the microscope with emulsion plate mounted. The Ames gauge dials and tap key are visible in the foreground. To the right is the motor-gear-flywheel assembly. The variable speed control is seen in the background.

scaler/timer model 890 which is resettable and may be started by shorting the gate-in BNC connector at the rear of the instrument. The circuit diagram in Appendix B shows how this and other components of the experiment are wired.

Remote Switching

As previously mentioned, one of the necessary features for the experiment is the ability to remotely control the acquiring and stopping functions of the multichannel analyzer. In both the Nuclear Data models this may be achieved by a set of external connectors located on the back panel of the analyzer. For the 2200 model, pin A of this external connector controls the stop mode of the analyzer. The normal state of this pin is +6V. The stop mode may be initiated by bringing the pin to zero volts. In practice this is done by shorting the pin to ground. Pin B of the external connector controls the acquire mode. The normal state of this pin is also +6V and the acquire mode may be initiated by grounding this pin.

In order for the analyzer to safely acquire or stop, it is essential that these two modes not be initiated while the memory unit of the analyzer is operating. Pin L of the external connector is called the memory pin and is at +6V when the memory is busy and is at ground when it is not busy. Hence, the ground signal for initiating the acquire and stop mode may be safely derived from pin L.

The actual shorting of the acquire and stop pins with the memory pin is accomplished with a mercury switch which is operated by the tap key, thus giving the observer control of the acquire-stop actions of the analyzer. The acquire function may be further interrupted by a

DPST switch and a microrelay which is operated by a foot switch. When the microrelay interrupts the acquire function it also bypasses the mercury switch and initiates the stop mode. Thus, depressing the foot switch puts the analyzer in the stop mode. If the DPST switch controlling the analyzer is switched so as to interrupt the acquire function, the analyzer will remain in the stop mode after the foot switch is released; otherwise the analyzer will continue to acquire when the foot switch is released.

The constant rate impulse into the scaler of the multichannel analyzer is supplied by an audio oscillator which generates square waves. The pulse rate normally used is 2500 cycles/sec. This, coupled with the .04 dwell time ordinarily used with the analyzer, provides 100 counts per channel when the analyzer is acquiring. The pulse rate is continually monitored and adjusted in order that a count rate of 100.0±.1 counts/channel can be maintained throughout the experiment.

The Measurements

Each measurement is begun by aligning the track to be measured with the x axis of the microscope stage. This is an easy task since the projected angles for all the tracks had been previously measured and recorded [6], and the rotating platform, on which the emulsion plate is mounted, is marked in degree increments. If the track is properly aligned, there is little perceptible displacement in the y direction from start to finish of the measurement.

The grain density measurement may be initiated by flipping up the left DPST switch (see Appendix B), which allows the analyzer to function, and the right DPST switch, which allows the motor and timer to function. This is impractical, however, since both hands of the observer are needed immediately for the measurement, the left hand to manipulate the fine focus of the microscope and the right hand to operate the tap key. Therefore, a foot switch is used to override the two DPST switches. The measurement begins by releasing the foot-switch. Similarly, the measurement is terminated by first depressing the foot switch and then flipping both DPST switches down before releasing the foot switch.

The track length measured during the run is read from the Ames gauge and the depth of the track in the emulsion is measured using the fine focus of the microscope. The depth measurement is made at the beginning and end of each of the track segments.

The information stored in the multichannel analyzer is read out in digital form by means of a high speed parallel printer. This data is then punched by hand onto computer cards for later analysis. Considerable effort must be expended to insure that the data is correctly transferred onto the cards. The few errors that go undetected will normally cause the computer either to stop processing the data or result in some abnormal behavior that is easily detected. Further, there are safeguards built into the data analysis program which will eliminate any data points which have substantial errors. This procedure is discussed more fully in the data analysis chapter.

Track Selection

The initial procedure was to relocate each event previously designated as a pion-nucleon interaction and make ionization measurements on those shower tracks which have been measured for $P\beta$ by the multiple

Coulomb scattering method. The multiple Coulomb scattering measurements were not made on tracks which traveled less than 2000 microns before leaving the plate; hence this was the lower limit to the length of the grain density measurements. When possible, the shower tracks were measured for lengths up to 3000 microns which normally yielded approximately 800 blobs, resulting in a statistical error of about 3.5%. It was hoped that by combining the three independent measurements of g that this error could be improved sufficiently to allow separation of the particles into clusters along the appropriate curves so that the particles could be identified and the actual shape of the relativistic rise determined. The shower tracks were each normalized to the grain density of the beam particle producing the event from which the shower track originated. The beam tracks were measured for about 4000 microns resulting in a blob count in the neighborhood of 1200. After a substantial amount of data had been taken using this procedure, it became apparent that the data was not clustering in a manner which would permit the determination of individual particle curves. The apparent reason for this was that the errors were larger than those due to statistical fluctuations alone. This indicated that unforeseen variables were influencing the results and that a more systematic approach was needed in order to determine the nature of these variables and to properly account for their presence in the data. Hence, this track selection procedure was abandonded in favor of the following method.

One hundred thirty-one shower tracks were selected which traveled at least 20,000 microns in a single emulsion pellicle. This selection was made for two reasons: first, it allowed for five to six thousand gap lengths to be measured resulting in statistical errors on the order of 1.5% and second, by so selecting the tracks, only the tracks with the best $P\beta$ measurements were considered. The ionization measurements were made in 5000 micron segments. If possible, five segments were measured for a total of 25,000 microns, or, if this was not possible, the measurement was terminated after four segments. Measuring the track by segments had the advantage of allowing a direct measurement of the error by using the different values of the grain density for the same track. Since most tracks are dipping, thereby causing them to traverse the pellicle at different depths, this also allows for a measurement of the change in the ionization parameters with depth in the emulsion. These points will be discussed in detail in the data analysis chapter which follows.

CHAPTER IV

ANALYSIS OF DATA

The Evaluation of Grain Density

The determination of the grain density for each track segment was done by processing the experimental data with the computer program GDEN which was written especially for this problem. The program is listed in Appendix C and the principal features incorporated into it will now be outlined.

The grain density for each track can be determined directly from the gap length distribution, $H(\ell) = B\, e^{-g\ell}$. This distribution has two parameters which may be adjusted in order to obtain a best fit to the data. The least squares method is the criterion for the best fit; therefore the quantity $S = D^2 \sum_i W_i [H(\ell_i) - B\ e^{-g\ell_i}]^2$ will be at its minimum value. D is the distance of the measurement and the weight W_i is the inverse of the variance of each data point. We assume the standard deviation for the ith point to be $\sigma_i = \sqrt{n_i}$, where n_i is the number of counts for this data point. This gives the weight $W_i = 1/n_i$.

In addition to finding the best value of g, the method provides a value of B that will, in general, be different from the measured value of B. These two values will be referred to as B_{meas} and B_{cal}, where B_{cal} is the intercept of the fitted distribution. The significance of these two values of blob density will be discussed at the conclusion of this section.

Probably the simplest method of finding the minimum of S is the grid search in which S is calculated over a large range of B and g. The values of B and g selected are those which give the smallest S; the range is then tightened and the search continued. This procedure is repeated until the desired accuracy is reached. Since it is not unreasonable to expect five hundred calculations of S before the end result is acceptable, another approach will be used. The method chosen converges on the best values of B and g after an average of five iteration steps, each of which requires only one calculation of S. This method will now be described.

Let us define the following,

$$F_k(N,g) = N\,e^{-g\ell_k} \qquad k = 1,\ldots m\ , \tag{4-1}$$

where N and g are the best fit values of the blob count and grain density. There are m of these equations corresponding to the total number of channels used. We further define:

$$Q_k = n_k - Ne^{-g\ell_k}\ , \tag{4-2}$$

where n_k is the count in the kth channel;

$$\Delta N = N - N'\ , \tag{4-3}$$

where N' is an intermediate estimate for N. This will initially be N_{meas} (again here we are speaking of blob count not density);

$$\Delta g = g - g'\ , \tag{4-4}$$

where g' is an intermediate estimate for g (this will initially be N_{meas}/D, D being the total distance of the measurement);

$$Q_k' = n_k - N'e^{-g'\ell_k} . \tag{4-5}$$

From these definitions, the quantity S becomes

$$S = \sum_{k=1}^{m} W_k Q_k^2 . \tag{4-6}$$

From the Taylor expansion, to a first order approximation, we get

$$F_k(N+dN, g+dg) = F_k(N,g) + \frac{\partial F_k}{\partial N} dN + \frac{\partial F_k}{\partial g} dg . \tag{4-7}$$

Comparing Eqs. (4-3) and (4-4) with

$$N + dN = N'$$

and

$$g + dg = g'$$

we rewrite Eq. (4-7) as follows:

$$F_k(N',g') = F_k(N,g) - \frac{\partial F_k}{\partial N} \Delta N - \frac{\partial F_k}{\partial g} \Delta g . \tag{4-8}$$

Subtracting both sides of Eq. (4-8) from n_k, we get

$$n_k - F_k(N',g') = n_k - F_k(N,g) + \frac{\partial F_k}{\partial N} \Delta N + \frac{\partial F_k}{\partial g} \Delta g$$

$$Q_k' = Q_k + \frac{\partial F_k}{\partial N} \Delta N + \frac{\partial F_k}{\partial g} \Delta g . \tag{4-9}$$

The minimizing of S gives us two conditions:

$$\frac{\partial S}{\partial N} = 0 \tag{4-10}$$

and

$$\frac{\partial S}{\partial g} = 0 \quad . \tag{4-11}$$

From Eq. (4-6),

$$\frac{\partial S}{\partial N} = 2\,\Sigma\, W_k Q_k \frac{\partial Q_k}{\partial N}$$

and further from Eq. (4-2), we see that

$$\frac{\partial Q_k}{\partial N} = - \frac{\partial F_k}{\partial N} \quad ;$$

hence, we get as our first condition

$$-2\,\Sigma\, W_k\, Q_k \frac{\partial F_k}{\partial N} = 0$$

or simply

$$\Sigma\, W_k Q_k \frac{\partial F_k}{\partial N} = 0 \quad . \tag{4-12}$$

Similarly, our second condition leads to

$$\Sigma\, W_k Q_k \frac{\partial F_k}{\partial g} = 0 \; . \tag{4-13}$$

Let us first use Eq. (4-12) to eliminate Q_k in Eq. (4-9). From Eq. (4-9), multiply each of the m equations by $W_k \frac{\partial F_k}{\partial N}$. We get the following m equations:

$$\begin{aligned}
W_1 \frac{\partial F_1}{\partial N} Q_1' &= W_1 \frac{\partial F_1}{\partial N} Q_1 + W_1 \left(\frac{\partial F_1}{\partial N}\right)^2 \Delta N + W_1 \frac{\partial F_1}{\partial N} \frac{\partial F_1}{\partial g} \Delta g \\
&\vdots \\
W_k \frac{\partial F_k}{\partial N} Q_k' &= W_k \frac{\partial F_k}{\partial N} Q_k + W_k \left(\frac{\partial F_k}{\partial N}\right)^2 \Delta N + W_k \frac{\partial F_k}{\partial N} \frac{\partial F_k}{\partial g} \Delta g \\
&\vdots \\
W_m \frac{\partial F_m}{\partial N} Q_m' &= W_m \frac{\partial F_m}{\partial N} Q_m + W_m \left(\frac{\partial F_m}{\partial N}\right)^2 \Delta N + W_m \frac{\partial F_m}{\partial N} \frac{\partial F_m}{\partial g} \Delta g \; .
\end{aligned}$$

Adding these m equations yields the single equation

$$\sum_{k=1}^{m} W_k \frac{\partial F_k}{\partial N} Q_k' = \sum_{k=1}^{m} W_k \frac{\partial F_k}{\partial N} Q_k + \Delta N \sum_{k=1}^{m} W_k \left(\frac{\partial F_k}{\partial N}\right)^2 + \Delta g \sum_{k=1}^{m} W_k \frac{\partial F_k}{\partial N} \frac{\partial F_k}{\partial g} .$$

We now apply the condition Eq. (4-12) to get

$$\sum_{k=1}^{m} W_k \frac{\partial F_k}{\partial N} Q_k' = \Delta N \sum_{k=1}^{m} W_k \left(\frac{\partial F_k}{\partial N}\right)^2 + \Delta g \sum_{k=1}^{m} W_k \left(\frac{\partial F_k}{\partial N}\right)\left(\frac{\partial F_k}{\partial g}\right) . \tag{4-14}$$

If we similarly multiply each of the m equations defined from Eq. (4-9) by

$$W_k \frac{\partial F_k}{\partial g} ,$$

add and apply Eq. (4-13), we get

$$\sum_{k=1}^{m} W_k \frac{\partial F_k}{\partial g} Q_k' = \Delta N \sum_{k=1}^{m} W_k \left(\frac{\partial F_k}{\partial N}\right)\left(\frac{\partial F_k}{\partial g}\right) + \Delta g \sum_{k=1}^{m} \left(\frac{\partial F_k}{\partial g}\right)^2 . \tag{4-15}$$

The differentials should be evaluated at our solution points N and g, but we will assume that the evaluation of these differentials at N' and g' will be close enough.

This leaves us with two equations and the two unknowns ΔN and Δg. After solving for ΔN and Δg, one gets a better estimate of the parameters N and g using Eq. (4-3) and Eq. (4-4) respectively. These estimates of N and g can now be used as new estimates of N and g and another iteration step can be performed to find a still better estimate of N and g. This process is continued until the corrections ΔN and Δg are as small as one desires them to be.

Equations (4-14) and (4-15) may be rewritten in matrix form,

$$\begin{pmatrix} F_1 \\ F_2 \end{pmatrix} = \begin{pmatrix} A_{11} & A_{12} \\ A_{21} & A_{22} \end{pmatrix} \begin{pmatrix} P_1 \\ P_2 \end{pmatrix} \tag{4-16}$$

or simply

$$F = AP \ . \tag{4-17}$$

In Eq. (4-16), P_1 and P_2 refer to the two parameters ΔN and Δg respectively, while

$$F_1 = \sum_{k=1}^{m} W_k \frac{\partial F_k}{\partial N} Q_k'$$

and

$$F_2 = \sum_{k=1}^{m} W_k \frac{\partial F_k}{\partial g} Q_k' \ .$$

The elements of the A matrix are:

$$A_{11} = \sum_{k=1}^{m} W_k \left(\frac{\partial F_k}{\partial N}\right)^2 ,$$

$$A_{12} = \sum_{k=1}^{m} W_k \left(\frac{\partial F_k}{\partial N}\right)\left(\frac{\partial F_k}{\partial g}\right) ,$$

$$A_{21} = \sum_{k=1}^{m} W_k \left(\frac{\partial F_k}{\partial g}\right)\left(\frac{\partial F_k}{\partial N}\right) = A_{12} ,$$

$$A_{22} = \sum_{k=1}^{m} W_k \left(\frac{\partial F_k}{\partial g}\right)^2 .$$

In solving the matrix Eq. (4-17) for P, we find

$$P = A^{-1}F \ .$$

The matrix A^{-1} is often referred to as the error matrix. From it we can calculate the standard deviations of the two parameters N and g as follows:

$$\sigma_N = \sqrt{\frac{S}{m-1} A_{11}^{-1}} \tag{4-18}$$

and

$$\sigma_g = \sqrt{\frac{S}{m-1} A_{22}^{-1}} \ . \tag{4-19}$$

These standard deviations normally vary from .3% to 1% depending on the quality of the fit and the number of gap lengths measured. The standard deviations give the limits which the two parameters may deviate from the calculated values and still represent an acceptable fit to the data. It is important to realize that they do not describe the variations found in the separate track segments measured. For this experiment, these variations are on the order 3%. Since this latter error is much larger and must also include the former error, we are justified in ignoring the errors associated with the calculation of the parameters N and g.

As previously pointed out, steps have been taken to eliminate gross errors from consideration in the data analysis. The chief source of these large errors is equipment failures resulting in bad output data from a single memory unit in the multichannel analyzer. Although this occurs infrequently, steps must be taken to eliminate their influence in the data analysis. In the computing program GDEN, all of the data points are continuously checked for large deviations from the best fit and those found which deviate by more than 3.5 $\sqrt{S/m-1}$ are eliminated from consideration. Assuming a normal distribution of error, this criterion would eliminate one valid data point out of a set of twenty-five thousand data points.

Figure 10 depicts the data from one of the grain density measurements along with the calculated best fit exponential. We note that although the intercepts do not coincide, the data clearly indicates that the assumption of the exponential nature of the gap length distribution is correct. The data departs from the exponential curve only at the short gap lengths where the measurement is most difficult and at long gap lengths where the statistics are poorest. The parameters of this fit are $g = .317 \pm .001$ and $N = 1251 \pm 7$. This last number is significantly lower than the measured blob count of 1357 which is found from the data intercept. The cause of this effect is seen by considering Eq. (2-21),

$$H(0) = B = g\, e^{-g\alpha} .$$

The intercept, $H(0) = B$, is obviously influenced by the values of the parameters g and α. Specifically, if we assume that the value of g remains constant but that α increases, then the parameter B decreases. (See Fig. 11) This has a simple interpretation in that a growth in α suggests a poorer resolution of blobs. This results in the coalescing of adjacent blobs with small intervening gaps into one single blob thus reducing the total blob count. This does not, however, affect the grain density parameter g. Physically, what happens is that the observer can see two blobs which are separated by a small gap and will depress the tap key twice, but the microscope stage is traveling too fast to allow for a sufficiently short response to measure the gap that the scanner can observe. The net effect is to shorten the gaps which follow by a slight amount thus, on the average, decreasing the population of all bins beyond the first two or four. This moves the distribution to the left but does not change the slope. The intercepts of the two distributions correspond to two different resolution parameters.

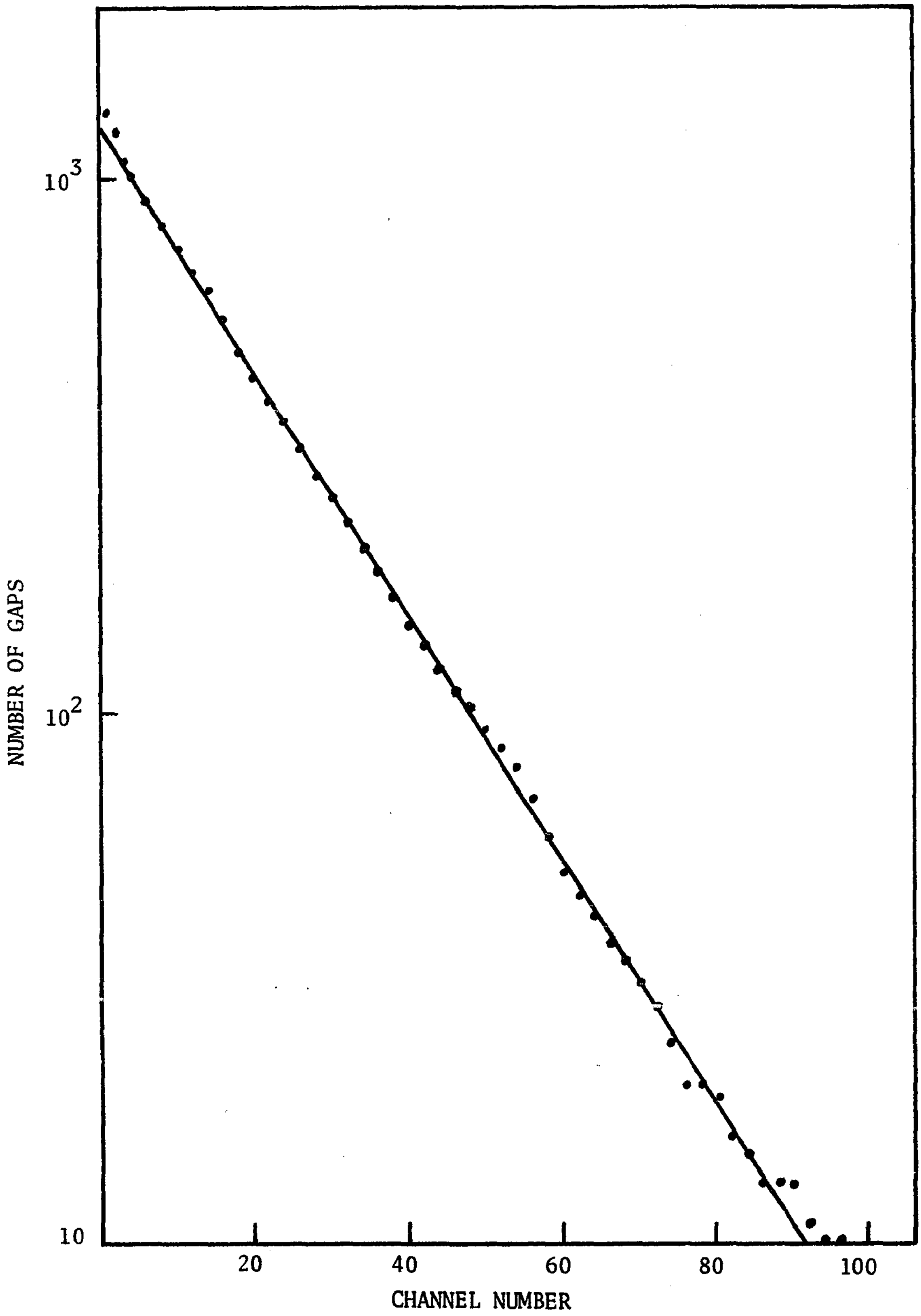

Figure 10. Example of a measured gap length distribution.

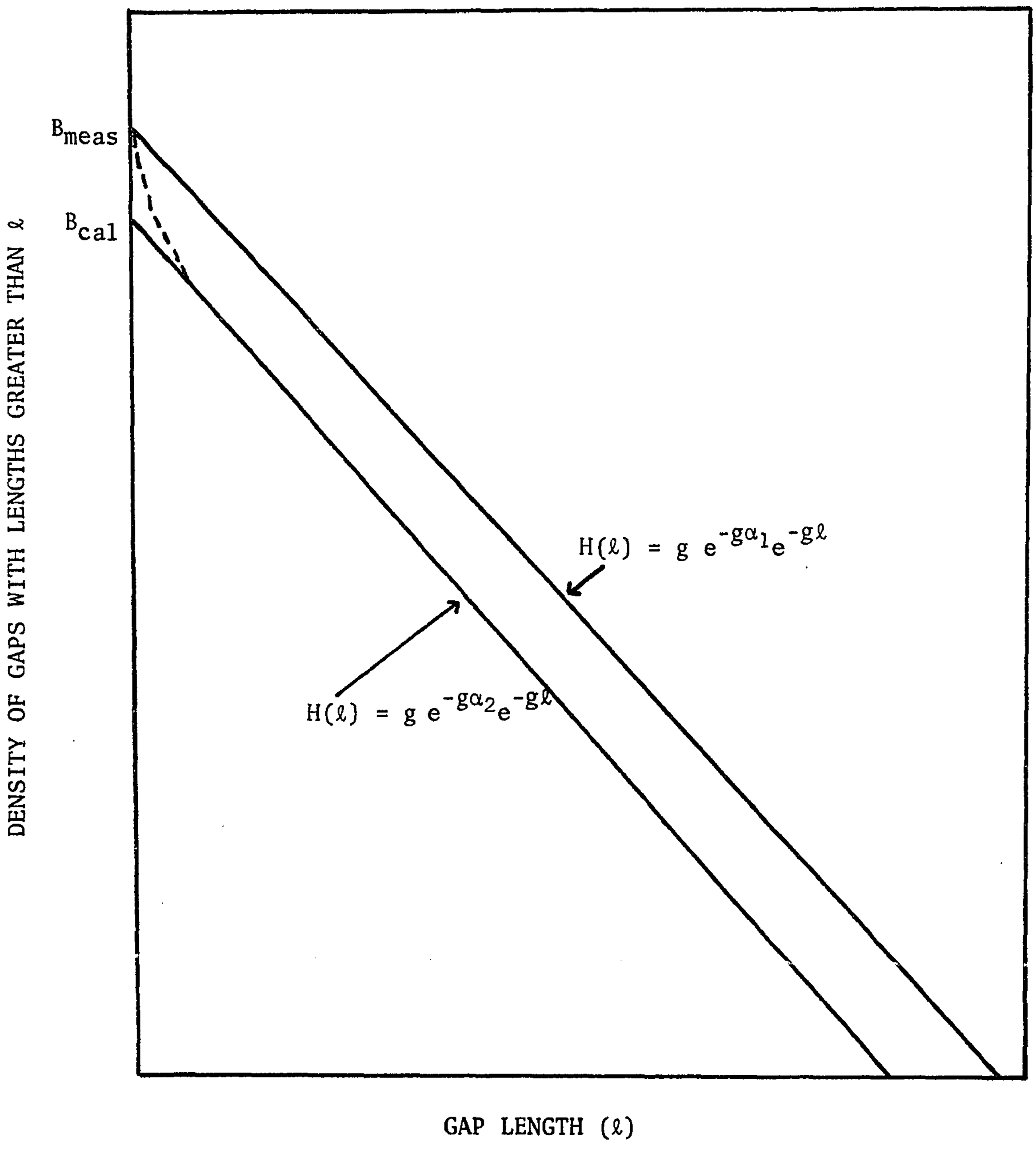

Figure 11. Schematic diagram of two gap length distributions such that $\alpha_2 > \alpha_1$.

We relate B_{meas} to the resolution of the blobs achieved visually by the observer, which we will henceforth refer to as the observer alpha α_o. Similarly, B_{cal} corresponds to the resolution resulting from the experimental contraints imposed, in this case principally by the speed of the microscope stage. We will refer to the latter resolution parameter as the apparatus alpha α_a. Since the experimental lacunarity is the area under the data distribution and this distribution is well described by $H(\ell) = B_{cal}\ e^{-g\alpha_a}$ at all but the first two or three bins, we see that we must use α_a in Eq. (2-23) in order to relate the grain density to the measured lacunarity. So, if we wish to obtain independent measurements of the grain density g, we must use

$$B_{meas} = g\ e^{-g\alpha_o} \tag{4-20}$$

and

$$L = e^{-g\alpha_a}\ . \tag{4-21}$$

Characteristics of the Track Parameters

Three scanners participated in measuring the grain densities of one hundred thirty-one tracks. The data from each scanner is initially analyzed separately so that characteristics particular to an individual scanner can be recognized and accounted for before the data is consolidated.

(1) The variations of grain density with depth in the emulsion.

The possible change in grain density with depth in the emulsion is investigated by first assuming that the variation is linear and searching for the slope which minimizes the quantity

$$S = \sum_j^{\text{tracks}} \sum_i^{\text{segments}} (g'_{ij} - \langle g' \rangle_j)^2$$

where each individual grain density is adjusted to the middle of the processed emulsion, which we take to be 125μ. Hence we have

$$g'_{ij} = g_{ij} + m(z_{ij}-125) \ .$$

Then

$$S = \sum_j^{\text{tracks}} \sum_i^{\text{segments}} [g_{ij}+m(z_{ij}-125)-\langle g\rangle_j -m(\langle z\rangle_j-125)]^2$$

or

$$S = \sum_j^{\text{tracks}} \sum_i^{\text{segments}} [g_{ij} - \langle g\rangle_j + m(z_{ij}-\langle z\rangle_j)]^2, \tag{4-22}$$

which is shown schematically in Fig. 12 for one event. This procedure is especially well suited here, because no knowledge of the overall normalization of the sample is required. Applying the condition $\partial S/\partial m = 0$, we find that

$$m = \frac{\sum_j^{\text{tracks}} \sum_i^{\text{segments}} (\langle g\rangle_j-g_{ij})(z_{ij}-\langle z\rangle_j)}{\sum_j^{\text{tracks}} \sum_i^{\text{segments}} (z_{ij} -\langle z\rangle_j)^2} \ . \tag{4-23}$$

We may abbreviate Eq. (4-23) as follows

$$m = \frac{\Sigma\ \Delta g\ \Delta z}{\Sigma\ \Delta z^2} \ .$$

Then by propagation of errors we see that

$$\sigma_m^2 = \Sigma\left(\frac{\Delta z}{\Sigma(\Delta z)^2}\right)^2 \sigma_{\Delta g_i}^2 \tag{4-24}$$

where we have ignored the small errors in the measurement of the track depths. For tracks with N segments, we find

$$\sigma_{\Delta g_i}^2 = \sigma_{g_i}^2 + \sigma_{\langle g\rangle}^2$$

or

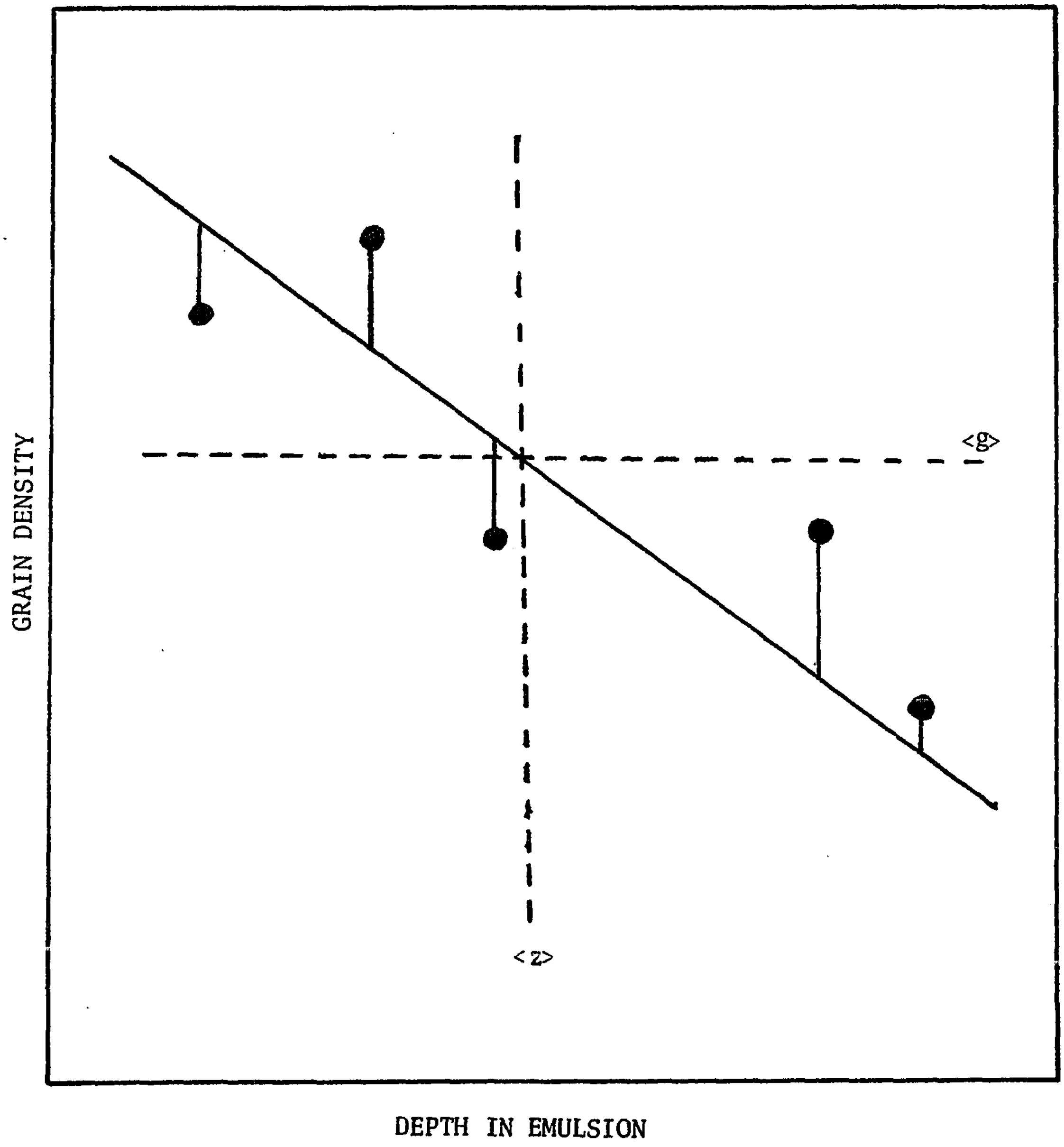

Figure 12. Idealized data points from five track segments depicting the variation of grain density with depth in the emulsion.

$$\sigma^2_{\Delta g_i} = \sigma^2_{g_i} + \frac{1}{N}\sigma^2_{g_i} = \frac{N+1}{N}\sigma^2_{g_i} \; .$$

As most tracks have five segments we may rewrite Eq. (4-24)

$$\sigma^2_m \simeq \frac{6}{5}\sigma^2_{g_i}\,\frac{1}{\Sigma(\Delta z)^2} \; .$$

For each scanner, the value of m yielding the minimum S was accepted as representing the change in grain density with depth in the emulsion. The slope parameters found for the three scanners are

$$m_1 = (-20.0\pm2.2)\times10^{-5},$$

$$m_2 = (-13.5\pm2.6)\times10^{-5},$$

$$m_3 = (-18\pm5)\times10^{-5}.$$

If we consider the grain density measurements that each scanner has made, then these slope parameters correspond to grain density decreases of approximately 16%, 13% and 18% from the top to the bottom of the emulsion. All three results are compatible with a general value of 15% for the decrease in grain density from the top to the bottom of the emulsion.

The linearity of the decrease in grain density is checked by dividing the emulsion into five depth levels of equal thickness and finding the deviations of the data points from the values predicted by the slope parameter m. The deviations are summed for each level and a non-zero result would indicate the general trend of the data to fall predominately to one side of the predicted curve. These results are shown in Fig. 13. Evidence is seen for a departure from linear

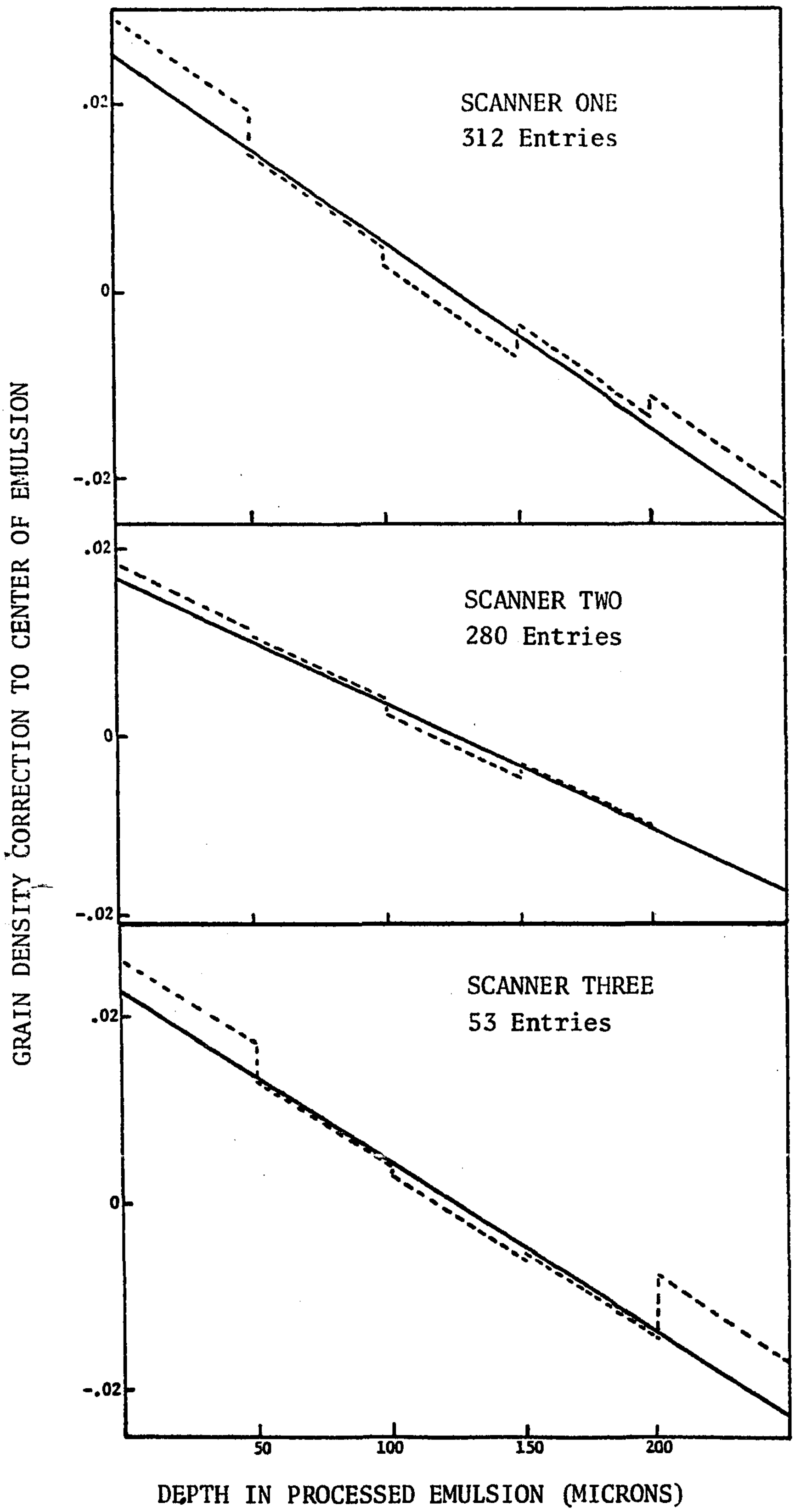

Figure 13. Grain density variation with depth in the emulsion. The solid lines indicate the assumed linear variations while the dashed lines show the actual variations.

behavior at both the extreme top and bottom of the emulsion. The effect consists of a 2% rise above the linear curve. Fortunately, 80% of the track segments are found in the middle three layers where the linear approximation to the grain density variations is valid to within 1%. Difficulties may occur, however, for tracks which have all or most of their segments lying in the top or bottom portions of the emulsion. This is especially true of the measurements of scanners one and three where the effect is most pronounced, suggesting that these tracks may warrant special attention. A review of tracks which have a majority of their segments in one of the outermost layers does reveal some with grain densities somewhat higher than expected but others which do not. Because these tracks are potentially unreliable, it was decided to discard all tracks which do not have at least two segments in the middle portions of the emulsion. This procedure was not, however, applied to scanner two where the effect is not as distinct. A total of four tracks were discarded by making this cut.

(2) Dependence of grain density measurements upon time.

The scanners were trained by having them make repeated measurements of shower tracks and having their results checked for consistency. Working one four-hour shift per day, this training period normally lasted about one-half month before the measurements were accepted as sufficiently consistent to commence data taking for this experiment. Although consistency was achieved, it was subsequently found that the normalization of each scanner had not yet stabilized. In this context, the normalization is defined as the grain density that would be measured by a given scanner for a standard track. In each case the normalization was found to rise after the start of data taking. Figure 14 shows this

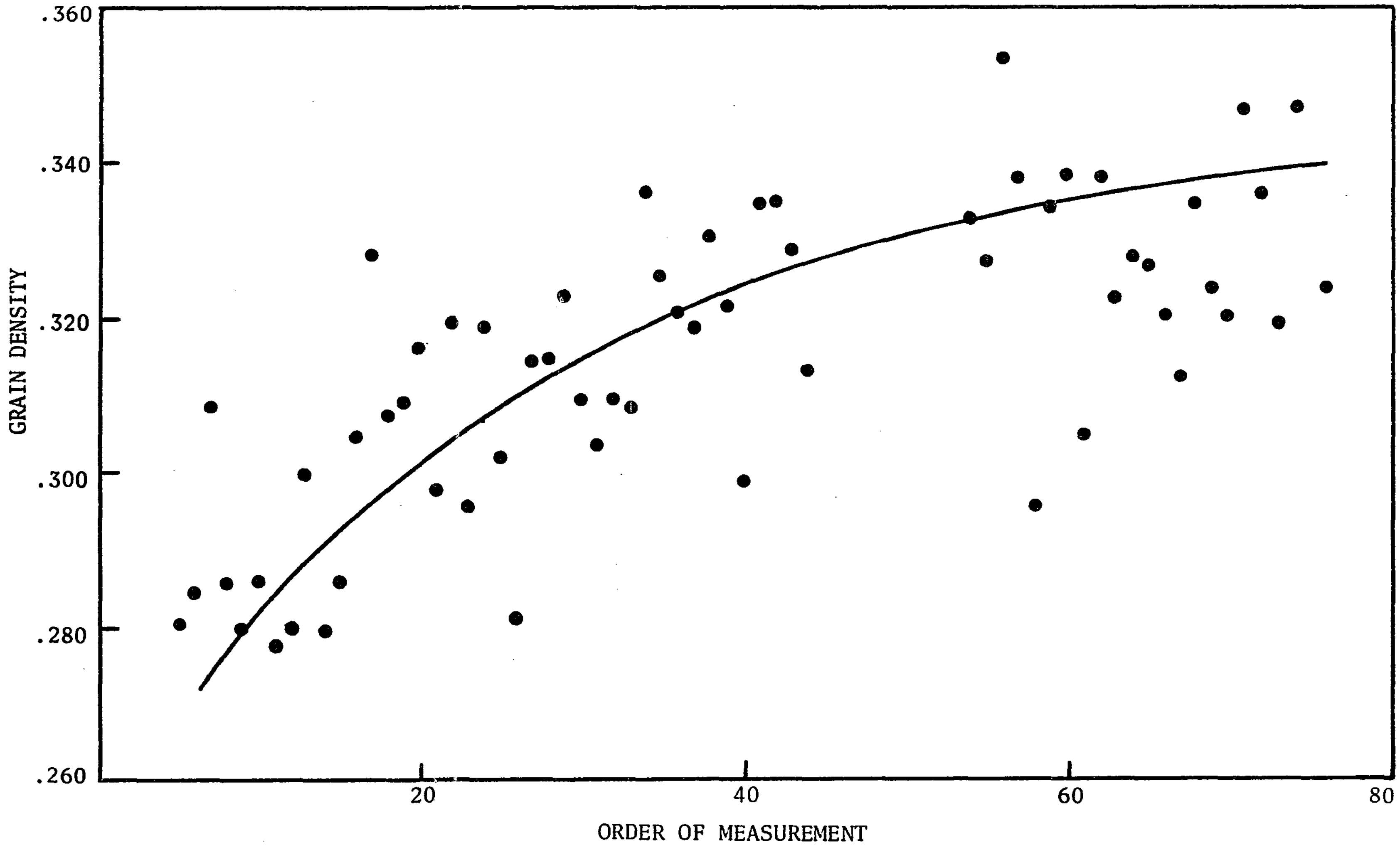

Figure 14. Track grain density by order of measurement (scanner one).

effect for one scanner. We notice a rise in the normalization for this scanner of about 20%. This effect was largely unanticipated and accounting for it is crucial to the data analysis.

A brief glance at Fig. 14 reveals that the data can be interpreted as an exponential rise to some asymptotic level. The curve drawn in Fig. 14 is the result of fitting the grain density to the three parameter exponential $g_N(1-\eta\, e^{-t/T})$ where the parameter t represents the order in which the data was taken and g_N is the grain density asymptote.

Similar results were obtained for a second scanner with the exception of two regions in which the data exhibits an inclination to dip below the rising exponential. Because of the nonavailability of a standard normalization, it is not possible to determine whether this results from the observers normalization decreasing in this region or from the two emulsion plates involved having lower average grain densities than the other plates. Because of this uncertainty, the two plates were discarded from the sample resulting in the loss of fifteen tracks. The remaining data is consistent with an uninterupted exponential rise in grain density normalization and is retained for further analysis.

The data from the third scanner is statistically insufficient to exhibit this exponential rise and has to be fitted with a straight line.

(3) The resolution parameter α.

(a) $\alpha_o = \alpha(B,g)$.

We calculate α_o using Eq. (2-20); thus,

$$\alpha_o = \frac{1}{g}\,\ell n\; g/B_{meas} \quad .$$

The results for each track are plotted in Figs. 15 and 16 for two scanners. It is noticed that the two scanners exhibit different characteristics. α_o of scanner one indicates little or no tendency to vary during the progression of the experiment. The results for scanner one are consistent with a constant $\alpha_o = .57 \pm .015\mu$ throughout the experiment. This is not the case, however, for scanner two. Here α_o is initially about .40μ and decreases throughout the experiment until it is in the vicinity of .20μ. It is problematical whether or not this actually represents an improvement in measurement by the observer. These results may be compared to the actual measured mean crystal-grain diameter in Ilford K-5 emulsion which is .210μ [20]. It is, nevertheless, apparent that the observers criterion for what constitutes blob separation has changed and that this must be taken into consideration if one is to calculate the grain density using Eq. (2-20). We assign a value in microns of $\alpha_o = .42 - .0043\ t$ for scanner two when we wish to determine the grain density from the measured blob density.

(b) $\alpha_a = \alpha(L,g)$

Using Eq. (2-23), we calculate

$$\alpha_a = \frac{1}{g} \ell n\ 1/L\ .$$

These results are plotted in Figs. 17 and 18. The principal feature of these plots is the tendency of the α_a parameter to remain constant throughout the experiment except for scanner one where an increase of about 15% is observed for the last twenty tracks measured. An inspection of the experimental data reveals that the speed in which the measurements were taken has fluctuated around 4.2 microns/sec for

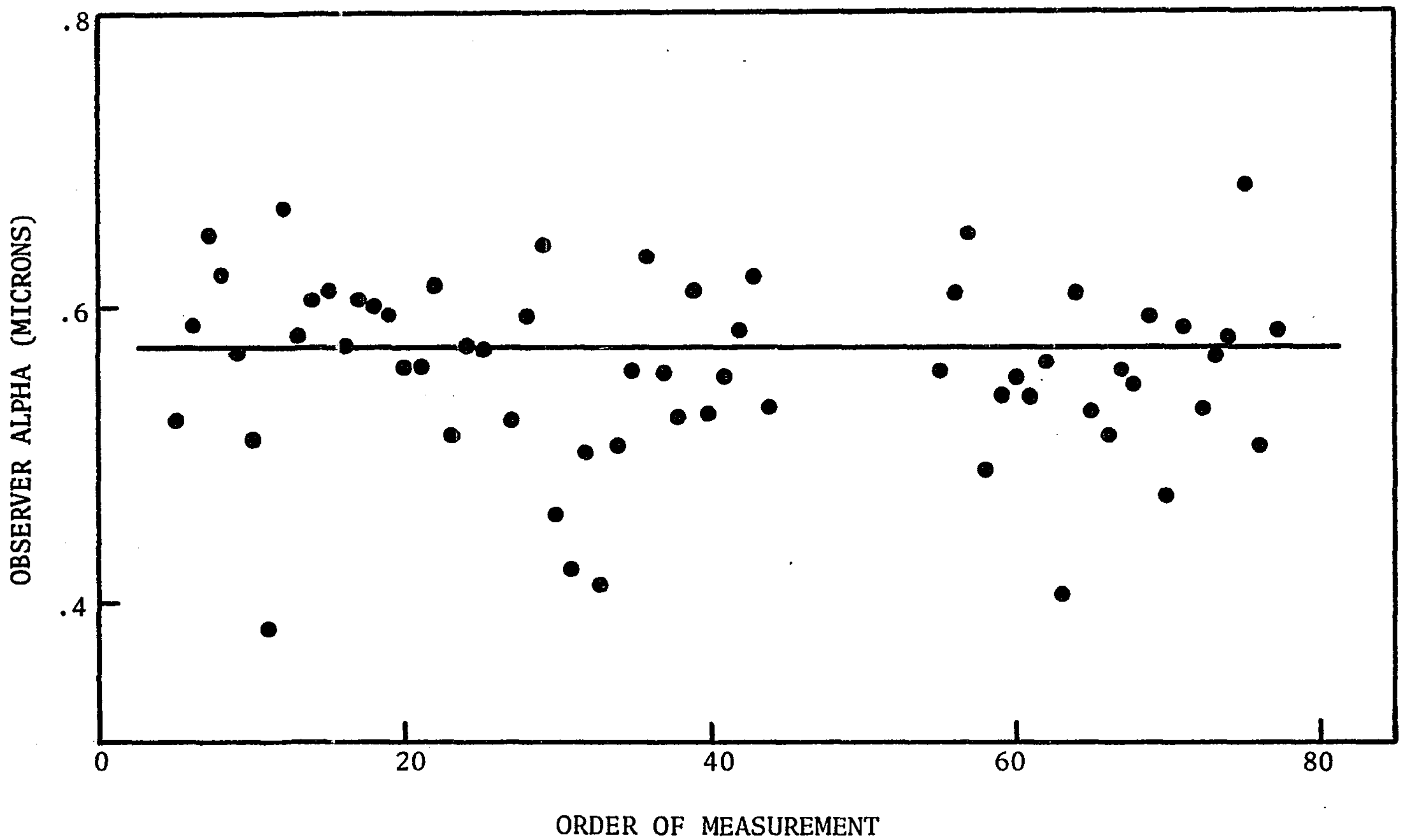

Figure 15. The observer alphas (α_o) for scanner one.

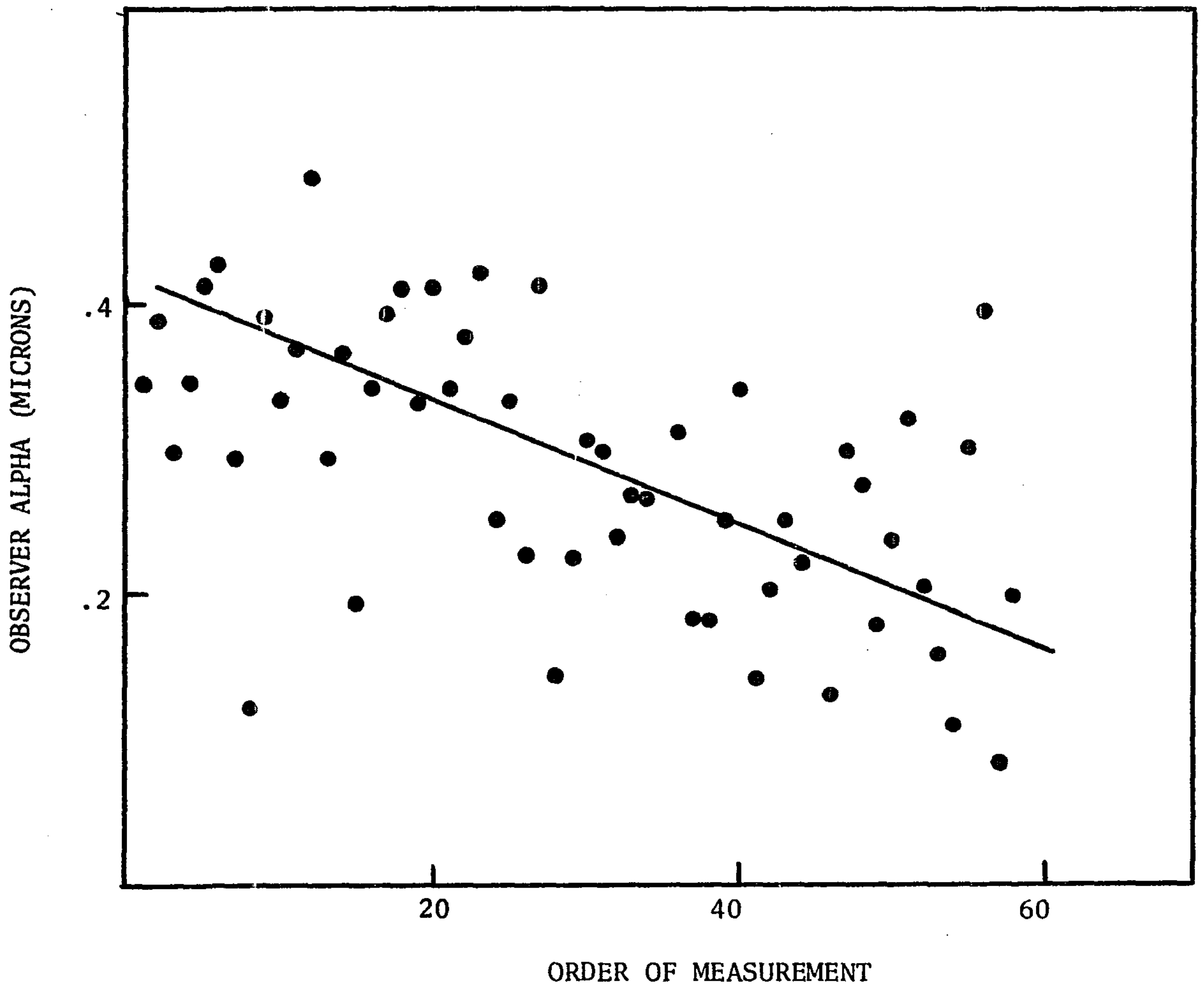

Figure 16. The observer alphas (α_o) for scanner two.

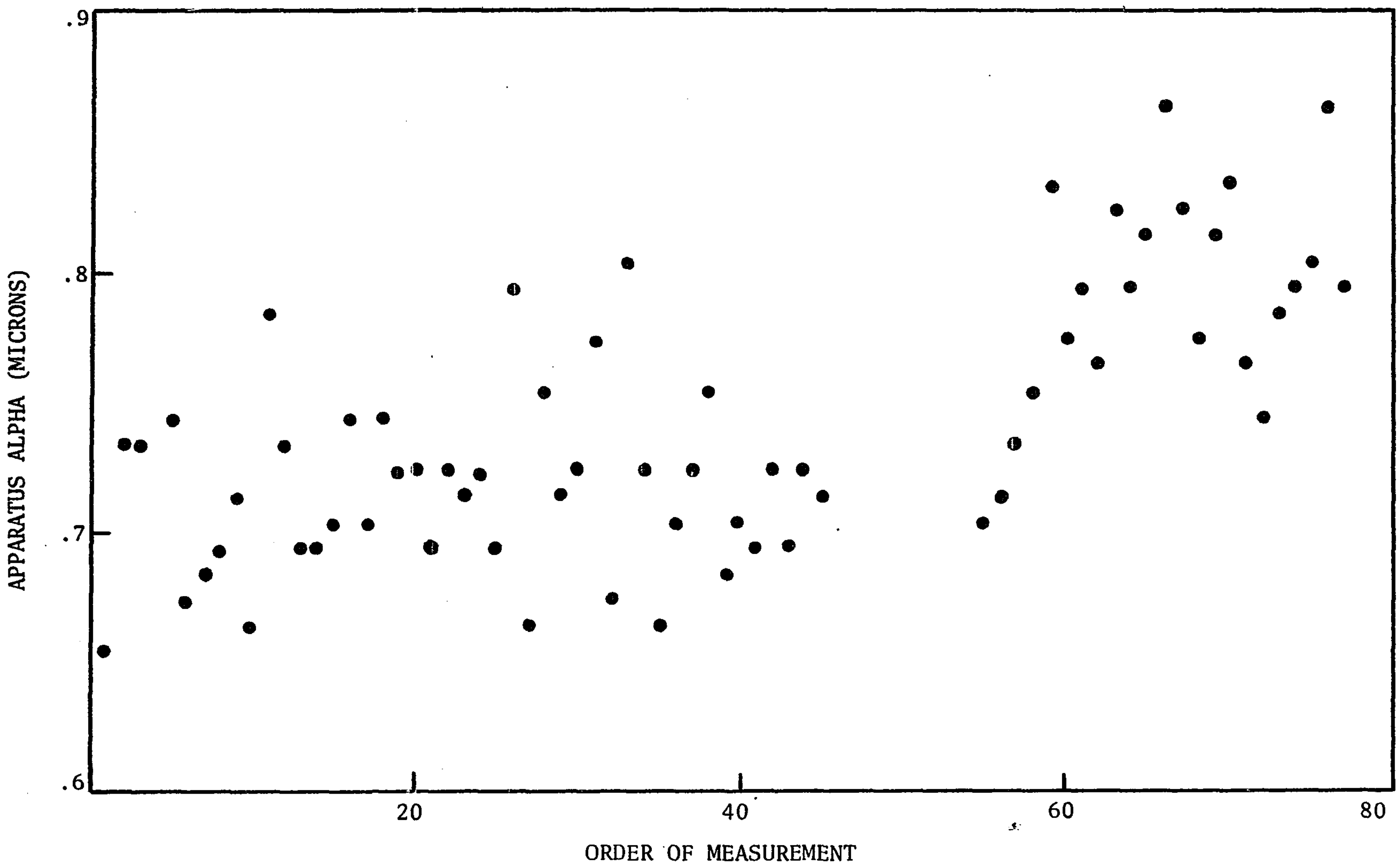

Figure 17. Apparatus alphas (α_a) for scanner one.

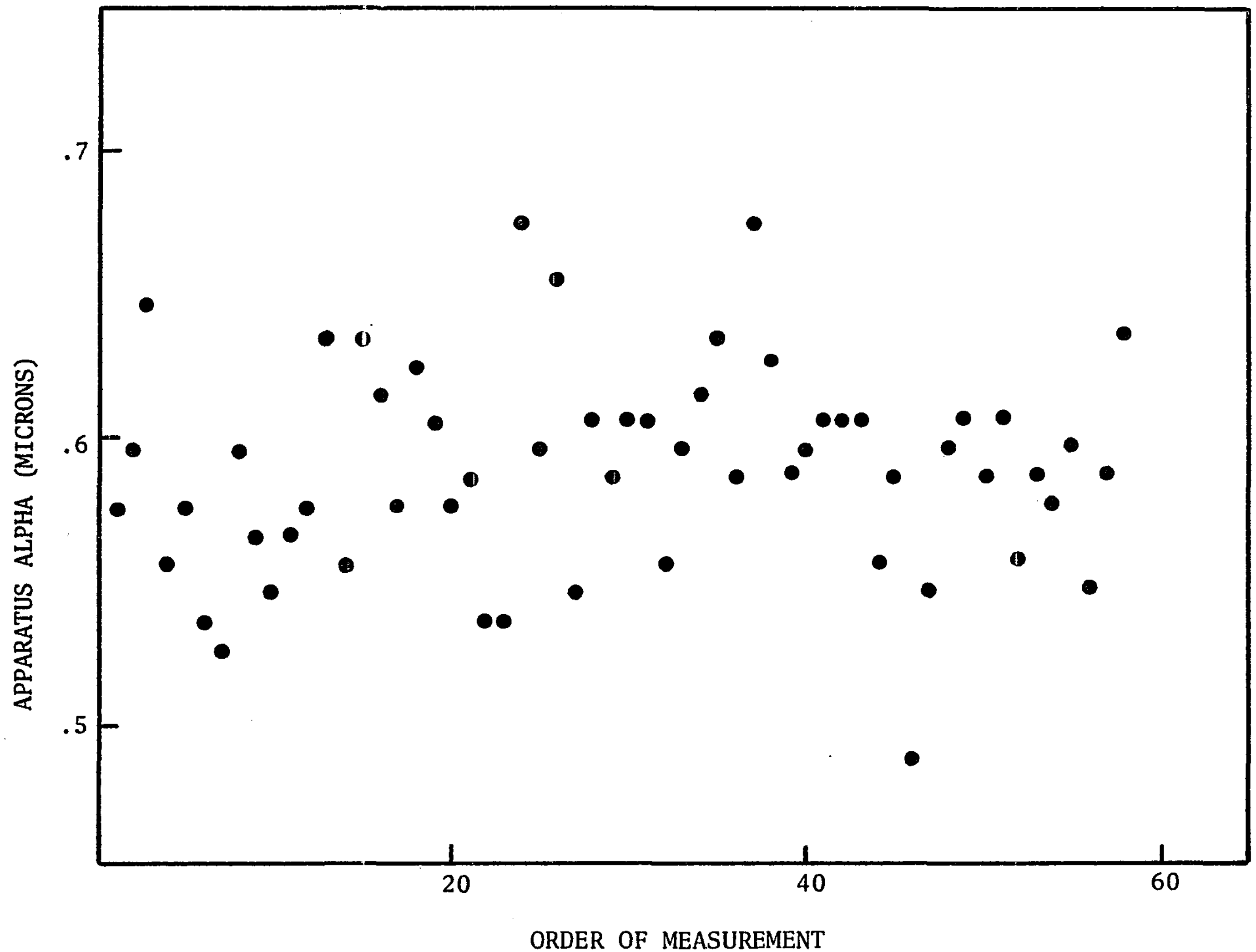

Figure 18. Apparatus alphas (α_a) for scanner two.

the entire experiment except for the final measurements of scanner one where the speed was increased to about 4.5 microns/sec. That this is, indeed, the cause of the observed increase in the parameter α_a is demonstrated in Fig. 19 where α_a is plotted versus the speed of the measurement for scanner one. The straight line fit in Fig. 19 is accepted as the best value of α_a for insertion into Eq. (2-23) in order to get a third independent value of the grain density g for the tracks measured by scanner one. Repeating this procedure for the other scanners also reveals results consistent with Fig. 19; however, because of the smaller spread in the speed of the measurements, the effect is not as clearly perceptible. Thus, it is of little consequence whether or not the corrections for speed of measurement are considered, although for completeness these corrections are also included for the remaining scanners.

These results clearly show that the two α's [$\alpha_o = \alpha(B,g)$ and $\alpha_a = \alpha(L,g)$] have different characteristics and must be treated as separate parameters in this and subsequent data analysis.

(4) Experimentally determined values of g*

The accepted value of the grain density for each track segment was found by forming a weighted average of the three independent measurements of g: g_S = g(slope of gap length distribution), g_B=g(blob density, α_o), and g_L = g(lacunarity, α_a). Therefore,

$$g = \frac{1}{T}\left(\frac{g_S}{\sigma^2_{g_S}} + \frac{g_B}{\sigma^2_{g_B}} + \frac{g_L}{\sigma^2_{g_L}}\right)$$

where

$$T = \frac{1}{\sigma^2_{g_S}} + \frac{1}{\sigma^2_{g_B}} + \frac{1}{\sigma^2_{g_L}} .$$

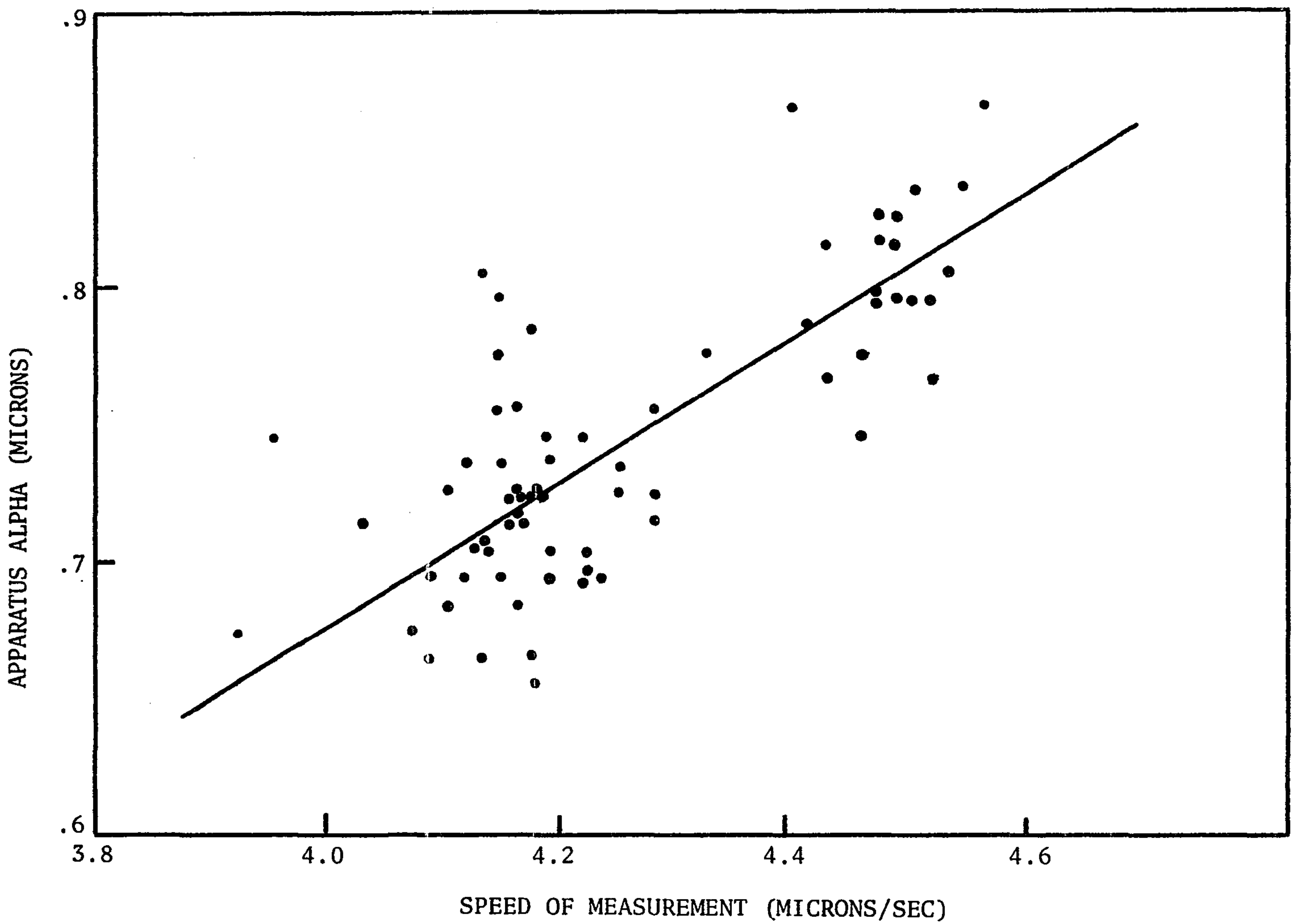

Figure 19. Apparatus alphas (α_a) for scanner one.

All grain density measurements are adjusted to the middle of the pellicle, while each σ is the spread of the individual grain density measurements. This spread can be found from the minimum S as defined in Eq. (4-22). Thus, $\sigma^2 = S_{min}/DF$, where DF = degrees of freedom = number of segments - number of tracks -1. Table 5 gives the results for all grain densities.

Table 5

EXPERIMENTAL SPREAD OF GRAIN DENSITIES OF TRACK SEGMENTS

Scanner	σ_g(slope)	$\sigma_g(B,\alpha_0)$	$\sigma_g(L,\alpha_a)$	σ_g(composite)
1	.017	.011	.014	.011
2	.014	.009	.017	.009
3	.012	.008	.012	.008

The standard deviation of the composite grain density was found by calculating the composite grain density for each individual track segment and then calculating the spread by the previously described method. This experimental spread is accepted as the error in the grain density measurement for each track segment.

The track grain density is found by a simple averaging of the component segments. Each segment is tested for the amount of its deviation from the track average. If this deviation exceeds the accepted standard deviation σ by a factor of three, the segment is discarded and the averaging repeated without the discarded segment. Because of the previously mentioned difficulties with the grain density measurements in the top and bottom portion of the emulsion pellicle, a more stringent rejection criterion has been applied to segments situated in these regions. These track segments are rejected if they deviate more than 2σ from the mean. In addition, the entire set of segments is closely scrutinized to insure that there is no substantial deviation from the grain density measurements recorded for the segments located in the middle portion of the emulsion. If such a pattern does exist for a track, only the segments in the middle portions of the emulsion are retained, for they are more reliable indicators of the true grain density of the particle track. After a careful review of the data, however, it is found necessary to apply this procedure to only four of the one hundred twelve remaining tracks.

The grain density error for each track is derived from

$$\sigma^2_{\text{track}} = \frac{1}{N}\,\sigma^2_{\text{segment}} \;,$$

where N is the total number of segments accepted for averaging.

In order to determine the g* for each track a knowledge of the beam grain density g_o is required. Because it was initially felt that the grain density measurements should have a stable overall normalization as the experiment progressed, the measurement of beam tracks was thought to be unnecessary. However, the unanticipated rise in normalization as displayed in Fig. 14 indicates that it does indeed change to such a large extent that failure to account for it would destroy the usefulness of the track density data for particle identification purposes. The solid line drawn in Fig. 14 gives a rough indication of how the grain density normalization changed as the experiment proceeded. To obtain a more precise relationship, we must estimate the value of the beam grain density for each track measured, plot these estimated grain densities, and fit a rising exponential to the resulting curve. We proceed as follows: a g^* vs $P\beta$ curve is assumed and the beam grain density estimations are found by dividing the measured grain densities of the tracks by the g^* appropriate for the $P\beta$ that each track possesses. These beam grain density estimations are then plotted and the resulting curve examined. There are five reasons for the curve not being smooth: (1) the grain density, $P\beta$ relationship is incorrect, (2) the track grain density measurements have errors, (3) the $P\beta$ measurements have errors, (4) all particles are not pions, (5) the normalization does not change in a smooth way. We shall assume that any change in normalization is not erratic and hence the fifth possibility is not considered.

Initially, the Sternheimer equation with T_{max} = 5 KeV was used and the resulting curve fitted with the best fit exponential rise. The values of g^* obtained, however, indicated that the per cent rise to the beam grain density was on the order of 12%; hence, the plot was repeated assuming the T_{max} parameter to be 100 KeV. This plot is shown in Fig. 20 along with the best exponential fit. Although most of the particles tend to cluster about the curve, it is noticed that a considerable number do not. These particles are non-pion candidates.

The curve shown in Fig. 20 is used for scanner one to give the values of g_0 at the emulsion's mid-depth as function of the track measuring order. The fact that this value changes as the experiment

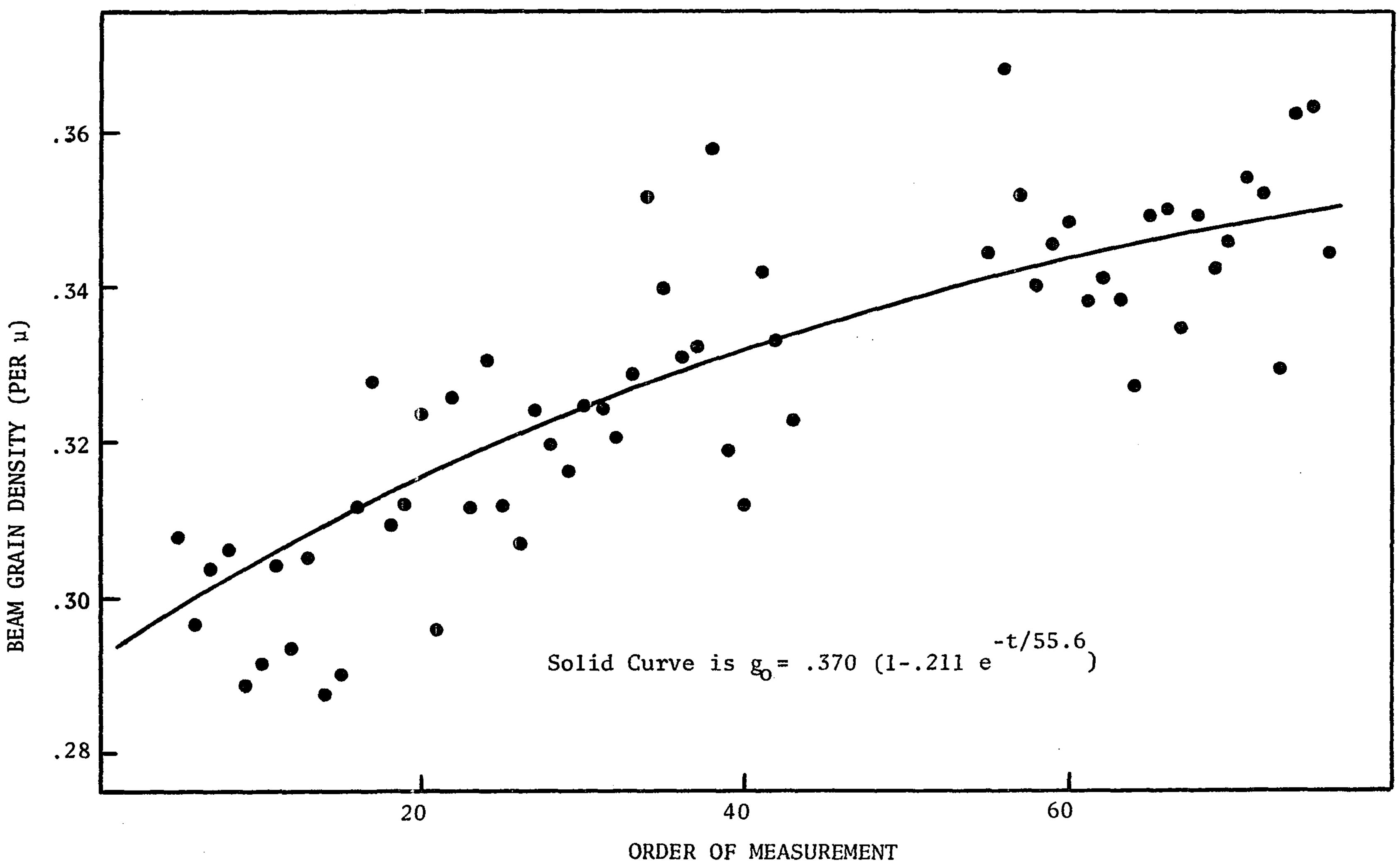

Figure 20. Normalization curve for scanner one.

progresses shows that the constant of proportionality Q in Eq. (2-1),

$$g = - Q \frac{1}{\rho} \left(\frac{dE}{dx}\right) \tag{2-1}$$

also depends on the measuring characteristics of the scanner. Notice that the resolution parameter α_o for scanner one does not change with the order of measurement while the grain density does. We can not associate this change in grain density normalization with an improvement in measurement but rather with a change, on the part of the scanner, of the notion as to what constitutes a developed grain along the particle path. Clearly, at latter stages in the experiment, developed grains, which would have been previously passed over, are being accepted as being associated with the path of the particle. From the time constants of the exponential curves, one can see that in this experiment the aymptotic region is not reached until over one hundred tracks (~600,000 gaps) have been measured.

Using similar normalization curves for each scanner, the quantity $g^* = g/g_o$ can be established. These results, along with the experimental results of space angle and $P\beta$ measurements previously done, are listed in Appendix D. The event type from which the measured tracks egress is given by prong number (an even number of prongs is interpreted as a pion-proton collision; an odd number of prongs is interpreted as a pion-neutron event). The letter P refers to events in which a dark or grey track is seen to emerge from the event. These tracks are normally assumed to be protons. See Ref. 6 for a more detailed account of these tracks.

CHAPTER V

EXPERIMENTAL RESULTS

General Observations

The data tabulated in Appendix D consists of measurements on one hundred twelve tracks. In Fig. 21 each particle is entered on a g^* vs $P\beta$ plot. We note several outstanding features in this plot. First, there is a clear separation of points in the region of the plot above 3 GeV, indicating the presence of particles that are not pions in the sample. Second, the presence of data points above the pion curve is observed. Third, a clustering of data points about the theoretical kaon curve indicates the presence of kaons in the sample. These features will now be discussed in more detail.

Characteristics of the g^* vs $P\beta$ Plot

In general, the data exhibits a tendency to cluster about the theoretical pion curve and, to a lesser extent, about the kaon curve. An interesting observation is that the data tends to fit the theoretical pion curve much better at higher momenta ($P\beta \gtrsim 6$ GeV) than at lower momenta. We notice, for example, the heavy scattering of data points between 2 and 5 GeV. This suggests that the excessive scattering of the data about the theoretical curve is due to large errors in the $P\beta$ measurements, for the region of the plot above 6 GeV is not very sensitive to the $P\beta$ measurement errors, while below 6 GeV these errors

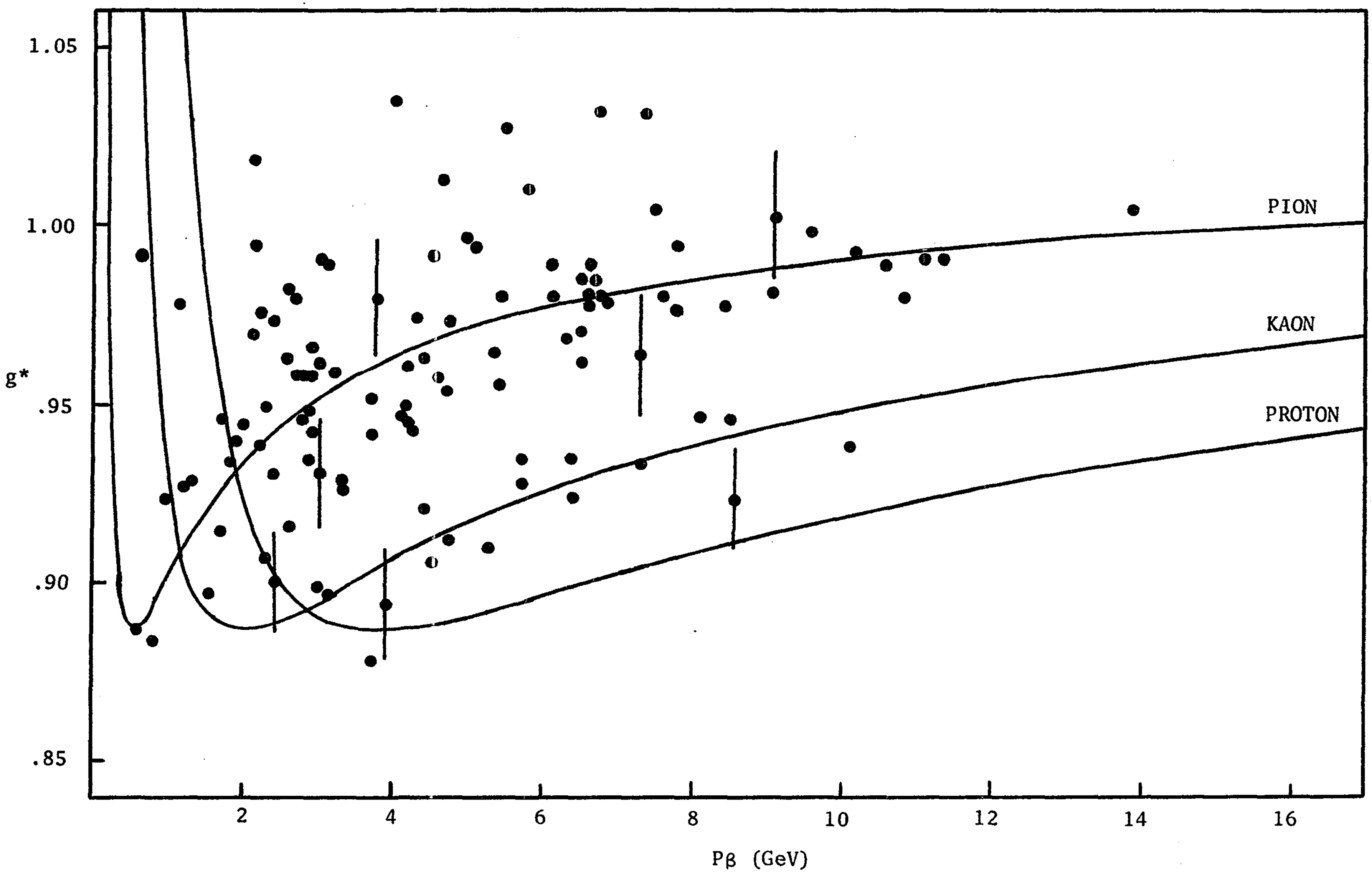

71

Figure 21. Experimental results. Theoretical curves are the Sternheimer equation with $T_{max} = 100$ KeV.

become more conspicuous. This interpretation is further supported by the clustering of points about the kaon curve, a curve which does not rise as steeply as the pion curve and hence is less sensitive to $P\beta$ errors.

The especially heavy population of data points in the region $P\beta \sim 2.5$ GeV and $g^* \sim .98$ suggests that there might also be an occasional tendency to underestimate the $P\beta$ values of particles by substantial amounts (on the order of ~60%). There is, however, no evidence that this underestimation of $P\beta$ is widespread; for, in general, the fit of the data points to the theoretical curve is quite good. A second difficulty that could add to the population of particles above the pion curve is the experimental difficulty encountered in the non-linear behavior of the grain density variation with depth in the emulsion.

The parameter T_{max} = 100 KeV is used for the theoretical curves drawn in Fig. 21, and good agreement to the experimental data is observed. In addition to Jongejans [12], this result agrees very well with the work of Herz and Stiller [21] who reported a relativistic blob density rise of 12% from minimum ionization to the ionization plateau for Ilford K-5 emulsion. This 12% rise in the blob density is equivalent to a 14% rise for grain density (see Table 4). Subtracting 2% for the difference between plateau and the beam ionization densities (the plateau ionization density g^* is 1.0195 from the Sternheimer equation for T_{max} = 100 KeV) leaves us with a 12% effect, which is observed in Fig. 21. Because of the errors in the measurements, it is difficult to determine how well the shape of the curve compares to the experimental data, but one does note remarkably good agreement for the kaon curve ($8 \lesssim \gamma \lesssim 20$) and for the high momentum portion of the pion curve ($\gamma \gtrsim 50$).

Possible Electrons

Seven particles appear well above the pion curve. They all lie in the region of $g^* \approx 1.02$ giving credibility to their possible interpretation as plateau ionizing particles and therefore most likely as electrons. Electrons with such high energies could only result as either direct pair production in coincidence with the strong interaction or as decay products of neutral particles which decay electromagnetically. This is known to occur for the decay of the Π°, which has two principal decay modes [18]:

$$\Pi^\circ \rightarrow \gamma\gamma \qquad 98.8\%$$

and

$$\Pi^\circ \rightarrow \gamma e^+ e^- \qquad 1.2\% \ .$$

If one makes the usual assumptions for the average number of Π°'s produced for each event $[n_{\Pi^\circ} = \frac{1}{2} n_{ch} = \frac{1}{2}(n_{\Pi^+} + n_{\Pi^-})]$, then we expect approximately two Π°'s per event. Utilizing the above decay ratios and noting that the one hundred twelve measured particles are emitted from one hundred events, we arrive at an expectation value of only one or two electrons to be included in the sample. Seven is clearly unexpected. A clear interpretation of these particles being electrons is hampered by the experimental difficulties mentioned in the previous section. Both of these possible difficulties, an overestimation of g^* or an underestimation of $P\beta$, could serve to place pions among the electron population, thereby casting doubt on the interpretation.

For electrons, the principal mode of energy loss is through radiation by bremsstrahlung rather than by ionizing collisions. For energies greater than one GeV this loss is exponential [13], but erratic; i.e., on the average, the energy remaining after traveling a distance t in a stopping material is

$$E = E_o \; e^{-t/T} \; , \tag{5-1}$$

where T is the radiation length of the material. Therefore, on the average, $E = .37\ E_o$ after the particle has traveled one radiation length. For Ilford emulsion, this radiation length is 2.91 cm [18]; thus in 20,000 microns, we would expect the electrons to lose 50% of their initial energy. If we divide the 20,000 micron path length into two segments of 10,000 microns each and integrate over each segment, we find a ratio of 1.4:1 for the average energy we would expect the electrons to have in each segment; i.e., the average energy that an electron possesses in the second half of the 20,000 micron path length should be about 30% less than what it possesses in the first half.

Pβ and energy are essentially equivalent for electrons; therefore, we may test each of the seven electron candidates for possible energy losses by investigating changes in Pβ along the particle path. We must, however, consider the role of errors in this analysis. The errors in Pβ are principally statistical; so that, if we designate the per cent error of the Pβ measurement for the entire track to be σ_o, it is not unreasonable to expect the per cent errors for the Pβ's calculated for each half to be $\sigma^2_{segment} = 2\sigma^2_o$. Now the per cent error in the ratio of the two segments will simply be

$$\sigma^2_{ratio} = \sigma^2_{segment} + \sigma^2_{segment} = 4\sigma^2_o;$$

hence, $\sigma_{ratio} = 2\sigma_o$. We see, then, that errors of 15% or more in the $P\beta$ measurements will result in errors greater than 30% in the $P\beta$ ratios, which is larger than the effect we seek. The uncertainty of the $P\beta$ ratio is further enhanced by the fact that the above analysis is based on average energy loss. We must note that, for electrons, the energy loss by bremsstrahlung is actually quite sporadic. We must therefore not expect to be able to unequivocally identify each individual particle as being an electron or a heavier particle. A review of the $P\beta$ measurements of each of the seven particles by segments reveals two which exhibit electron-like behavior in that the $P\beta$ ratios for the two half segments have values of 1.7 and 2.7. This can by no means be considered to be conclusive evidence that the particles are electrons, but it does lend support to a conclusion that electrons are included in the sample of seven. The precise number is difficult to estimate but it is likely more than two.

Kaons

Above 3 GeV in Fig. 21, there is a clear separation of low points from those fitting the pion curve. Further, it is evident that the great bulk of these particles are kaons. There is no evidence to suggest that protons with $P\beta$ greater than 4 GeV are present in the data sample. If we consider the identified particles with momenta greater than 3.5 GeV/c ($\beta \simeq 1$ for such high momenta), then we observe thirteen kaons and forty-six pions which gives a kaon population of (22 ± 6) per cent for these fast particles. This is substantially higher than previous experiments have suggested. Bartke, *et al.* have reported the following cross sections for 16 GeV/c Π^--proton collisions [22]:

$$\sigma_{K\bar{K}} = 2.21 \pm 0.25 \text{ mb}$$

and

$$\sigma_{YK} = 1.32 \pm 0.15 \text{ mb} .$$

These can be compared with the total cross section for this reaction,

$$\sigma_{Total} = 25.68 \pm 0.10 \text{ mb [23]} .$$

When one considers that the average number of charged particles produced in these reactions is $\langle n_{ch} \rangle = 4.2$ [24] and that the great majority of these particles are pions, then it is seen that the ratio K_{ch}/Π_{ch} should be less than 10%.

There are several factors which one should be aware of when the K_{ch}/Π_{ch} ratio found in this experiment is considered. First, the $\sigma_{K\bar{K}}$ ratio reported in Ref. 22 is derived almost exclusively from observed K° decays. If the assumption is made that the four possible charge states of $K\bar{K}$ ($K^+K^-, K^+\bar{K}^\circ, K^-K^\circ, K^\circ\bar{K}^\circ$) occur with equal frequency, then it is possible to calculate the cross section $\sigma_{K\bar{K}}$ solely from the observed K° decays. This situation arises because of the extreme difficulties encountered in distinguishing charged kaons from charged pions. In a bubble chamber, for example, it is not possible to distinguish the two by ionization if the momenta are greater than ~500 MeV/c. The only method available, other than kinematical fitting, is to look at the decays which the particles may suffer before leaving the chamber. These observed decays become rarer as the energy increases, both because the probability for the decay to occur in the chamber decreases and because the decays that do occur become more difficult to detect due to the increasing similarity of the lab momenta of the primary particle and the decay products. For example, in Ref. 22, the number of seen K° decays was one hundred twenty-six while the seen charged K decays was only four.

A second factor to be considered is that the sample presented in this work is biased due to the selection procedure used to obtain the tracks. Because we are selecting tracks which must travel at least 20,000 microns before leaving an emulsion pellicle which is only 600μ thick unprocessed, we are obviously dealing mainly with those particles which are ejected forward in a narrow jet. Hence, our sample is populated principally by the fast forward produced particles which are often referred to as the projectile fragments. In this experiment we are examining the identities of particles in a kinematic region in which - as far as the direct identification of particles is concerned - data is currently unavailable.

A third consideration is that the experimental biases which could influence the population of the electron candidates can only serve to transfer points from the proton curve to the kaon curve but not from the pion curve to the kaon curve; consequently, these particles remain solid non-pion candidates.

The pion and kaon distributions are plotted in Fig. 22 as functions of the variable $\chi = P^*_{\parallel}/P_o$ where $P^*_{\parallel}$ is the center of mass longitudinal momentum of the particles and P_o is the center of mass momentum of the pion beam particles. Note that the great bulk of the

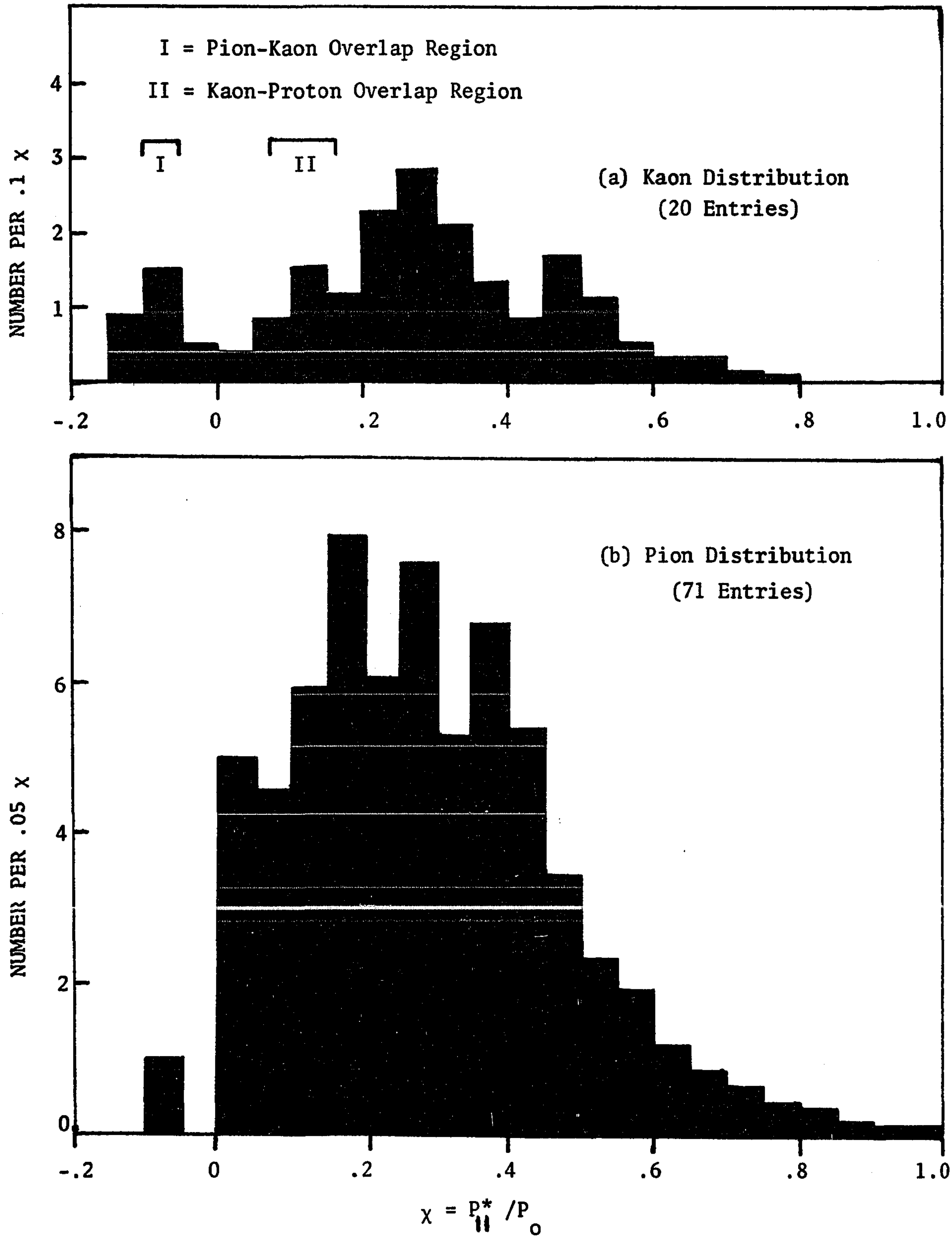

Figure 22. Unweighted particle distribution. The abscissa is the center of mass longitudinal momentum divided by the center of mass beam momentum.

sample involves particles with $\chi > 0$ confirming the earlier assertion that the data consists almost entirely of the fast forward produced particles. The kaons included in Fig. 22a consist of fourteen entries listed in Appendix D which are solely identified as kaons, six entries which are identified as either kaons or protons and one entry which is either a kaon or pion. The regions where the kaon curve overlaps the pion and proton curves are marked on the figure. Of the six entries identified as either kaons or protons, only the four which lie in the kaon-proton overlap region can have a serious influence on the results. The entry at 8.6 GeV is more likely a kaon than a proton while the entry at 1.1 GeV is beyond the negative χ limit of the plot and is of little importance to this analysis. Similarly, the pion-kaon overlap region is in the negative χ region, and the one pion-kaon entry will therefore not contribute significantly to this analysis. As can be seen from Fig. 22a, the kaon-proton overlap contributes to the histogram in the region of $.08 \lesssim \chi \lesssim .17$, and it is here that the kaon distribution could be too high.

Of the seventy-one pion entries, only four have alternate identification possibilities. Due to the fact that pions are produced more prolifically than any other particle, little error should occur by assuming these particles to be pions.

As already seen in Fig. 22, we are interested in the positive χ portion of the pion and kaon distributions. In order to better see the shape of these distributions, it will be necessary to apply a geometrical weighting factor to each particle in order to account for experimental biases incurred by the track selection procedure. This bias occurs because the tracks with large space angles θ have less probability to travel 20,000 microns without leaving the emulsion than do tracks with smaller space angles. This is illustrated in Fig. 23. In Fig. 23a, we visualize a cone along which any shower track with a space angle θ must travel. The base of this cone has a radius R = 20,000 sin θ. If this cone base remains inside the emulsion, there is no chance of this track leaving the emulsion before it has traveled 20,000 microns (cone with base R_1 in Fig. 23b). If, on the other hand, the cone base extends beyond the limits of the emulsion, then the probability is less than 100% that the track will travel at least 20,000 microns in the emulsion, or that it will be selected for measurement (cone with base R_2 in Fig. 23b). This probability is given by

$$P = \frac{\text{Portion of Cone Base Circumference Inside Emulsion}}{\text{Total Circumference of Cone Base}} \, . \tag{5-2}$$

Clearly,

$$\lim_{\theta \to \text{large}} P = \frac{2 \times 600\mu \times 100}{2\Pi(20{,}000\,)\sin\theta}\,\% = \frac{3}{\Pi\ \sin\theta}\,\% \, . \tag{5-3}$$

This limit is already reached at $\theta = 3°$ where the diameter of the cone is approximately three times the width of the emulsion. At this point, Eq. (5-2) and Eq. (5-3) agree to within ½%. Below 3°, the probability P is found by allowing the event to originate at different depths in the emulsion and then by numerically integrating to find the total probability for the track to remain in the emulsion using Eq. (5-2). The results are shown in Table 6.

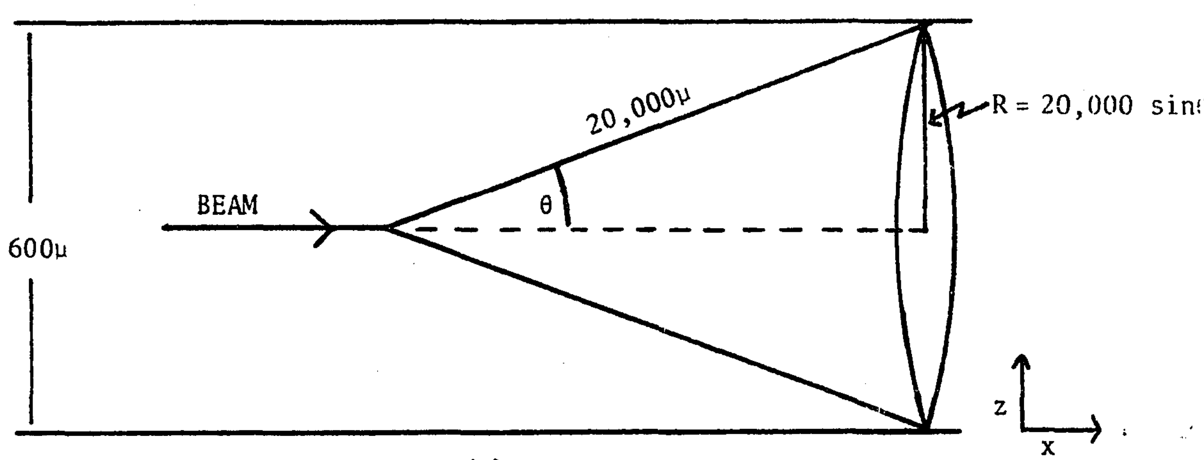

(a)

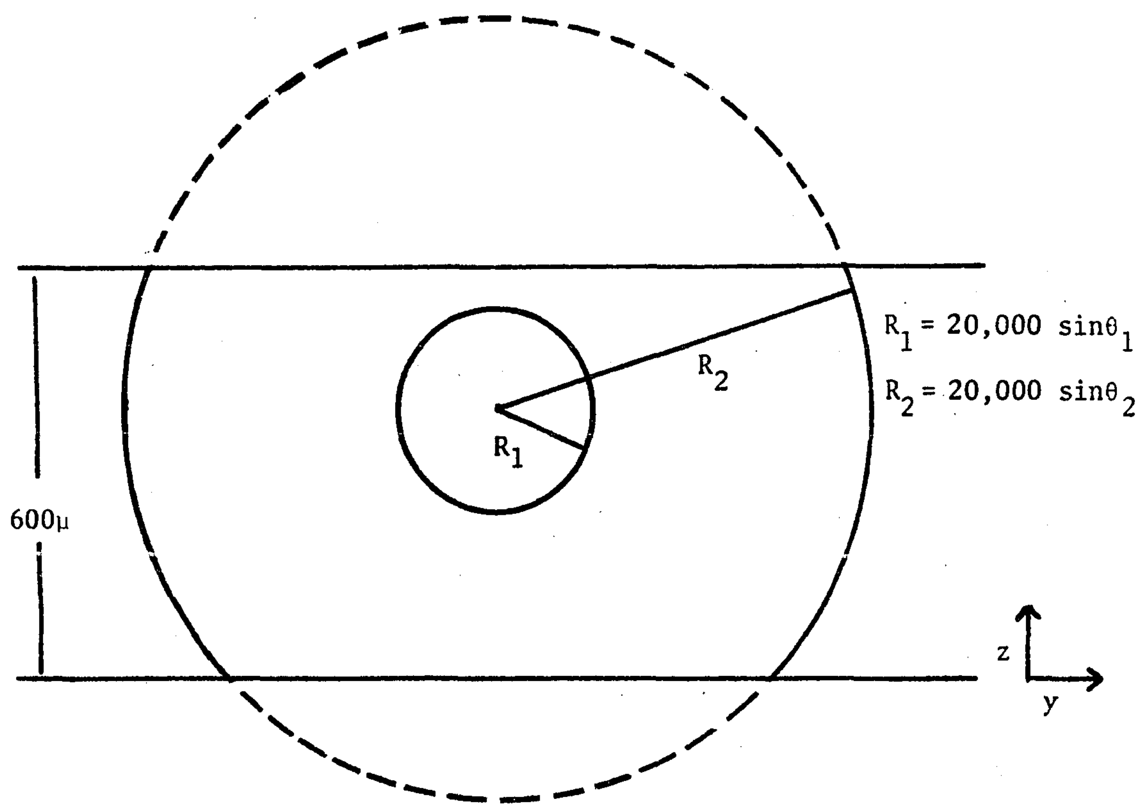

(b)

Figure 23. (a) Diagram of a cone produced by shower particles, all with a space angle θ

(b) Cone bases for two space angles θ_1 and θ_2 such that $\theta_2 > \theta_1$.

Table 6

GEOMETRICAL WEIGHTS

Space Angle (Degrees)	Probability for Track Selection (Per Cent)
.1	100.0
.2	100.0
.3	100.0
.4	97.6
.5	93.9
.6	89.7
.7	84.4
.8	79.5
.9	73.2
1.0	67.2
2.0	28.8
3.0	18.6
4.0	13.8
5.0	11.0
6.0	9.2
7.0	7.9
8.0	6.9
9.0	6.1

The weighted pion and kaon positive χ distributions are displayed in Figs. 24 and 25. The pion distribution may be described by the exponential $d\sigma/d\chi \simeq Ce^{-5\chi}$. The kaon distribution does not, however, display this simple exponential behavior. There is a shoulder appearing at $\chi \simeq .3$. It should be pointed out that the region of kaon-proton overlap does not contribute events for $\chi \gtrsim .2$, and accordingly can not contribute to this enhancement. It appears that the bulk of the

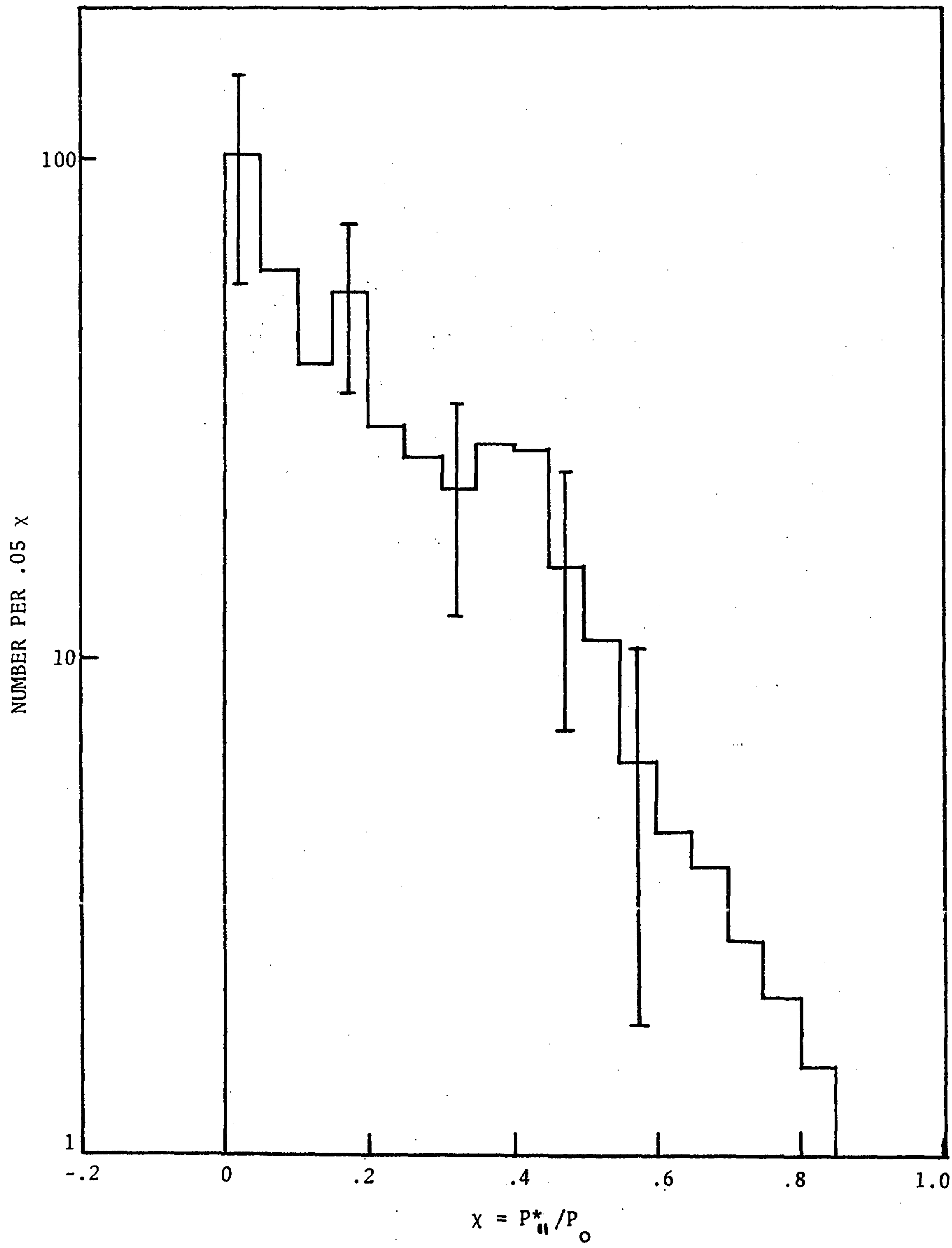

Figure 24. Weighted pion distribution.

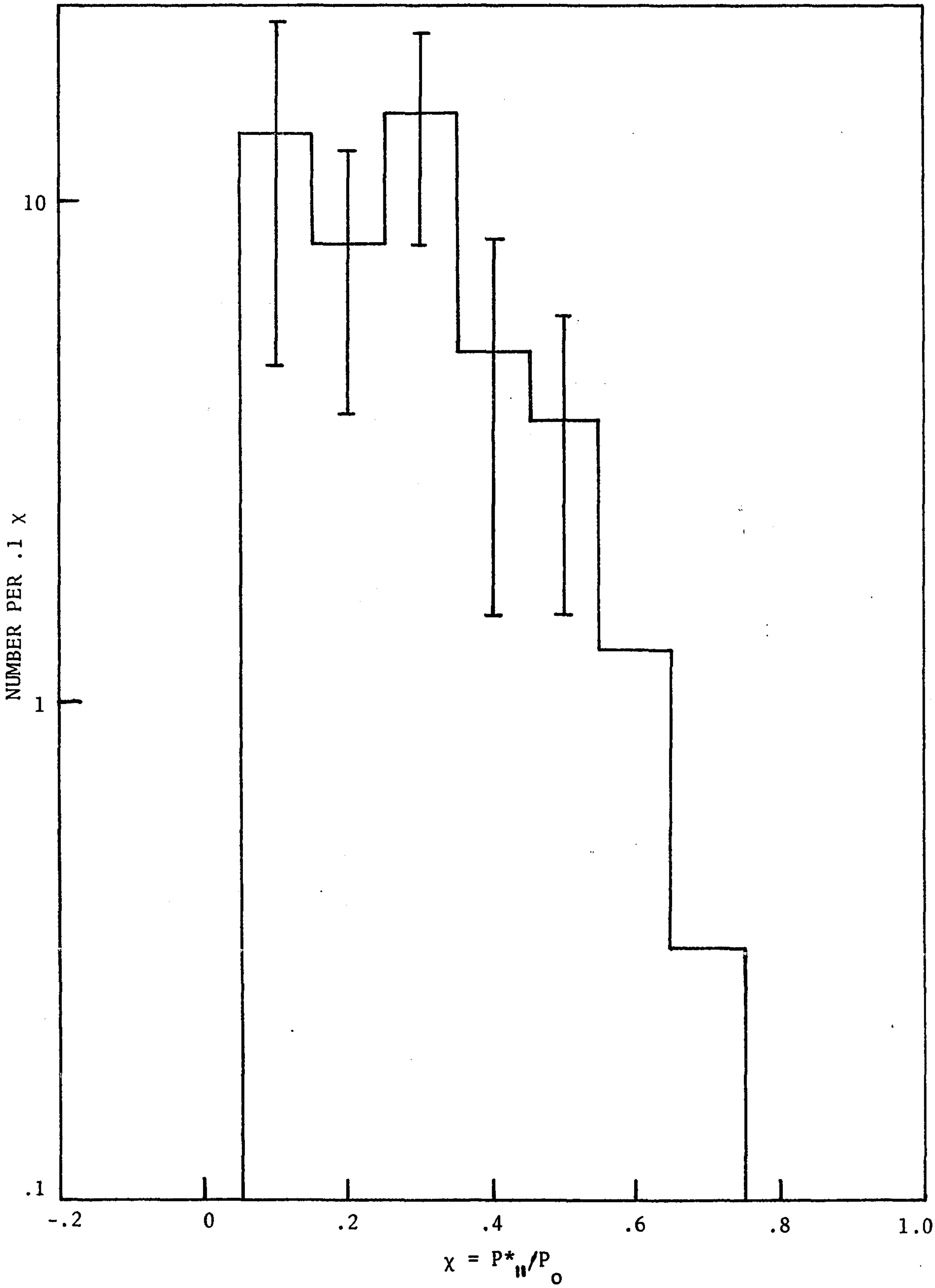

Figure 25. Weighted kaon distribution.

identified kaons contributes to the $.2 \leq \chi \leq .4$ region of the χ distribution.

The K_{ch}/Π_{ch} ratio is computed using the weighted kaon and pion distributions and is plotted as a function of the variable χ in Fig. 26. Although the statistical errors are quite large, an enhancement in the K_{ch}/Π_{ch} ratio is clearly seen in the region of $\chi \approx .3$.

These results give evidence for greater production of fast forward kaons than previously recognized for pion-nucleon collisions. This could indicate the formation of a meson resonance during the collision process which then continues on as a leading particle and subsequently decays with a rather large $K\bar{K}$ branching ratio.

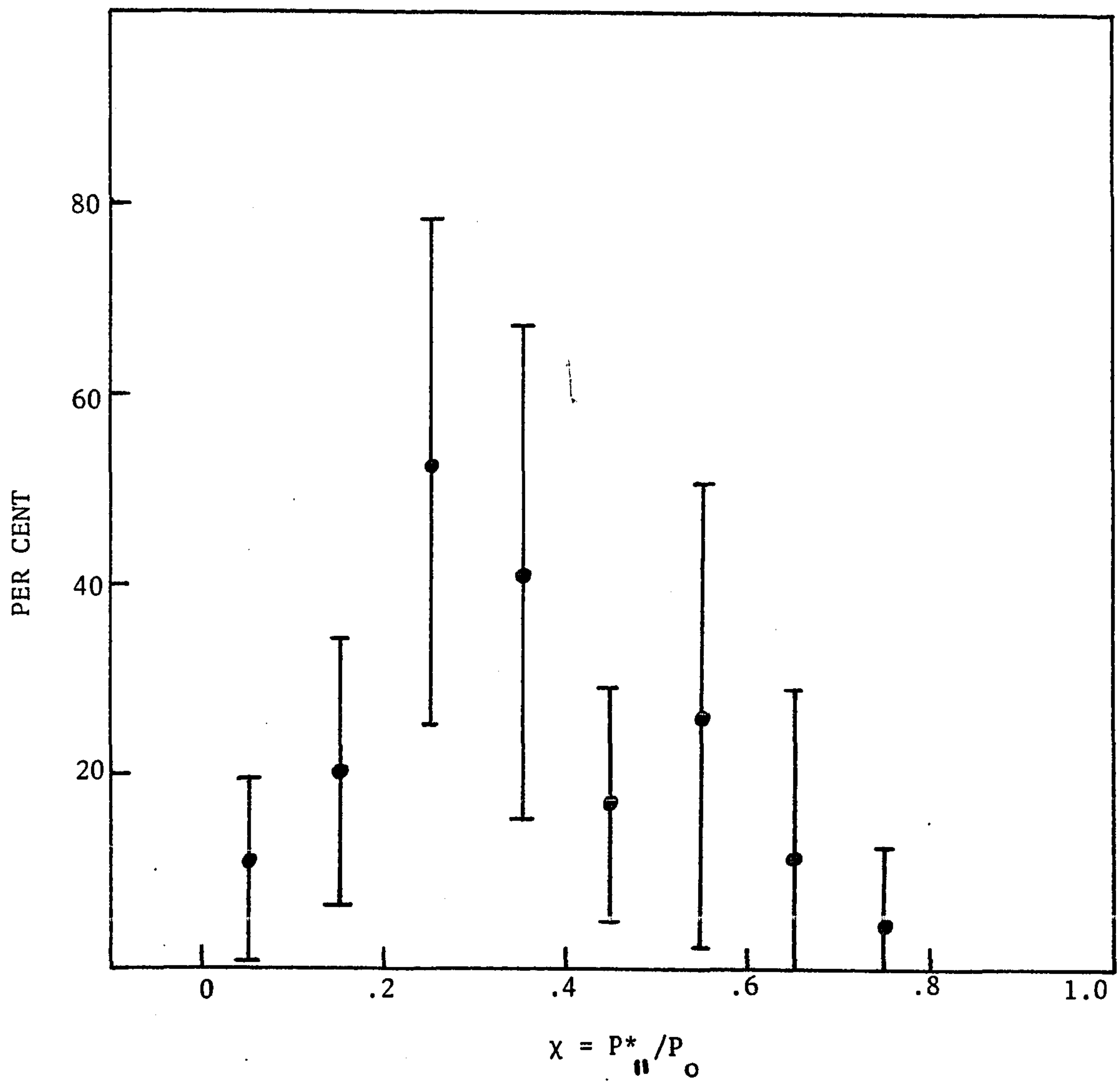

Figure 26. Ratio of charged kaons to charged pions (K_{ch}/Π_{ch})

CHAPTER VI

SUMMARY AND CONCLUSIONS

The experimental procedure used in this work differs from previous experiments in that the grain densities of relativistic particle tracks have been determined directly from the measured gap length distributions. No knowledge of individual scanner characteristics which are incorporated in a resolution parameter α is required. These parameters may, however, be found for each measurement and observations made as to how they vary for each scanner. The resolution parameters can then be used to calculate alternate values of the grain density which, when combined with the original, yield a composite grain density that has a reduced error spread.

It is found that a serious difficulty encountered in this type of experiment is the determination of the normalization of the grain density. In addition to previously recognized factors which can cause the grain density of tracks to vary, we find that idiosyncrasies of the observer can also influence the determination of grain densities. An individual can measure the same track at different times in the course of the experiment and get different results. Apparently the criteria as to what constitutes a developed grain along the path of particle changes for each scanner as the experiment progresses. Remeasuring of standard tracks throughout the run of an experiment would be of great help in determining the nature of the normalization change.

The track selection was confined largely to fast forward charged particles produced in π^--nucleon collisions. We find that the bulk of these particles are pions with kaons and possibly some electrons included. These electrons most likely originate from π° decays. There is no evidence for protons being emitted with $P_{lab} > 4$ GeV/c. Most of the non-pions with $P_{lab} > 4$ GeV/c appear to be kaons.

We enumerate the major conclusions of this experiment.

(1) For Ilford K-5 emulsion, the grain density of singly charged particles is well described by the Sternheimer equation with the parameter T_{max} = 100 KeV.

(2) Great care must be taken in order to achieve a normalization accuracy of ~1%. Grain densities vary by about 15% from top to bottom in the emulsion pellicle. The grain density, as measured, can change for each scanner as the experiment progresses. Two months may be required before the grain density measurements reach an asymptotic level. The resolution parameter α also can vary during the course of the experiment.

(3) Evidence, though not compelling, does exist for a greater abundance of electrons found among the fast forward particles than would be expected from previous experimental evidence.

(4) Considerable evidence exists for a larger number of kaons emitted in the forward direction of pion-nucleon collisions than has been previously recognized.

BIBLIOGRAPHY

1. A. J. Swinnerton and C. Waller. *Sci.Et Ind.Phot.* *2*, 28, 481 (1957).

2. P. D. Bharadwaj and P. L. Jain. *Nuovo Cimento 55A*, 765 (1968).

3. B. Bhowmik and R. K. Shivpuri. *Phys. Rev. 160*, 5, 1227 (1967).

4. A. A. Kamel and G. K. Rao. *Nuclear Physics B2*, 135 (1967).

5. A. A. Kamel, *et al. Nuclear Physics B6*, 523 (1968).

6. J. Samimi. Ph.D. Dissertation, University of Oklahoma (1969).

7. H. Bethe. *Ann. Physik 7*, 5, 325 (1930).

8. F. Bloch. *Z. Physik 81*, 363 (1933).

9. H. J. Bhabha. *Pro. Roy. Soc. A164*, 257 (1937).

10. H. Messel and D. M. Ritson. *Phil. Mag. 7*, 41, 1129 (1950).

11. G. Alexander and R.H.W. Johnston. *Nuovo Cimento 10*, 5, 363 (1957).

12. B. Jongejans. *Nuovo Cimento 16*, 4, 625 (1960).

13. B. Rossi. *High Energy Physics.* New York: Prentice-Hall (1952).

14. H. Bethe. *Z. Physik 76*, 293 (1932).

15. R. M. Sternheimer. *Phys. Rev. 88*, 851 (1952); *91*, 256 (1953); *93*, 351, 1434 (1954).

16. R. M. Sternheimer. *Phys. Rev. 103*, 3, 511 (1956).

17. E. Pickup and L. Voyvodic. *Phys. Rev. 80*, 89 (1950).

18. Particle Data Group. *Rev. Mod. Phys. 42*, 1, 87 (Jan. 1970).

19. C. O'Ceallaigh. *Nuovo Cimento Suppl. 12*, 412 (1954).

20. W. H. Barkas. *Nuclear Research Emulsions.* New York: Academic Press (1963).

21. A. J. Herz and B. Stiller. *Vth International Conference on Nuclear Photography Cern.*, IX-23 (1965).

22. J. Bartke, *et al. Nuovo Cimento 24,* 5, 876 (1962).

23. W. Galbraith, *et al. Phys. Rev. 138B,* 913 (1965).

24. R. Honecker, *et al. Nuclear Physics B13,* 571 (1969).

APPENDIX A

TABLES OF $P\beta$ vs g^*

TABLE OF PBETA VS G* FOR 16.2 GEV PIONS

TMAX=1.0 KEV

PB/M	PB(PION)	PB(KAON)	PB(PROTON)	PB(SIGMA)	PB(DEUT)	G*
0.1	0.01396	0.04938	0.09383	0.11973	0.18755	4.72464
0.2	0.02792	0.09876	0.18765	0.23946	0.37511	2.77012
0.3	0.04187	0.14815	0.28148	0.35920	0.56266	2.05626
0.4	0.05583	0.19753	0.37530	0.47893	0.75022	1.63451
0.5	0.06979	0.24691	0.46913	0.59866	0.93777	1.45739
0.6	0.08375	0.29629	0.56295	0.71839	1.12532	1.30537
0.7	0.09770	0.34567	0.65678	0.83812	1.31288	1.19749
0.8	0.11166	0.39506	0.75060	0.95786	1.50043	1.11778
0.9	0.12562	0.44444	0.84443	1.07759	1.68799	1.05715
1.0	0.13958	0.49382	0.93826	1.19732	1.87554	1.01003
1.1	0.15354	0.54320	1.03208	1.31705	2.06309	0.97280
1.2	0.16749	0.59258	1.12591	1.43678	2.25065	0.94303
1.3	0.18145	0.64197	1.21973	1.55652	2.43820	0.91899
1.4	0.19541	0.69135	1.31356	1.67625	2.62576	0.89945
1.5	0.20937	0.74073	1.40738	1.79598	2.81331	0.88348
1.6	0.22332	0.79011	1.50121	1.91571	3.00086	0.87040
1.7	0.23728	0.83949	1.59504	2.03544	3.18842	0.85966
1.8	0.25124	0.88888	1.68886	2.15518	3.37597	0.84978
1.9	0.26520	0.93826	1.78269	2.27491	3.56353	0.84322
2.0	0.27916	0.98764	1.87651	2.39464	3.75108	0.83781
2.1	0.29311	1.03702	1.97034	2.51437	3.93863	0.83336
2.2	0.30707	1.08640	2.06416	2.63410	4.12619	0.82973
2.3	0.32103	1.13579	2.15799	2.75384	4.31374	0.82678
2.4	0.33499	1.18517	2.25181	2.87357	4.50130	0.82442
2.5	0.34894	1.23455	2.34564	2.99330	4.68885	0.82255
2.6	0.36290	1.28393	2.43947	3.11303	4.87640	0.82111
2.7	0.37686	1.33331	2.53329	3.23276	5.06396	0.82004
2.8	0.39082	1.38270	2.62712	3.35250	5.25151	0.81928
2.9	0.40478	1.43208	2.72094	3.47223	5.43907	0.81879
3.0	0.41873	1.48146	2.81477	3.59196	5.62662	0.81854
3.1	0.43269	1.53084	2.90859	3.71169	5.81417	0.81848
3.2	0.44665	1.58022	3.00242	3.83142	6.00173	0.81860
3.3	0.46061	1.62961	3.09624	3.95116	6.18928	0.81887
3.4	0.47457	1.67899	3.19007	4.07089	6.37684	0.81927
3.5	0.48852	1.72837	3.28390	4.19062	6.56439	0.81978
3.6	0.50248	1.77775	3.37772	4.31035	6.75194	0.82038
3.7	0.51644	1.82713	3.47155	4.43008	6.93950	0.82107
3.8	0.53040	1.87652	3.56537	4.54982	7.12705	0.82184
3.9	0.54435	1.92590	3.65920	4.66955	7.31461	0.82266
4.0	0.55831	1.97528	3.75302	4.78928	7.50216	0.82354
4.1	0.57227	2.02466	3.84685	4.90901	7.68971	0.82446
4.2	0.58623	2.07404	3.94068	5.02874	7.87727	0.82542
4.3	0.60019	2.12343	4.03450	5.14848	8.06482	0.82641
4.4	0.61414	2.17281	4.12833	5.26821	8.25238	0.82743
4.5	0.62810	2.22219	4.22215	5.38794	8.43993	0.82847
4.6	0.64206	2.27157	4.31598	5.50767	8.62748	0.82953
4.7	0.65602	2.32095	4.40980	5.62740	8.81504	0.83060
4.8	0.66997	2.37034	4.50363	5.74714	9.00259	0.83169
4.9	0.68393	2.41972	4.59745	5.86687	9.19015	0.83278
5.0	0.69789	2.46910	4.69128	5.98660	9.37770	0.83388

PB/M	PB(PION)	PB(KAON)	PB(PROTON)	PB(SIGMA)	PB(DEUT)	G*
5.5	0.76768	2.71601	5.16041	6.58526	10.31547	0.83942
6.0	0.83747	2.96292	5.62954	7.18392	11.25324	0.84439
6.5	0.90726	3.20983	6.09866	7.78258	12.19101	0.85018
7.0	0.97705	3.45674	6.56779	8.38124	13.12878	0.85525
7.5	1.04683	3.70365	7.03692	8.97990	14.06655	0.86003
8.0	1.11662	3.95056	7.50605	9.57856	15.00432	0.86467
8.5	1.18641	4.19747	7.97518	10.17722	15.94209	0.86902
9.0	1.25620	4.44438	8.44430	10.77588	16.87936	0.87313
9.5	1.32599	4.69129	8.91343	11.37454	17.81763	0.87703
10.0	1.39578	4.93820	9.38256	11.97320	18.75540	0.88072
10.5	1.46557	5.18511	9.85169	12.57186	19.69317	0.88423
11.0	1.53536	5.43202	10.32082	13.17052	20.63094	0.88755
11.5	1.60515	5.67893	10.78994	13.76918	21.56871	0.89071
12.0	1.67494	5.92584	11.25907	14.36784	22.50648	0.89371
12.5	1.74472	6.17275	11.72820	14.96650	23.44425	0.89657
13.0	1.81451	6.41966	12.19733	15.56516	24.38202	0.89930
13.5	1.88430	6.66657	12.66646	16.16382	25.31979	0.90190
14.0	1.95409	6.91348	13.13558	16.76248	26.25756	0.90438
14.5	2.02388	7.16039	13.60471	17.36114	27.19533	0.90676
15.0	2.09367	7.40730	14.07384	17.95980	28.13310	0.90904
16.0	2.23325	7.90112	15.01210	19.15712	30.00864	0.91331
17.0	2.37283	8.39494	15.95035	20.35444	31.88418	0.91725
18.0	2.51240	8.88876	16.88861	21.55176	33.75972	0.92089
19.0	2.65198	9.38258	17.82686	22.74908	35.63526	0.92427
20.0	2.79156	9.87640	18.76512	23.94640	37.51080	0.92742
21.0	2.93114	10.37022	19.70338	25.14372	39.38634	0.93036
22.0	3.07072	10.86404	20.64163	26.34104	41.26188	0.93312
23.0	3.21029	11.35786	21.57989	27.53836	43.13742	0.93570
24.0	3.34987	11.85168	22.51814	28.73568	45.01296	0.93813
25.0	3.48945	12.34550	23.45640	29.93300	46.88850	0.94043
26.0	3.62903	12.83932	24.39466	31.13032	48.76404	0.94259
27.0	3.76861	13.33314	25.33291	32.32764	50.63958	0.94464
28.0	3.90818	13.82696	26.27117	33.52496	52.51512	0.94659
29.0	4.04776	14.32078	27.20942	34.72228	54.39066	0.94843
30.0	4.18734	14.81460	28.14768	35.91960	56.26620	0.95019
40.0	5.58312	19.75280	37.53024	47.89280	75.02160	0.96401
50.0	6.97890	24.69100	46.91280	59.86600	93.77700	0.97343
60.0	8.37468	29.62920	56.29536	71.83920	112.53240	0.98033
70.0	9.77046	34.56740	65.67792	83.81240	131.28780	0.98563
80.0	11.16624	39.50560	75.06048	95.78560	150.04320	0.98985
90.0	12.56202	44.44380	84.44304	107.75880	168.79360	0.99329
100.0	13.95780	49.38200	93.82560	119.73200	187.55400	0.99616
110.0	15.35358	54.32020	103.20816	131.70520	206.30940	0.99860
120.0	16.74936	59.25840	112.59072	143.67840	225.06480	1.00069
130.0	18.14514	64.19660	121.97328	155.65160	243.82020	1.00251
140.0	19.54092	69.13480	131.35584	167.62480	262.57560	1.00411
150.0	20.93670	74.07300	140.73840	179.59800	281.33100	1.00552
160.0	22.33248	79.01120	150.12096	191.57120	300.08640	1.00678
170.0	23.72826	83.94940	159.50352	203.54440	318.84180	1.00791
180.0	25.12404	88.88760	168.88608	215.51760	337.59720	1.00893
190.0	26.51982	93.82580	178.26864	227.49080	356.35260	1.00986

TABLE OF PBETA VS G* FOR 16.2 GEV PIONS

TMAX=2.0 KEV

PB/M	PB(PION)	PB(KAON)	PB(PROTON)	PB(SIGMA)	PB(DEUT)	G*
0.1	0.01396	0.04938	0.09383	0.11973	0.18755	5.02533
0.2	0.02792	0.09876	0.18765	0.23946	0.37511	2.91324
0.3	0.04187	0.14815	0.28148	0.35920	0.56266	2.15052
0.4	0.05583	0.19753	0.37530	0.47893	0.75022	1.75542
0.5	0.06979	0.24691	0.46913	0.59866	0.93777	1.51475
0.6	0.08375	0.29629	0.56295	0.71839	1.12532	1.35393
0.7	0.09770	0.34567	0.65678	0.83812	1.31288	1.23959
0.8	0.11166	0.39506	0.75060	0.95736	1.50043	1.15563
0.9	0.12562	0.44444	0.84443	1.07759	1.68799	1.09150
1.0	0.13958	0.49332	0.93826	1.19732	1.87554	1.04161
1.1	0.15354	0.54320	1.03208	1.31705	2.06309	1.00214
1.2	0.16749	0.59258	1.12591	1.43678	2.25065	0.97050
1.3	0.18145	0.64197	1.21973	1.55652	2.43820	0.94466
1.4	0.19541	0.69135	1.31356	1.67625	2.62576	0.92399
1.5	0.20937	0.74073	1.40738	1.79598	2.81331	0.90635
1.6	0.22332	0.79011	1.50121	1.91571	3.00086	0.89273
1.7	0.23728	0.83949	1.59504	2.03544	3.18842	0.88108
1.8	0.25124	0.88888	1.68886	2.15518	3.37597	0.87044
1.9	0.26520	0.93826	1.78269	2.27491	3.56353	0.86310
2.0	0.27916	0.98764	1.87651	2.39464	3.75108	0.85700
2.1	0.29311	1.03702	1.97034	2.51437	3.93863	0.85191
2.2	0.30707	1.08640	2.06416	2.63410	4.12619	0.84770
2.3	0.32103	1.13579	2.15799	2.75384	4.31374	0.84422
2.4	0.33499	1.18517	2.25181	2.87357	4.50130	0.84137
2.5	0.34894	1.23455	2.34564	2.99330	4.68885	0.83906
2.6	0.36290	1.28393	2.43947	3.11303	4.87640	0.83720
2.7	0.37686	1.33331	2.53329	3.23276	5.06396	0.83574
2.8	0.39082	1.38270	2.62712	3.35250	5.25151	0.83461
2.9	0.40478	1.43208	2.72094	3.47223	5.43907	0.83378
3.0	0.41873	1.48146	2.81477	3.59196	5.62662	0.83320
3.1	0.43269	1.53084	2.90859	3.71169	5.81417	0.83285
3.2	0.44665	1.58022	3.00242	3.83142	6.00173	0.83268
3.3	0.46061	1.62961	3.09624	3.95116	6.18928	0.83267
3.4	0.47457	1.67899	3.19007	4.07089	6.37684	0.83281
3.5	0.48852	1.72837	3.28390	4.19062	6.56439	0.83308
3.6	0.50248	1.77775	3.37772	4.31035	6.75194	0.83345
3.7	0.51644	1.82713	3.47155	4.43008	6.93950	0.83392
3.8	0.53040	1.87652	3.56537	4.54982	7.12705	0.83447
3.9	0.54435	1.92590	3.65920	4.66955	7.31461	0.83509
4.0	0.55831	1.97528	3.75302	4.78928	7.50216	0.83577
4.1	0.57227	2.02466	3.84685	4.90901	7.68971	0.83650
4.2	0.58623	2.07404	3.94068	5.02874	7.87727	0.83728
4.3	0.60019	2.12343	4.03450	5.14848	8.06482	0.83810
4.4	0.61414	2.17281	4.12833	5.26821	8.25238	0.83895
4.5	0.62810	2.22219	4.22215	5.38794	8.43993	0.83983
4.6	0.64206	2.27157	4.31598	5.50767	8.62748	0.84073
4.7	0.65602	2.32095	4.40980	5.62740	8.81504	0.84165
4.8	0.66997	2.37034	4.50363	5.74714	9.00259	0.84259
4.9	0.68393	2.41972	4.59745	5.86687	9.19015	0.84355
5.0	0.69789	2.46910	4.69128	5.98660	9.37770	0.84451

PB/M	PB(PION)	PB(KAON)	PB(PROTON)	PB(SIGMA)	PB(DEUT)	G*
5.5	0.76768	2.71601	5.16041	6.58526	10.31547	0.84943
6.0	0.83747	2.96292	5.62954	7.18392	11.25324	0.85435
6.5	0.90726	3.20983	6.09866	7.78258	12.19101	0.85916
7.0	0.97705	3.45674	6.56779	8.38124	13.12878	0.86381
7.5	1.04683	3.70365	7.03692	8.97990	14.06655	0.86826
8.0	1.11662	3.95056	7.50605	9.57856	15.00432	0.87250
8.5	1.18641	4.19747	7.97518	10.17722	15.94209	0.87653
9.0	1.25620	4.44438	8.44430	10.77588	16.87986	0.88035
9.5	1.32599	4.69129	8.91343	11.37454	17.81763	0.88399
10.0	1.39578	4.93820	9.38256	11.97320	18.75540	0.88743
10.5	1.46557	5.18511	9.85169	12.57186	19.69317	0.89071
11.0	1.53536	5.43202	10.32082	13.17052	20.63094	0.89382
11.5	1.60515	5.67893	10.78994	13.76918	21.56871	0.89677
12.0	1.67494	5.92584	11.25907	14.36784	22.50648	0.89959
12.5	1.74472	6.17275	11.72820	14.96650	23.44425	0.90227
13.0	1.81451	6.41966	12.19733	15.56516	24.38202	0.90483
13.5	1.88430	6.66657	12.66646	16.16382	25.31979	0.90728
14.0	1.95409	6.91348	13.13558	16.76248	26.25756	0.90961
14.5	2.02388	7.16039	13.60471	17.36114	27.19533	0.91185
15.0	2.09367	7.40730	14.07384	17.95980	28.13310	0.91399
16.0	2.23325	7.90112	15.01210	19.15712	30.00864	0.91801
17.0	2.37283	8.39494	15.95035	20.35444	31.88418	0.92172
18.0	2.51240	8.88876	16.88861	21.55176	33.75972	0.92516
19.0	2.65198	9.38258	17.82686	22.74908	35.63526	0.92835
20.0	2.79156	9.87640	18.76512	23.94640	37.51080	0.93132
21.0	2.93114	10.37022	19.70338	25.14372	39.38634	0.93409
22.0	3.07072	10.86404	20.64163	26.34104	41.26188	0.93669
23.0	3.21029	11.35786	21.57989	27.53836	43.13742	0.93914
24.0	3.34987	11.85168	22.51814	28.73568	45.01296	0.94143
25.0	3.48945	12.34550	23.45640	29.93300	46.88850	0.94360
26.0	3.62903	12.83932	24.39466	31.13032	48.76404	0.94565
27.0	3.76861	13.33314	25.33291	32.32764	50.63958	0.94759
28.0	3.90818	13.82696	26.27117	33.52496	52.51512	0.94942
29.0	4.04776	14.32078	27.20942	34.72228	54.39066	0.95117
30.0	4.18734	14.81460	28.14768	35.91960	56.26620	0.95283
40.0	5.58312	19.75280	37.53024	47.89280	75.02160	0.96591
50.0	6.97890	24.69100	46.91280	59.86600	93.77700	0.97483
60.0	8.37468	29.62920	56.29536	71.83920	112.53240	0.98136
70.0	9.77046	34.56740	65.67792	83.81240	131.28780	0.98638
80.0	11.16624	39.50560	75.06048	95.78560	150.04320	0.99038
90.0	12.56202	44.44380	84.44304	107.75880	168.79860	0.99364
100.0	13.95780	49.38200	93.82560	119.73200	187.55400	0.99636
110.0	15.35358	54.32020	103.20816	131.70520	206.30940	0.99867
120.0	16.74936	59.25840	112.59072	143.67840	225.06480	1.00065
130.0	18.14514	64.19660	121.97328	155.65160	243.82020	1.00238
140.0	19.54092	69.13480	131.35584	167.62480	262.57560	1.00389
150.0	20.93670	74.07300	140.73840	179.59800	281.33100	1.00523
160.0	22.33248	79.01120	150.12096	191.57120	300.08640	1.00643
170.0	23.72826	83.94940	159.50352	203.54440	318.84180	1.00750
180.0	25.12404	88.88760	168.88608	215.51760	337.59720	1.00847
190.0	26.51982	93.82580	178.26864	227.49080	356.35260	1.00935

TABLE OF PBETA VS G* FOR 16.2 GEV PIONS

TMAX=5.0 KEV

PB/M	PB(PION)	PB(KAON)	PB(PROTON)	PB(SIGMA)	PB(DEUT)	G*
0.1	0.01396	0.04938	0.09383	0.11973	0.18755	5.37795
0.2	0.02792	0.09876	0.18765	0.23946	0.37511	3.08107
0.3	0.04187	0.14815	0.28148	0.35920	0.56266	2.26106
0.4	0.05583	0.19753	0.37530	0.47893	0.75022	1.83858
0.5	0.06979	0.24691	0.46913	0.59866	0.93777	1.58202
0.6	0.08375	0.29629	0.56295	0.71839	1.12532	1.41087
0.7	0.09770	0.34567	0.65678	0.83812	1.31288	1.28960
0.8	0.11166	0.39506	0.75060	0.95786	1.50043	1.20001
0.9	0.12562	0.44444	0.84443	1.07759	1.68799	1.13179
1.0	0.13958	0.49382	0.93826	1.19732	1.87554	1.07865
1.1	0.15354	0.54320	1.03208	1.31705	2.06309	1.03654
1.2	0.16749	0.59258	1.12591	1.43678	2.25065	1.00271
1.3	0.18145	0.64197	1.21973	1.55652	2.43820	0.97525
1.4	0.19541	0.69135	1.31356	1.67625	2.62576	0.95277
1.5	0.20937	0.74073	1.40738	1.79598	2.81331	0.93425
1.6	0.22332	0.79011	1.50121	1.91571	3.00086	0.91893
1.7	0.23728	0.83949	1.59504	2.03544	3.18842	0.90620
1.8	0.25124	0.88888	1.68886	2.15518	3.37597	0.89466
1.9	0.26520	0.93826	1.78269	2.27491	3.56353	0.88642
2.0	0.27916	0.98764	1.87651	2.39464	3.75108	0.87949
2.1	0.29311	1.03702	1.97034	2.51437	3.93863	0.87367
2.2	0.30707	1.08640	2.06416	2.63410	4.12619	0.86878
2.3	0.32103	1.13579	2.15799	2.75384	4.31374	0.86468
2.4	0.33499	1.18517	2.25181	2.87357	4.50130	0.86126
2.5	0.34894	1.23455	2.34564	2.99330	4.68885	0.85841
2.6	0.36290	1.28393	2.43947	3.11303	4.87640	0.85607
2.7	0.37686	1.33331	2.53329	3.23276	5.06396	0.85414
2.8	0.39082	1.38270	2.62712	3.35250	5.25151	0.85259
2.9	0.40478	1.43208	2.72094	3.47223	5.43907	0.85136
3.0	0.41873	1.48146	2.81477	3.59196	5.62662	0.85041
3.1	0.43269	1.53084	2.90859	3.71169	5.81417	0.84969
3.2	0.44665	1.58022	3.00242	3.83142	6.00173	0.84919
3.3	0.46061	1.62961	3.09624	3.95116	6.18928	0.84886
3.4	0.47457	1.67899	3.19007	4.07089	6.37684	0.84870
3.5	0.48852	1.72837	3.28390	4.19062	6.56439	0.84868
3.6	0.50248	1.77775	3.37772	4.31035	6.75194	0.84878
3.7	0.51644	1.82713	3.47155	4.43008	6.93950	0.84898
3.8	0.53040	1.87652	3.56537	4.54982	7.12705	0.84928
3.9	0.54435	1.92590	3.65920	4.66955	7.31461	0.84966
4.0	0.55831	1.97528	3.75302	4.78928	7.50216	0.85011
4.1	0.57227	2.02466	3.84685	4.90901	7.68971	0.85062
4.2	0.58623	2.07404	3.94068	5.02874	7.87727	0.85119
4.3	0.60019	2.12343	4.03450	5.14848	8.06482	0.85180
4.4	0.61414	2.17281	4.12833	5.26821	8.25238	0.85246
4.5	0.62810	2.22219	4.22215	5.38794	8.43993	0.85315
4.6	0.64206	2.27157	4.31598	5.50767	8.62748	0.85387
4.7	0.65602	2.32095	4.40980	5.62740	8.81504	0.85461
4.8	0.66997	2.37034	4.50363	5.74714	9.00259	0.85538
4.9	0.68393	2.41972	4.59745	5.86687	9.19015	0.85617
5.0	0.69789	2.46910	4.69128	5.98660	9.37770	0.85698

PB/M	PB(PION)	PB(KAON)	PB(PROTON)	PB(SIGMA)	PB(DEUT)	G*
5.5	0.76768	2.71601	5.16041	6.58526	10.31547	0.86116
6.0	0.83747	2.96292	5.62954	7.18392	11.25324	0.86544
6.5	0.90726	3.20933	6.09866	7.78258	12.19101	0.86970
7.0	0.97705	3.45674	6.56779	8.38124	13.12878	0.87384
7.5	1.04683	3.70365	7.03692	8.97990	14.06655	0.87784
8.0	1.11662	3.95056	7.50605	9.57856	15.00432	0.88168
8.5	1.18641	4.19747	7.97518	10.17722	15.94209	0.88534
9.0	1.25620	4.44438	8.44430	10.77588	16.87986	0.88882
9.5	1.32599	4.69129	8.91343	11.37454	17.81763	0.89214
10.0	1.39578	4.93820	9.38256	11.97320	18.75540	0.89530
10.5	1.46557	5.13511	9.85169	12.57186	19.69317	0.89830
11.0	1.53536	5.43202	10.32082	13.17052	20.63094	0.90116
11.5	1.60515	5.67893	10.78994	13.76918	21.56871	0.90389
12.0	1.67494	5.92584	11.25907	14.36784	22.50648	0.90646
12.5	1.74472	6.17275	11.72820	14.96650	23.44425	0.90896
13.0	1.81451	6.41966	12.19733	15.56516	24.38202	0.91132
13.5	1.88430	6.66657	12.66646	16.16382	25.31979	0.91358
14.0	1.95409	6.91348	13.13558	16.76248	26.25756	0.91574
14.5	2.02388	7.16039	13.60471	17.36114	27.19533	0.91781
15.0	2.09367	7.40730	14.07384	17.95980	28.13310	0.91980
16.0	2.23325	7.90112	15.01210	19.15712	30.00864	0.92353
17.0	2.37283	8.39494	15.95035	20.35444	31.88418	0.92697
18.0	2.51240	8.88876	16.88861	21.55176	33.75972	0.93016
19.0	2.65198	9.38258	17.82686	22.74908	35.63526	0.93312
20.0	2.79156	9.87640	18.76512	23.94640	37.51080	0.93589
21.0	2.93114	10.37022	19.70338	25.14372	39.38634	0.93847
22.0	3.07072	10.86404	20.64163	26.34104	41.26188	0.94089
23.0	3.21029	11.35786	21.57989	27.53836	43.13742	0.94316
24.0	3.34987	11.85168	22.51814	28.73568	45.01296	0.94530
25.0	3.48945	12.34550	23.45640	29.93300	46.88850	0.94732
26.0	3.62903	12.83932	24.39466	31.13032	48.76404	0.94923
27.0	3.76861	13.33314	25.33291	32.32764	50.63958	0.95104
28.0	3.90818	13.82696	26.27117	33.52496	52.51512	0.95275
29.0	4.04776	14.32078	27.20942	34.72228	54.39066	0.95438
30.0	4.18734	14.81460	28.14768	35.91960	56.26620	0.95593
40.0	5.58312	19.75280	37.53024	47.89280	75.02160	0.96813
50.0	6.97890	24.69100	46.91280	59.86600	93.77700	0.97647
60.0	8.37468	29.62920	56.29536	71.83920	112.53240	0.98257
70.0	9.77046	34.56740	65.67792	83.81240	131.28780	0.98727
80.0	11.16624	39.50560	75.06048	95.78560	150.04320	0.99100
90.0	12.56202	44.44380	84.44304	107.75880	168.79860	0.99405
100.0	13.95780	49.38200	93.82560	119.73200	187.55400	0.99660
110.0	15.35358	54.32020	103.20816	131.70520	206.30940	0.99376
120.0	16.74936	59.25840	112.59072	143.67840	225.06480	1.00061
130.0	18.14514	64.19660	121.97328	155.65160	243.82020	1.00222
140.0	19.54092	69.13480	131.35584	167.62480	262.57560	1.00364
150.0	20.93670	74.07300	140.73840	179.59800	281.33100	1.00489
160.0	22.33248	79.01120	150.12096	191.57120	300.08640	1.00601
170.0	23.72826	83.94940	159.50352	203.54440	318.84180	1.00701
160.0	25.12404	88.88760	168.88608	215.51760	337.59720	1.00792
190.0	26.51982	93.82580	178.26864	227.49080	356.35260	1.00874

TABLE OF PBETA VS G* FOR 16.2 GEV PIONS

TMAX= 20.0 KEV

PB/M	PB(PION)	PB(KAON)	PB(PROTON)	PB(SIGMA)	PB(DEUT)	G*
0.1	0.01396	0.04938	0.09383	0.11973	0.18755	5.83337
0.2	0.02792	0.09876	0.18765	0.23946	0.37511	3.29787
0.3	0.04187	0.14815	0.28148	0.35920	0.56266	2.40386
0.4	0.05583	0.19753	0.37530	0.47893	0.75022	1.94603
0.5	0.06979	0.24691	0.46913	0.59866	0.93777	1.66394
0.6	0.08375	0.29629	0.56295	0.71839	1.12532	1.48446
0.7	0.09770	0.34567	0.65678	0.83812	1.31288	1.35335
0.8	0.11166	0.39506	0.75060	0.95786	1.50043	1.25737
0.9	0.12562	0.44444	0.84443	1.07759	1.68799	1.18386
1.0	0.13955	0.49382	0.93826	1.19732	1.87554	1.12653
1.1	0.15354	0.54320	1.03208	1.31705	2.06309	1.08101
1.2	0.16749	0.59258	1.12591	1.43678	2.25065	1.04436
1.3	0.18145	0.64197	1.21973	1.55652	2.43820	1.01451
1.4	0.19541	0.69135	1.31356	1.67625	2.62576	0.98998
1.5	0.20937	0.74073	1.40738	1.79598	2.81331	0.96969
1.6	0.22332	0.79011	1.50121	1.91571	3.00086	0.95280
1.7	0.23728	0.83949	1.59504	2.03544	3.18842	0.93869
1.8	0.25124	0.88888	1.68886	2.15518	3.37597	0.92599
1.9	0.26520	0.93826	1.78269	2.27491	3.56353	0.91657
2.0	0.27916	0.98764	1.87651	2.39464	3.75108	0.90859
2.1	0.29311	1.03702	1.97034	2.51437	3.93863	0.90181
2.2	0.30707	1.08640	2.06416	2.63410	4.12619	0.89604
2.3	0.32103	1.13579	2.15799	2.75384	4.31374	0.89115
2.4	0.33499	1.18517	2.25181	2.87357	4.50130	0.88699
2.5	0.34894	1.23455	2.34564	2.99330	4.68885	0.88346
2.6	0.36290	1.28393	2.43947	3.11303	4.87640	0.88048
2.7	0.37686	1.33331	2.53329	3.23276	5.06396	0.87796
2.8	0.39082	1.38270	2.62712	3.35250	5.25151	0.87586
2.9	0.40478	1.43208	2.72094	3.47223	5.43907	0.87411
3.0	0.41873	1.48146	2.81477	3.59196	5.62662	0.87267
3.1	0.43269	1.53084	2.90859	3.71169	5.81417	0.87149
3.2	0.44665	1.58022	3.00242	3.83142	6.00173	0.87056
3.3	0.46061	1.62961	3.09624	3.95116	6.13928	0.86982
3.4	0.47457	1.67899	3.19007	4.07089	6.37684	0.86927
3.5	0.48852	1.72837	3.28390	4.19062	6.56439	0.86888
3.6	0.50248	1.77775	3.37772	4.31035	6.75194	0.86862
3.7	0.51644	1.82713	3.47155	4.43008	6.93950	0.86849
3.8	0.53040	1.87652	3.56537	4.54982	7.12705	0.86846
3.9	0.54435	1.92590	3.65920	4.66955	7.31461	0.86853
4.0	0.55831	1.97528	3.75302	4.78928	7.50216	0.86869
4.1	0.57227	2.02466	3.84685	4.90901	7.68971	0.86891
4.2	0.58623	2.07404	3.94068	5.02874	7.87727	0.86921
4.3	0.60019	2.12343	4.03450	5.14848	8.06482	0.86956
4.4	0.61414	2.17281	4.12833	5.26821	8.25238	0.86976
4.5	0.62810	2.22219	4.22215	5.38794	8.43993	0.87040
4.6	0.64206	2.27157	4.31598	5.50767	8.62743	0.87089
4.7	0.65602	2.32095	4.40980	5.62740	8.81504	0.87141
4.8	0.66997	2.37034	4.50363	5.74714	9.00259	0.87195
4.9	0.68393	2.41972	4.59745	5.86687	9.19015	0.87253
5.0	0.69789	2.46910	4.69128	5.98660	9.37770	0.87313

PB/M	PB(PIØN)	PB(KAØN)	PB(PRØTØN)	PB(SIGMA)	PB(DEUT)	G*
5.5	0.76768	2.71601	5.16041	6.58526	10.31547	0.87636
6.0	0.83747	2.96292	5.62954	7.18392	11.25324	0.87983
6.5	0.90726	3.20983	6.09866	7.78258	12.19101	0.88336
7.0	0.97705	3.45674	6.56779	8.38124	13.12878	0.88686
7.5	1.04683	3.70365	7.03692	8.97990	14.06655	0.89023
8.0	1.11662	3.95056	7.50605	9.57856	15.00432	0.89359
8.5	1.18641	4.19747	7.97518	10.17722	15.94209	0.89677
9.0	1.25620	4.44438	8.44430	10.77588	16.87986	0.89982
9.5	1.32599	4.69129	8.91343	11.37454	17.81763	0.90274
10.0	1.39578	4.93820	9.38256	11.97320	18.75540	0.90552
10.5	1.46557	5.18511	9.85169	12.57186	19.69317	0.90818
11.0	1.53536	5.43202	10.32082	13.17052	20.63094	0.91071
11.5	1.60515	5.67893	10.78994	13.76918	21.56871	0.91313
12.0	1.67494	5.92584	11.25907	14.36784	22.50648	0.91545
12.5	1.74472	6.17275	11.72820	14.96650	23.44425	0.91766
13.0	1.81451	6.41966	12.19733	15.56516	24.38202	0.91977
13.5	1.88430	6.66657	12.66646	16.16382	25.31979	0.92179
14.0	1.95409	6.91348	13.13558	16.76248	26.25756	0.92373
14.5	2.02388	7.16039	13.60471	17.36114	27.19533	0.92558
15.0	2.09367	7.40730	14.07384	17.95980	28.13310	0.92736
16.0	2.23325	7.90112	15.01210	19.15712	30.00864	0.93071
17.0	2.37283	8.39494	15.95035	20.35444	31.88418	0.93381
18.0	2.51240	8.88876	16.88861	21.55176	33.75972	0.93669
19.0	2.65198	9.38258	17.82686	22.74908	35.63526	0.93936
20.0	2.79156	9.87640	18.76512	23.94640	37.51080	0.94186
21.0	2.93114	10.37022	19.70338	25.14372	39.38634	0.94419
22.0	3.07072	10.86404	20.64163	26.34104	41.26188	0.94638
23.0	3.21029	11.35786	21.57989	27.53836	43.13742	0.94844
24.0	3.34987	11.85168	22.51814	28.73568	45.01296	0.95037
25.0	3.48945	12.34550	23.45640	29.93300	46.88850	0.95220
26.0	3.62903	12.83932	24.39466	31.13032	48.76404	0.95393
27.0	3.76861	13.33314	25.33291	32.32764	50.63958	0.95557
28.0	3.90818	13.82696	26.27117	33.52496	52.51512	0.95712
29.0	4.04776	14.32078	27.20942	34.72228	54.39066	0.95860
30.0	4.18734	14.81460	28.14768	35.91960	56.26620	0.96000
40.0	5.58312	19.75280	37.53024	47.89280	75.02160	0.97108
50.0	6.97890	24.69100	46.91280	59.86600	93.77700	0.97866
60.0	8.37468	29.62920	56.29536	71.83920	112.53240	0.98421
70.0	9.77046	34.56740	65.67792	83.81240	131.28780	0.98849
80.0	11.16624	39.50560	75.06048	95.78560	150.04320	0.99189
90.0	12.56202	44.44380	84.44304	107.75880	168.79860	0.99466
100.0	13.95780	49.38200	93.82560	119.73200	187.55400	0.99698
110.0	15.35358	54.32020	103.20816	131.70520	206.30940	0.99895
120.0	16.74936	59.25840	112.59072	143.67840	225.06480	1.00064
130.0	18.14514	64.19660	121.97328	155.65160	243.82020	1.00211
140.0	19.54092	69.13480	131.35584	167.62480	262.57560	1.00340
150.0	20.93670	74.07300	140.73840	179.59800	281.33100	1.00454
160.0	22.33248	79.01120	150.12096	191.57120	300.08640	1.00556
170.0	23.72826	83.94940	159.50352	203.54440	318.84180	1.00647
180.0	25.12404	88.88760	168.88608	215.51760	337.59720	1.00729
190.0	26.51982	93.82580	178.26864	227.49080	356.35260	1.00804

TABLE OF PBETA VS G* FOR 16.2 GEV PIONS

TMAX= 50.0 KEV

PB/M	PB(PION)	PB(KAON)	PB(PROTON)	PB(SIGMA)	PB(DEUT)	G*
0.1	0.01396	0.04938	0.09383	0.11973	0.18755	6.09226
0.2	0.02792	0.09876	0.18765	0.23946	0.37511	3.42109
0.3	0.04187	0.14815	0.28148	0.35920	0.56266	2.48501
0.4	0.05583	0.19753	0.37530	0.47893	0.75022	2.00708
0.5	0.06979	0.24691	0.46913	0.59866	0.93777	1.71832
0.6	0.08375	0.29629	0.56295	0.71839	1.12532	1.52626
0.7	0.09770	0.34567	0.65678	0.83812	1.31288	1.39035
0.8	0.11166	0.39506	0.75060	0.95786	1.50043	1.28995
0.9	0.12562	0.44444	0.84443	1.07759	1.68799	1.21343
1.0	0.13958	0.49382	0.93826	1.19732	1.87554	1.15372
1.1	0.15354	0.54320	1.03208	1.31705	2.06309	1.10627
1.2	0.16749	0.59258	1.12591	1.43678	2.25065	1.06801
1.3	0.18145	0.64197	1.21973	1.55652	2.43820	1.03630
1.4	0.19541	0.69135	1.31356	1.67625	2.62576	1.01111
1.5	0.20937	0.74073	1.40738	1.79598	2.81331	0.98931
1.6	0.22332	0.79011	1.50121	1.91571	3.00086	0.97203
1.7	0.23728	0.83949	1.59504	2.03544	3.18842	0.95713
1.8	0.25124	0.88888	1.68886	2.15518	3.37597	0.94377
1.9	0.26520	0.93826	1.78269	2.27491	3.56353	0.93369
2.0	0.27916	0.98764	1.87651	2.39464	3.75108	0.92510
2.1	0.29311	1.03702	1.97034	2.51437	3.93863	0.91773
2.2	0.30707	1.08640	2.06416	2.63410	4.12619	0.91152
2.3	0.32103	1.13579	2.15799	2.75384	4.31374	0.90616
2.4	0.33499	1.18517	2.25181	2.87357	4.50130	0.90158
2.5	0.34894	1.23455	2.34564	2.99330	4.68885	0.89767
2.6	0.36290	1.28393	2.43947	3.11303	4.87640	0.89432
2.7	0.37686	1.33331	2.53329	3.23276	5.06396	0.89148
2.8	0.39082	1.38270	2.62712	3.35250	5.25151	0.88906
2.9	0.40478	1.43208	2.72094	3.47223	5.43907	0.88701
3.0	0.41873	1.48146	2.81477	3.59196	5.62662	0.88530
3.1	0.43269	1.53084	2.90859	3.71169	5.81417	0.88386
3.2	0.44665	1.58022	3.00242	3.83142	6.00173	0.88267
3.3	0.46061	1.62961	3.09624	3.95116	6.18928	0.88171
3.4	0.47457	1.67899	3.19007	4.07089	6.37684	0.88093
3.5	0.48852	1.72837	3.28390	4.19062	6.56439	0.88033
3.6	0.50248	1.77775	3.37772	4.31035	6.75194	0.87987
3.7	0.51644	1.82713	3.47155	4.43008	6.93950	0.87954
3.8	0.53040	1.87652	3.56537	4.54982	7.12705	0.87933
3.9	0.54435	1.92590	3.65920	4.66955	7.31461	0.87923
4.0	0.55831	1.97528	3.75302	4.78928	7.50216	0.87921
4.1	0.57227	2.02466	3.84685	4.90901	7.68971	0.87928
4.2	0.58623	2.07404	3.94068	5.02874	7.87727	0.87942
4.3	0.60019	2.12343	4.03450	5.14848	8.06482	0.87962
4.4	0.61414	2.17281	4.12833	5.26821	8.25238	0.87987
4.5	0.62810	2.22219	4.22215	5.38794	8.43993	0.88018
4.6	0.64206	2.27157	4.31598	5.50767	8.62748	0.88053
4.7	0.65602	2.32095	4.40930	5.62740	8.81504	0.88092
4.8	0.66997	2.37034	4.50363	5.74714	9.00259	0.88134
4.9	0.68393	2.41972	4.59745	5.86687	9.19015	0.88180
5.0	0.69789	2.46910	4.69128	5.98660	9.37770	0.88228

PB/M	PB(PION)	PB(KAON)	PB(PROTON)	PB(SIGMA)	PB(DEUT)	G*
5.5	0.76768	2.71601	5.16041	6.58526	10.31547	0.88497
6.0	0.83747	2.96292	5.62954	7.18392	11.25324	0.88797
6.5	0.90726	3.20983	6.09866	7.78258	12.19101	0.89109
7.0	0.97705	3.45674	6.56779	8.38124	13.12878	0.89422
7.5	1.04683	3.70365	7.03692	8.97990	14.06655	0.89732
8.0	1.11662	3.95056	7.50605	9.57856	15.00432	0.90033
8.5	1.18641	4.19747	7.97518	10.17722	15.94209	0.90324
9.0	1.25620	4.44438	8.44430	10.77588	16.87986	0.90604
9.5	1.32599	4.69129	8.91343	11.37454	17.81763	0.90872
10.0	1.39578	4.93820	9.38256	11.97320	18.75540	0.91129
10.5	1.46557	5.18511	9.85169	12.57186	19.69317	0.91375
11.0	1.53536	5.43202	10.32082	13.17052	20.63094	0.91610
11.5	1.60515	5.67893	10.78994	13.76918	21.56871	0.91835
12.0	1.67494	5.92584	11.25907	14.36784	22.50648	0.92050
12.5	1.74472	6.17275	11.72820	14.96650	23.44425	0.92256
13.0	1.81451	6.41966	12.19733	15.56516	24.38202	0.92453
13.5	1.88430	6.66657	12.66646	16.16382	25.31979	0.92642
14.0	1.95409	6.91348	13.13558	16.76248	26.25756	0.92822
14.5	2.02388	7.16039	13.60471	17.36114	27.19533	0.92996
15.0	2.09367	7.40730	14.07384	17.95980	28.13310	0.93162
16.0	2.23325	7.90112	15.01210	19.15712	30.00864	0.93476
17.0	2.37283	8.39494	15.95035	20.35444	31.88418	0.93766
18.0	2.51240	8.88876	16.88861	21.55176	33.75972	0.94036
19.0	2.65198	9.38258	17.82686	22.74908	35.63526	0.94287
20.0	2.79156	9.87640	18.76512	23.94640	37.51080	0.94521
21.0	2.93114	10.37022	19.70338	25.14372	39.38634	0.94740
22.0	3.07072	10.86404	20.64163	26.34104	41.26188	0.94946
23.0	3.21029	11.35786	21.57989	27.53836	43.13742	0.95139
24.0	3.34987	11.85168	22.51814	28.73568	45.01296	0.95321
25.0	3.48945	12.34550	23.45640	29.93300	46.88850	0.95493
26.0	3.62903	12.83932	24.39466	31.13032	48.76404	0.95656
27.0	3.76861	13.33314	25.33291	32.32764	50.63958	0.95810
28.0	3.90818	13.82696	26.27117	33.52496	52.51512	0.95956
29.0	4.04776	14.32078	27.20942	34.72228	54.39066	0.96095
30.0	4.18734	14.81460	28.14768	35.91960	56.26620	0.96227
40.0	5.58312	19.75280	37.53024	47.89280	75.02160	0.97271
50.0	6.97890	24.69100	46.91280	59.86600	93.77700	0.97986
60.0	8.37468	29.62920	56.29536	71.83920	112.53240	0.98510
70.0	9.77046	34.56740	65.67792	83.81240	131.28780	0.98913
80.0	11.16624	39.50560	75.06048	95.78560	150.04320	0.99234
90.0	12.56202	44.44380	84.44304	107.75880	168.79860	0.99496
100.0	13.95780	49.38200	93.82560	119.73200	187.55400	0.99715
110.0	15.35358	54.32020	103.20816	131.70520	206.30940	0.99901
120.0	16.74936	59.25840	112.59072	143.67840	225.06480	1.00060
130.0	18.14514	64.19660	121.97328	155.65160	243.82020	1.00199
140.0	19.54092	69.13480	131.35584	167.62480	262.57560	1.00321
150.0	20.93670	74.07300	140.73840	179.59800	281.33100	1.00428
160.0	22.33248	79.01120	150.12096	191.57120	300.08640	1.00525
170.0	23.72826	83.94940	159.50352	203.54440	318.84180	1.00611
180.0	25.12404	88.88760	168.88608	215.51760	337.59720	1.00689
190.0	26.51982	93.82580	178.26864	227.49080	356.35260	1.00760

TABLE ØF PBETA VS G* FØR 16.2 GEV PIØNS

TMAX=100.0 KEV

PB/M	PB(PIØN)	PB(KAØN)	PB(PRØTØN)	PB(SIGMA)	PB(DEUT)	G*
0.1	0.01396	0.04938	0.09383	0.11973	0.18755	6.26938
0.2	0.02792	0.09876	0.18765	0.23946	0.37511	3.50535
0.3	0.04187	0.14815	0.28148	0.35920	0.56266	2.54049
0.4	0.05583	0.19753	0.37530	0.47893	0.75022	2.04881
0.5	0.06979	0.24691	0.46913	0.59866	0.93777	1.75207
0.6	0.08375	0.29629	0.56295	0.71839	1.12532	1.55482
0.7	0.09770	0.34567	0.65678	0.83812	1.31288	1.41528
0.8	0.11166	0.39506	0.75060	0.95786	1.50043	1.31221
0.9	0.12562	0.44444	0.84443	1.07759	1.68799	1.23363
1.0	0.13958	0.49382	0.93826	1.19732	1.87554	1.17229
1.1	0.15354	0.54320	1.03208	1.31705	2.06309	1.12351
1.2	0.16749	0.59258	1.12591	1.43678	2.25065	1.08415
1.3	0.18145	0.64197	1.21973	1.55652	2.43820	1.05201
1.4	0.19541	0.69135	1.31356	1.67625	2.62576	1.02553
1.5	0.20937	0.74073	1.40738	1.79598	2.81331	1.00353
1.6	0.22332	0.79011	1.50121	1.91571	3.00086	0.98515
1.7	0.23728	0.83949	1.59504	2.03544	3.18842	0.96971
1.8	0.25124	0.88888	1.68886	2.15518	3.37597	0.95590
1.9	0.26520	0.93826	1.78269	2.27491	3.56353	0.94536
2.0	0.27916	0.98764	1.87651	2.39464	3.75108	0.93636
2.1	0.29311	1.03702	1.97034	2.51437	3.93863	0.92866
2.2	0.30707	1.08640	2.06416	2.63410	4.12619	0.92206
2.3	0.32103	1.13579	2.15799	2.75384	4.31374	0.91640
2.4	0.33499	1.18517	2.25181	2.87357	4.50130	0.91153
2.5	0.34894	1.23455	2.34564	2.99330	4.68885	0.90735
2.6	0.36290	1.28393	2.43947	3.11303	4.87640	0.90376
2.7	0.37686	1.33331	2.53329	3.23276	5.06396	0.90068
2.8	0.39082	1.38270	2.62712	3.35250	5.25151	0.89805
2.9	0.40478	1.43208	2.72094	3.47223	5.43907	0.89580
3.0	0.41873	1.48146	2.81477	3.59196	5.62662	0.89389
3.1	0.43269	1.53084	2.90859	3.71169	5.81417	0.89228
3.2	0.44665	1.58022	3.00242	3.83142	6.00173	0.89092
3.3	0.46061	1.62961	3.09624	3.95116	6.18928	0.88979
3.4	0.47457	1.67899	3.19007	4.07089	6.37684	0.88887
3.5	0.48852	1.72837	3.28390	4.19062	6.56439	0.88812
3.6	0.50248	1.77775	3.37772	4.31035	6.75194	0.88752
3.7	0.51644	1.82713	3.47155	4.43008	6.93950	0.88706
3.8	0.53040	1.87652	3.56537	4.54982	7.12705	0.88673
3.9	0.54435	1.92590	3.65920	4.66955	7.31461	0.88650
4.0	0.55831	1.97528	3.75302	4.78928	7.50216	0.88637
4.1	0.57227	2.02466	3.84685	4.90901	7.68971	0.88633
4.2	0.58623	2.07404	3.94068	5.02874	7.87727	0.88636
4.3	0.60019	2.12343	4.03450	5.14848	8.06482	0.88645
4.4	0.61414	2.17281	4.12833	5.26821	8.25238	0.88661
4.5	0.62810	2.22219	4.22215	5.38794	8.43993	0.88682
4.6	0.64206	2.27157	4.31598	5.50767	8.62748	0.88708
4.7	0.65602	2.32095	4.40980	5.62740	8.81504	0.88738
4.8	0.66997	2.37034	4.50363	5.74714	9.00259	0.88772
4.9	0.68393	2.41972	4.59745	5.86687	9.19015	0.88809
5.0	0.69789	2.46910	4.69128	5.98660	9.37770	0.88849

PB/M	PB(PI∅N)	PB(KA∅N)	PB(PR∅T∅N)	PB(SIGMA)	PB(DEUT)	G*
5.5	0.76768	2.71601	5.16041	6.58526	10.31547	0.89081
6.0	0.83747	2.96292	5.62954	7.18392	11.25324	0.89349
6.5	0.90726	3.20983	6.09866	7.78258	12.19101	0.89633
7.0	0.97705	3.45674	6.56779	8.38124	13.12878	0.89921
7.5	1.04683	3.70365	7.03692	8.97990	14.06655	0.90208
8.0	1.11662	3.95056	7.50605	9.57856	15.00432	0.90488
8.5	1.18641	4.19747	7.97518	10.17722	15.94209	0.90760
9.0	1.25620	4.44438	8.44430	10.77588	16.87986	0.91023
9.5	1.32599	4.69129	8.91343	11.37454	17.81763	0.91276
10.0	1.39578	4.93820	9.38256	11.97320	18.75540	0.91519
10.5	1.46557	5.18511	9.85169	12.57186	19.69317	0.91751
11.0	1.53536	5.43202	10.32082	13.17052	20.63094	0.91974
11.5	1.60515	5.67893	10.78994	13.76918	21.56871	0.92187
12.0	1.67494	5.92584	11.25907	14.36784	22.50648	0.92390
12.5	1.74472	6.17275	11.72820	14.96650	23.44425	0.92586
13.0	1.81451	6.41966	12.19733	15.56516	24.38202	0.92773
13.5	1.88430	6.66657	12.66646	16.16382	25.31979	0.92952
14.0	1.95409	6.91348	13.13558	16.76248	26.25756	0.93124
14.5	2.02388	7.16039	13.60471	17.36114	27.19533	0.93289
15.0	2.09367	7.40730	14.07384	17.95980	28.13310	0.93448
16.0	2.23325	7.90112	15.01210	19.15712	30.00864	0.93747
17.0	2.37283	8.39494	15.95035	20.35444	31.88418	0.94024
18.0	2.51240	8.88876	16.88861	21.55176	33.75972	0.94281
19.0	2.65198	9.38258	17.82686	22.74908	35.63526	0.94520
20.0	2.79156	9.87640	18.76512	23.94640	37.51080	0.94744
21.0	2.93114	10.37022	19.70338	25.14372	39.38634	0.94953
22.0	3.07072	10.86404	20.64163	26.34104	41.26188	0.95150
23.0	3.21029	11.35786	21.57989	27.53836	43.13742	0.95335
24.0	3.34987	11.85168	22.51814	28.73568	45.01296	0.95509
25.0	3.48945	12.34550	23.45640	29.93300	46.88850	0.95673
26.0	3.62903	12.83932	24.39466	31.13032	48.76404	0.95829
27.0	3.76861	13.33314	25.33291	32.32764	50.63958	0.95976
28.0	3.90818	13.82696	26.27117	33.52496	52.51512	0.96116
29.0	4.04776	14.32078	27.20942	34.72228	54.39066	0.96249
30.0	4.18734	14.81460	28.14768	35.91960	56.26620	0.96376
40.0	5.58312	19.75280	37.53024	47.89280	75.02160	0.97376
50.0	6.97890	24.69100	46.91280	59.86600	93.77700	0.98061
60.0	8.37468	29.62920	56.29536	71.83920	112.53240	0.98563
70.0	9.77046	34.56740	65.67792	83.31240	131.28780	0.98950
80.0	11.16624	39.50560	75.06048	95.78560	150.04320	0.99258
90.0	12.56202	44.44380	84.44304	107.75880	168.79860	0.99510
100.0	13.95780	49.38200	93.82560	119.73200	187.55400	0.99719
110.0	15.35358	54.32020	103.20816	131.70520	206.30940	0.99897
120.0	16.74936	59.25840	112.59072	143.67840	225.06480	1.00050
130.0	18.14514	64.19660	121.97328	155.65160	243.82020	1.00184
140.0	19.54092	69.13480	131.35584	167.62480	262.57560	1.00300
150.0	20.93670	74.07300	140.73840	179.59800	281.33100	1.00404
160.0	22.33248	79.01120	150.12096	191.57120	300.08640	1.00496
170.0	23.72826	83.94940	159.50352	203.54440	318.84180	1.00579
180.0	25.12404	88.88760	168.88608	215.51760	337.59720	1.00654
190.0	26.51982	93.82580	178.26864	227.49080	356.35260	1.00722

APPENDIX B

CIRCUIT DIAGRAM FOR EXPERIMENT

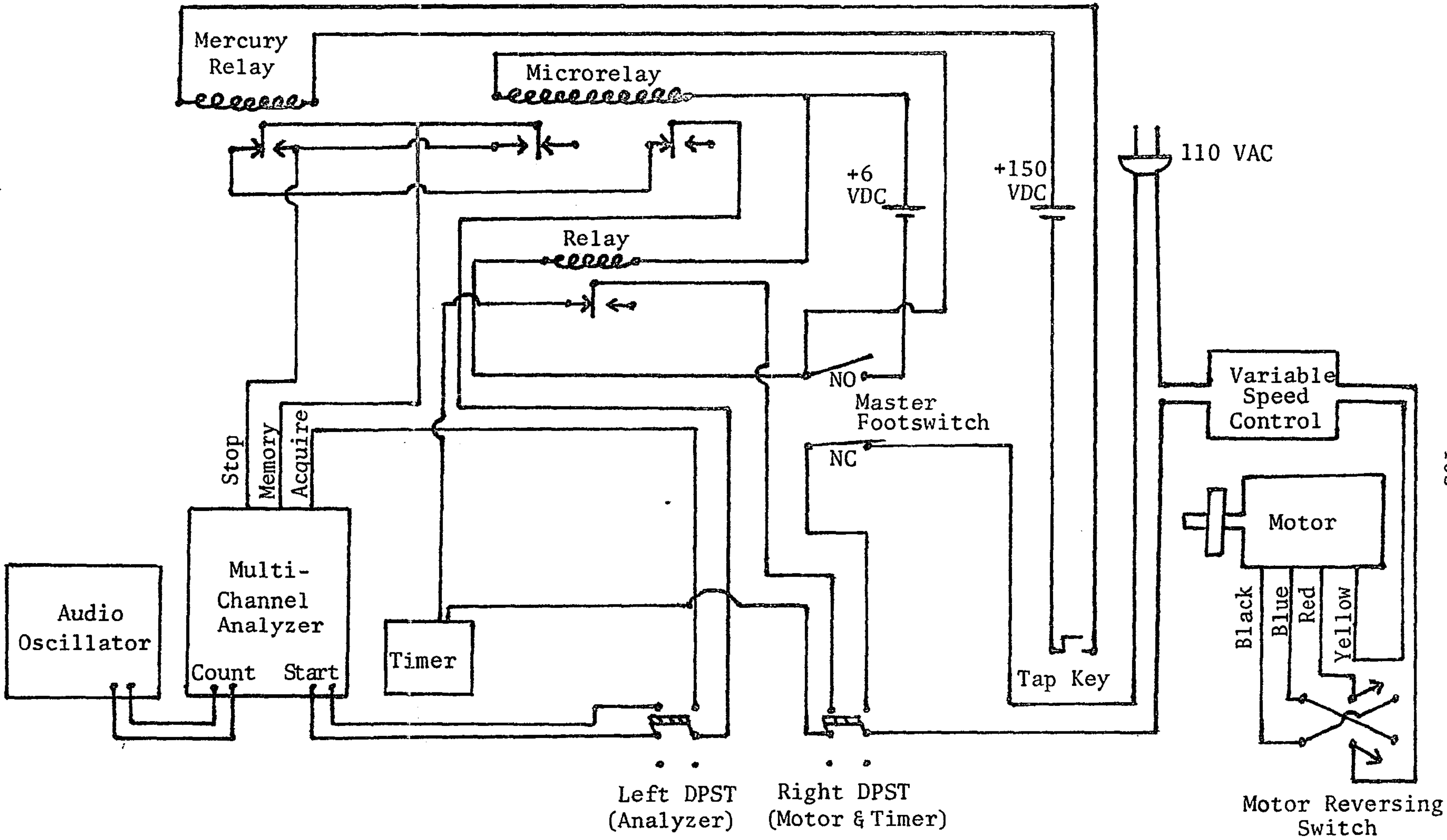
Mercury Relay
Microrelay
Relay
+6 VDC
+150 VDC
110 VAC
NO
Master Footswitch
NC
Variable Speed Control
Motor
Black
Blue
Red
Yellow
Stop
Memory
Acquire
Multi-Channel Analyzer
Count
Start
Audio Oscillator
Timer
Tap Key
Left DPST (Analyzer)
Right DPST (Motor & Timer)
Motor Reversing Switch

APPENDIX C

COMPUTER PROGRAM GDEN

```
C      GDEN      CALCULATION OF G FOR HIGH ENERGY PARTICLES
C      THIS PROGRAM CALCULATES THE TRACK PARAMETERS (G(H),B,L,ALPHA) FOR
C      HIGH ENERGY PARTICLES AND PLOTS THE GAP LENGTH DISTRIBUTION
       DIMENSION Y(260),SY(260),W(260),DY(260),A(5),YP(135)
       INTEGER A,YP
     1 READ(5,2)IDEN,IPR,ITR,ZST,ZEND,X,B,T,DT,CCH,DIP,DIPER,N
       IF(IDEN.EQ.0) STOP
     2 FORMAT(I6,I3,I3,2F4.0,2F5.0,F7.1,F4.2,F7.1,2F5.1,I5)
       LIM=N+1
       READ(5,3)(Y(I),I=1,LIM)
     3 FORMAT(10F7.0)
       SPEED=X/T
       B=(((Y(2)-Y(3))/4.0)+Y(2))/CCH
       BDEN=B/X
       ZAVG=(ZST+ZEND)/2.0
       YSUM=0.0
       DO 4 I=2,LIM
       YSUM=YSUM+Y(I)
       IF(Y(I))101,101,102
   101 W(I)=0.0
       GO TO 4
   102 W(I)=CCH/Y(I)
     4 CONTINUE
       Y(1)=B*CCH
       C=((YSUM+0.5*Y(1))*DT*SPEED/CCH)/X
       GPR=BDEN/C
C      CALCULATE THE BEST FIT FOR THE VARIABLES G AND B
       P1=B
       P2=GPR
       W(1)=1/B
       NN=N
       ITER=0
     5 ITER=ITER+1
       F1=0.0
       F2=0.0
       A11=0.0
       A22=0.0
       A12=0.0
       SSQ=0.0
       DO 6 I=1,LIM
       CI=I-1
       YC=P1*EXP(-P2*CI*DT*SPEED)
       DY(I)=Y(I)/CCH-YC
C      THE FOLLOWING CALCULATIONS APPLY TO THE F=AP MATRIX EQUATION
       F1=F1+DY(I)*W(I)*YC/P1
       F2=F2+DY(I)*W(I)*(-CI*DT*SPEED)*YC
       A11=A11+W(I)*(YC/P1)**2
       A22=A22+W(I)*(-CI*DT*SPEED*YC)**2
       A12=A12+W(I)*(-CI*DT*SPEED)*YC**2/P1
       SY(I)=W(I)*DY(I)*DY(I)
       SSQ=SSQ+SY(I)
     6 CONTINUE
   106 CONTINUE
       XN=NN
```

```
      S=SQRT(SSQ/(XN-1.0))
C     ELIMINATE OBVIOUSLY BAD READINGS BY THROWING AWAY DEVIATIONS > 3.5S
      IN=0
      DO 8 I=1,LIM
      IF(3.5*S-SQRT(SY(I)))7,7,8
    7 NN=NN-1
      IN=IN+1
      F1=F1-CY(I)*W(I)*YC/P1
      F2=F2-CY(I)*W(I)*(-CI*DT*SPEED)*YC
      A11=A11-W(I)*(YC/P1)**2
      A22=A22-W(I)*(-CI*DT*SPEED*YC)**2
      A12=A12-W(I)*(-CI*DT*SPEED)*YC**2/P1
      SSQ=SSQ-SY(I)
      W(I)=0.0
      SY(I)=0.0
    8 CONTINUE
      IF(IN)9,9,106
    9 A21=A12
C     CALCULATE AND TEST THE TWO PARAMETERS B=P1 AND G=P2
      DET=A11*A22-A12*A21
      DP1=(A22*F1-A12*F2)/DET
      DP2=(A11*F2-A21*F1)/DET
      P1=P1+DP1
      P2=P2+DP2
      IF(ABS(DP1)-.01)10,10,5
   10 IF(ABS(DP2)-.00001)11,11,5
C     CALCULATE THE ERRORS FOR THE TWO PARAMETERS
   11 ERP1=S*SQRT(A22/DET)
      ERP2=S*SQRT(A11/DET)
      ALPHA=-ALOG(BDEN/P2)/P2
      DIP=DIP*3.1459/180.0
      GPR=GPR*COS(DIP)
      PG=P2*COS(DIP)
C     PRINT THE RESULTS
      WRITE(7,999)IDEN,IPR,ITR,X,T,ZAVG,C,P2,ERP2,B,P1,ERP1,DIP,DIPER
  999 FORMAT(I6,2I2,F5.0,F6.1,F5.1,3F5.4,2F6.1,2F5.1,F3.1)
      WRITE(6,12)IDEN,IPR,ITR
   12 FORMAT(1H1,10X,'EVENT NUMBER',I7,20X,'NUMBER OF PRONGS',I3,20X,'TR
     1ACK NUMBER',I3)
      WRITE(6,13)SPEED,N,ZAVG,BDEN,C,ALPHA
   13 FORMAT(///,' SPEED OF MEASUREMENT=',F6.3,' MICRONS/SEC',30X,'NUMBE
     1R OF CHANNELS USED=',I4,///,' AVERAGE Z(FROM TOP) OF TRACK=',F6.1,
     2' MICRONS',25X,'BLOB DENSITY=',F6.4,' BLOBS/MICRON',///,' LACUNARI
     3TY=',F6.4,52X,'ALPHA=',F6.4)
      WRITE(6,51)ITER
   51 FORMAT(///,10X,'THE FOLLOWING RESULTS OF G AND B WERE ACHIEVED AFT
     1ER',I3,' ITERATIONS')
      WRITE(6,14)GPR,PG,ERP2,B,P1,ERP1
   14 FORMAT(//,17X,'    G=1/LBAR',40X,'G(H)',15X,'ERROR',//,20X,F7.5,40X
     1,F7.5,9X,F10.5,///,17X,'B(MEASUREMENT)',32X,'B(CALCULATION)',10X,'
     2ERROR',//,21X,F6.1,41X,F6.1,9X,F10.1,///////,' THE FOLLOWING CHANN
     3ELS WERE DELETED FROM THE CALCULATION ')
      DO 17 I=1,LIM
      K=I-1
      IF(W(I))15,15,17
```

```
   15 WRITE(6,16)K
   16 FORMAT(1H ,I3)
   17 CONTINUE
C     PLOT THE DATA AND THE FITTED CURVE
      WRITE(6,18)
   18 FORMAT(//////,' ON THE FOLLOWING PAGES THE RESULT IS PLOTTED. THE
     1HORIZONTAL AXIS IS LNY---THE VERTICAL AXIS IS CHANNEL NUMBER',//,'
     2 MEASURED DATA POINTS ARE X,S   CALCULATED DATA POINTS ARE +,S    B
     3OTH DATA POINTS COINCIDING ARE PLOTTED WITH O,S')
      DATA A/'X','+','O',' ','*'/
C     CALCULATION OF MAXIMUM VALUE AND SCALING FACTOR
      IF(B-P1)19,19,20
   19 YMAX=ALOG(P1)
      YEND=P1
      GO TO 21
   20 YMAX=ALOG(B)
      YEND=B
   21 SC=YMAX/126.0
C     SET UP BORDER AND PRINT SCALE
      WRITE(6,22)YEND
   22 FORMAT(1H1,4X,'1',118X,F8.1)
      WRITE(6,23)
   23 FORMAT(1H ,4X,'*',125X,'*')
      WRITE(6,24)(A(5),I=1,128)
   24 FORMAT(1H ,3X,128A1)
C     PLOTTING OF DATA
      LIM=N+1
      DO 33 I=1,LIM
      I1=I-1
      IF(I1-N)43,43,36
   43 CI=I-1
      IF(Y(I))103,103,104
  103 NY=1
      GO TO 105
  104 NY=ALOG(Y(I)/CCH)/SC+1
      IF(NY.LE.1) NY=1
      IF(NY.GT.127) NY=127
  105 NYC=ALOG(P1*EXP(-P2*CI*DT*SPEED))/SC+1
      IF(NYC.LE.1) NYC=1
      IF(NYC-NY)25,31,28
   25 DO 26 J=1,NYC
   26 YP(J)=A(4)
      YP(NYC)=A(2)
      K=NYC+1
      DO 27 J=K,NY
   27 YP(J)=A(4)
      YP(NY)=A(1)
      MAX=NY
      GO TO 33
   28 DO 29 J=1,NY
   29 YP(J)=A(4)
      YP(NY)=A(1)
      K=NY+1
      DO 30 J=K,NYC
   30 YP(J)=A(4)
```

```
      YP(NYC)=A(2)
      MAX=NYC
      GO TO 33
   31 DO 32 J=1,NY
   32 YP(J)=A(4)
      YP(NY)=A(3)
      MAX=NY
   33 WRITE(6,34)I1,(YP(J),J=1,MAX)
   34 FORMAT(1H ,I3,'*',127A1)
C     FINAL BORDER
   36 WRITE(6,24)(A(5),I=1,128)
      WRITE(6,35)SC
   35 FORMAT(1H0,' SCALE= ',F8.5,' LN(COUNTS)/CHANNEL')
      GO TO 1
      END
```

APPENDIX D

DATA FOR MEASURED SHOWER TRACKS

Event	Type	Track	Space Angle (Degrees)	g*	Pβ (MeV)	Identification
182981	3	3	4.3±0.1	.992±.016	655±55	K
182988	3	1	1.6±0.1	.978±.016	6628±1270	Π
182988	3	2	0.4±0.1	.971±.015	6561±1262	Π
183077	3	2	2.1±0.2	.981±.016	7693±613	Π
183160	3	2	0.7±0.1	.946±.015	8537±5467	K
183247	3	2	0.9±0.1	.991±.016	11404±6076	Π
183247	3	3	5.7±0.1	.947±.017	1740±134	Π,P
182926	4P	2	4.0±0.1	.967±.020	2987±534	Π
182926	4P	3	2.4±0.2	.985±.020	6744±384	Π
183035	4P	2	1.1±0.3	.978±.016	8501±1404	Π
183148	4P	2	2.8±0.2	1.014±.016	4715±265	e
182984	4	1	1.3±0.1	.990±.016	6129±567	Π
183036	4	3	0.9±0.1	.975±.016	4349±866	Π
182955	4	3	0.6±0.4	.963±.015	2606±198	Π
183134	5	2	23.1±0.1	.942±.015	3775±478	Π
183048	5P	4	3.9±0.3	.945±.015	4266±303	Π
182966	8P	5	6.8±0.1	.878±.016	3771±179	P
190214	3	1	2.7±0.1	.956±.015	5442±660	Π
221575	2P	1	1.9±0.1	1.033±.016	6790±2045	e
221814	3P	2	2.3±0.3	.962±.015	6570±736	Π
221859	3	2	1.0±0.1	1.028±.016	5550±511	e
221695	3	2	1.6±0.3	1.003±.018	9180±2156	Π
221681	4	1	5.3±0.1	.995±.016	2189±156	
221681	4	2	2.1±0.1	.986±.025	6558±638	Π
221642	4	2	2.5±0.1	1.005±.016	13969±7771	Π
221565	4	3	3.5±0.1	.992±.016	4567±394	Π
221791	6	2	2.0±0.1	.995±.016	7893±1695	Π
221715	7P	5	16.9±0.1	.940±.015	1922±342	Π,P
221781	8P	3	1.4±0.1	.943±.015	4309±1730	Π
221703	8	4	1.9±0.1	.897±.014	3153±164	K,P
240508	3	2	1.8±0.1	.965±.017	5400±552	Π
240508	3	3	2.7±0.1	.964±.017	7335±680	Π

Event	Type	Track	Space Angle (Degrees)	g*	Pβ (MeV)	Identi-fication
262699	3	2	0.4±0.1	.981±.016	5432±504	π
262590	4	3	3.1±0.1	.990±.016	6652±1020	π
262636	4	3	6.7±0.1	.962±.015	3017±472	π
262600	5	5	11.1±0.1	.884±.014	807±86	π
262594	7	6	6.1±0.1	.945±.017	2042±282	π
300241	3	3	1.1±0.1	.938±.017	10118±1559	K
310323	8	7	7.6±0.1	.907±.016	2302±305	P
330031	2P	1	1.4±0.1	.981±.016	6639±872	π
330256	2	2	1.0±0.1	1.033±.016	7415±757	e
330374	2	1	2.5±0.1	.980±.016	10898±2545	π
330137	3	3	2.7±0.1	.977±.016	7828±1154	π
330240	3	3	1.9±0.1	.923±.015	8594±956	K,P
330244	3	3	3.1±0.1	.995±.016	5118±814	π
330333	3	1	5.9±0.1	.931±.015	3050±324	π
330333	3	3	2.5±0.1	.929±.015	3383±1015	
330141	4	3	13.8±0.1	.935±.015	2901±399	π
330135	6	5	6.6±0.1	.991±.018	3029±290	
350584	2	1	2.1±0.1	.938±.015	2285±299	π
350584	2	2	2.8±0.2	.991±.018	11172±3171	π
351286	2	1	2.8±0.1	1.005±.016	7568±2494	π
350659	3	1	2.8±0.1	.915±.015	1715±142	π
351230	3	1	3.7±0.1	.997±.016	5002±887	π
351262	4	3	3.7±0.2	.926±.016	3362±297	
350729	5	4	7.3±0.1	.990±.016	8279±2151	π
351214	6	5	6.8±0.1	.898±.014	3040±122	K,P
351240	6	3	1.9±0.1	.942±.015	2945±744	π
351267	6	6	6.4±0.1	.934±.015	1856±199	π,P
370358	2P	1	1.9±0.3	.959±.017	2711±951	π
370052	3	1	3.3±0.2	.969±.015	6314±734	π
370110	3	2	0.6±0.1	.981±.016	6772±1022	π
370385	3	2	0.7±0.1	.954±.017	4789±481	π

Event	Type	Track	Space Angle (Degrees)	g*	Pβ (MeV)	Identi-fication
370507	3	1	2.3±0.1	.976±.017	2212±460	
370398	4P	3	0.4±0.1	.979±.016	6903±842	Π
370041	5	2	8.5±0.1	.981±.020	6185±1599	Π
370095	5	2	0.9±0.1	1.036±.015	4040±2383	e
370190	6P	1	6.7±0.1	.960±.020	3216±1029	Π
370338	6P	4	2.4±0.1	1.019±.018	2185±253	e
370084	6	3	2.4±0.1	.974±.017	4794±874	Π
380160	2P	1	0.9±0.1	1.011±.016	5827±515	e
380040	2	2	2.0±0.1	.993±.016	10231±2137	Π
380071	3	2	3.4±0.2	.948±.017	2913±330	Π
380275	3	1	1.8±0.3	.990±.018	3174±929	
380095	4P	1	7.7±0.1	.980±.016	2726±215	
380095	4P	2	3.2±0.1	.924±.015	6428±1027	K
380266	4	2	1.6±0.3	.950±.017	4208±308	Π
380036	6P	4	10.0±0.1	.924±.016	993±123	Π,K
392102	3	2	5.0±0.1	.959±.017	2987±861	Π
392065	4P	2	1.2±0.3	.980±.017	3792±381	Π
392026	4	2	0.3±0.1	.931±.016	2450±714	Π
392026	4	3	3.4±0.1	.946±.017	2819±152	Π
392042	4	3	3.3±0.2	.950±.017	2326±133	Π
392136	5P	1	3.9±0.1	.928±.015	5765±802	K
392136	5P	4	33.1±0.1	.897±.016	1557±174	K
392178	6P	5	17.3±0.1	.982±.016	2663±360	
392159	8	5	2.3±0.2	.912±.016	4805±1118	K
400391	2P	1	0.6±0.1	.982±.016	9106±1528	Π
400395	2P	1	0.7±0.1	.978±.016	1170±423	K,P
400251	3P	2	1.7±0.1	.952±.015	3748±244	Π
400438	3P	1	1.9±0.1	.999±.016	9658±1685	Π
400330	3	2	2.5±0.3	.921±.015	4445±642	K
400060	4P	3	5.4±0.1	.929±.015	1347±84	Π
400133	4	1	4.1±0.1	.935±.017	5734±1010	K
400146	4	3	0.4±0.1	.963±.015	4442±304	Π

Event	Type	Track	Space Angle (Degrees)	g*	Pβ (MeV)	Identi-fication
400237	5	2	8.8±0.1	.900±.014	2475±437	K,P
400319	5	3	3.3±0.3	.894±.016	3938±1180	K,P
400300	6	4	5.2±0.1	.958±.017	4654±642	Π
400245	10P	8	6.3±0.1	.910±.016	5358±1040	K
443374	3	1	2.4±0.4	.935±.015	6395±2296	K
443513	3	2	4.5±0.1	.916±.015	2668±153	P
443513	4	4	12.3±0.1	.928±.015	1274±96	Π
481081	2	1	1.4±0.4	.974±.016	2432±137	
481081	2	2	2.1±0.4	.989±.016	10637±4402	Π
480837	3	2	0.7±0.1	.947±.015	8161±606	K
480892	4P	2	5.3±0.1	.959±.015	2851±226	Π
481110	4	2	2.2±0.1	.906±.016	4588±617	K
481148	4	3	1.1±0.4	.970±.017	2165±100	
480939	5	3	4.9±0.1	.961±.015	4215±644	Π
480939	5	4	1.7±0.1	.933±.015	7346±1118	K
480942	5	1	5.9±0.1	.888±.016	599±26	Π
513335	5	3	1.4±0.1	.947±.017	4163±310	Π